Phase Transitions and Symmetry Breaking in Disordered Quantum Hall Edge States

by

Joel Ellis Moore

Submitted to the Department of Physics
in partial fulfillment of the requirements for the degree of

Doctor of Philosophy

at the

MASSACHUSETTS INSTITUTE OF TECHNOLOGY

February 2001

Author ....
Department of Physics
October 5, 2000

Certified by... .....
Xiao-Gang Wen
Professor
Thesis Supervisor

Accepted by .....
Thomas J. Greytak
Professor, Associate Department Head for Education

Phase Transitions and Symmetry Breaking in Disordered Quantum Hall Edge States

by

Joel Ellis Moore

Submitted to the Department of Physics
on October 5, 2000, in partial fulfillment of the
requirements for the degree of
Doctor of Philosophy

Abstract

Tunneling into the edge of a quantum Hall droplet is a sensitive probe of the topological orders believed to exist in fractional quantum Hall states. The tunneling behavior of a general hierarchy state is studied within the chiral-Luttinger-liquid model of low-energy edge dynamics. Adding random hopping of quasiparticles between edge modes results in "symmetry restoration by disorder" and universal weak tunneling behavior in edges with modes traveling in both directions. We develop a boost coordinate technique and apply it to find the edge phases and tunneling exponents of all topologically stable principal hierarchy states. States with neutral modes in both directions along the edge have multiple stable fixed points which can be classified by their symmetries. When the tunneling current into an edge is large, the system can cross over from the weak-tunneling fixed point to a different strongly coupled fixed point with different conductance and effective charge. Edges with multiple modes can have multiple strongly coupled fixed points. We develop a general formalism to analyze weakly and strongly coupled fixed points of point tunneling. Adding interactions to tunneling between two Laughlin edges is shown to lead to a continuous variation of effective quasiparticle charge and conductance with interaction strength.

Thesis Supervisor: Xiao-Gang Wen
Title: Professor

Acknowledgments

I like to think that my advisor, Xiao-Gang Wen, has taught me something about a physicist's proper attitude toward his work and toward the scientific community. He has also taught me a great deal of physics, but whatever inadequacies are revealed by this thesis are entirely my own. Xiao-Gang has always been willing to share his ideas and to listen to any proposal of mine, however far-fetched, while helping me find the proper path. Most of all, his genuine and wide-ranging curiosity is a reminder of what the scientific enterprise is really about and a model for his students to emulate. It has been a pleasure being his student and learning as much from his example as from his words. I have also learned from fellow Wen alumni and future alumni Claudio Chamon, Sven Heemeyer, Christopher Mudry, Walter Rantner, and Anna Lopatnikova.

I would also like to thank Patrick Lee, who generously shares his encyclopedic knowledge of condensed matter physics with any student who asks. Professors Wen and Lee and my other teachers (A. Nihat Berker, John Joannopoulos, Mehran Kardar, and Barton Zwiebach) have made MIT a wonderful place to learn and do physics, and I doubt any place I find myself later on will compare.

My many discussions on Kondo physics with Marc Kastner and David Goldhaber-Gordon helped me greatly on a piece of research which was an important part of my graduate education but is not reported here. Nat Fisch and Duncan Haldane of Princeton also deserve mention for making my first experience of physics research a positive one. Two of my high school teachers, Donald Brown and Robert Morse, succeeded in occasionally difficult circumstances by being as committed to their profession as any scientist I have met at any level.

Margaret O'Meara in the CMT office and my fellow CMT students (especially Darren Segall, Tairan Wang, Mehmet Ozgür Oktel, and Rava da Silveira) have earned my sincere thanks for too many things to list over the past four years. I spent the best part of my free time in my first three years at MIT with my Somerville housemates John Lettow, Russell Mann, and Salil Vadhan, who all became close friends.

My graduate work was supported by a fellowship from the Fannie and John Hertz Foundation. I would also like to acknowledge a supplemental Karl Taylor Compton fellowship which I held during my first two years at MIT. The Center for Theoretical Sciences at Hsinchu, Taiwan, hosted me graciously for a two-month visit.

Finally, my abiding thanks go to my parents Janet and Bill and sister Lindsay for their constant encouragement and support. My wife Rageshree has been the ideal confidant and companion these four years, all while succeeding admirably in her own scientific career.

Contents

Chapter 1

Introduction

The first two sections of this introduction review the relevant aspects of the integer and fractional quantum Hall effects. The third section covers the experimental technique of cleaved-edge overgrowth, which allows the observation of non-Fermi-liquid behavior at the edge. The fourth and fifth sections explain how the properties of bulk quantum Hall liquids and of one-dimensional interacting electron systems combine to yield novel behavior at the one-dimensional edge of a quantum Hall droplet. The final section outlines the organization and main results of this thesis.

1.1 Integer quantum Hall effect

The integer quantum Hall effect, discovered by Klaus von Klitzing in 1980 [1], is a quantum-mechanical property of effectively two-dimensional electron gases (2DEGs). When electrons are trapped at the planar interface of a layered GaAs-AlGaAs structure, at sufficiently low temperatures their transverse motion is "frozen out," as essentially all of the electrons occupy the lowest eigenstate in the transverse direction, of width $\sim 100\mathring{A}$. The relevant experimental aspects are described in more detail in section 3 below. Henceforth we neglect the transverse direction and assume that the electrons move in two dimensions. Under these assumptions it turns out that the transverse conductance is quantized to better than one part in 10^9, in real samples with some amount of disorder; this is the famous quantized Hall effect, which we now review.

When a magnetic field B is applied to the 2DEG, the single-electron orbital eigenstates (i.e., ignoring the Zeeman energy) can be grouped into Landau levels of energies $E_n = (n + \frac{1}{2})\hbar\omega_c$, with $n = 0, 1, 2, \ldots$ and $\omega_c = eB/mc$ the classical cyclotron frequency. Each of these levels is highly degenerate, with $N = A/2\pi\ell^2$ states per spin-polarized level in a 2DEG of area A, $\ell = \sqrt{\frac{hc}{eB}}$ the magnetic length. The single-electron density of states in a clean magnetized 2DEG consists of δ-funcion peaks at the Landau level energies E_n. In the presence of a weak spatially random potential, some of the weight in these δ-functions moves into localized states at nearby energies. The only extended states are at exactly the Landau level energies, but there do remain extended states in the presence of (sufficiently weak) disorder. This is quite

different from the situation with $B = 0$, when it is believed that an arbitrarily weak random potential is sufficient to localize all states in two dimensions.

The Hall coefficient is defined as

$$R = \frac{V_y}{I_x B}, \tag{1.1}$$

where I_x is the current through the sample and V_y the associated transverse voltage. For free electrons the Hall coefficient is $\frac{1}{nec}$, where n is the areal electron density. This holds both classically and quantum-mechanically in a perfectly clean system: in the frame moving with velocity cV_y/B, the electric field is zero, so the electrons are stationary on average in this frame. Hence the current in the original frame is $necV_y/B$.

At sufficiently low temperatures in a slightly disordered system, the transverse conductance shows plateaus as the magnetic field is varied with electron density constant. The plateaus are at the values ke^2/h for integers k, so the Hall coefficient is

$$R = \frac{h}{e^2 kB} = \frac{2\pi\ell^2}{kec}. \tag{1.2}$$

This corresponds to the free electron density $k/2\pi\ell^2$, or k filled Landau levels. When the chemical potential is in a region with localized states between the Landau level energies $\hbar\omega_c(k + 1/2)$ and $\hbar\omega_c(k + 3/2)$, the system behaves as if it had exactly k filled Landau levels of free electrons.

The amazing precision of the Hall coefficient's quantization and its insensitivity to details of sample geometry and weak impurity scattering suggest that the reason for its quantization must be topological in nature. Note that in two dimensions conductance and conductivity have the same engineering dimensions, so independence of sample size and geometry is at least possible. The quantization of the Hall coefficient when the chemical potential is in a region of localized states was first explained by Laughlin [2] and Halperin [3]. The important feature for what follows is that when all states at the chemical potential are strongly localized on the experimental length scale, there is a "mobility gap" and the diagonal conductivity is zero. Hence there is no dissipation in the bulk sample.

Under these conditions a gauge-invariance argument shows that an adiabatic change in flux through a hole in the 2DEG by one flux quantum does not change the bulk state of the system, except that an integer number k of electrons may be transferred across the sample. Then averaging to obtain a transverse conductance gives ke^2/h if k Landau levels are filled, as the extended states in each Landau band are sensitive to the flux through the center through the Aharonov-Bohm effect. In the fractional case discussed in the next section, several flux quanta must be added in order to transport a single electron across the sample, and a gapped bulk state emerges at certain fractional fillings as a result of strong electron-electron interactions.

1.2 Fractional quantum Hall effect

The key property for quantization is a gapped ("incompressible") state in the bulk, at least for extended states, but with occupied extended states surviving below the Fermi level. At certain fractional filling factors $\nu = n/n_B$, $n_B = 1/2\pi\ell^2$, there are strongly correlated states which have a true gap in the bulk as a result of Coulomb interactions between the electrons. In order to understand how such states arise at $\nu = 1/3$ and other fractions, it is useful to work in a particular basis for the Landau eigenfunctions, which we now describe.

Instead of using the original coordinate system (x, y) on the plane, we can use the complex coordinates $(z, \bar{z})$, with $z = x + iy$, $\bar{z} = x - iy$. The choice of vector potential $\mathbf{A} = \frac{B}{2}(y\hat{\mathbf{x}} - x\hat{\mathbf{y}})$ gives a constant magnetic field B along the z-direction. The single-particle Hamiltonian is

$$H = \frac{1}{2m}(\frac{\hbar}{i}\nabla + \frac{e}{c}\mathbf{A})^2, \tag{1.3}$$

and in the above gauge the lowest-Landau-level (LLL) normalized eigenfunctions are

$$\psi_m(z, \bar{z}) = \frac{z^m e^{-|z|^2/4}}{\sqrt{2\pi 2^m m!}} \tag{1.4}$$

Here the integer m is the angular momentum of the eigenstate around the origin: $L_z = m\hbar$. The eigenfunctions for higher Landau levels $n > 1$ are of similar form with prefactors $\bar{z}^{(n-1)}$. The $\nu = 1$ ground state for a noninteracting rotationally symmetric system of N electrons is the Slater determinant of $\psi_0, \psi_1, \ldots \psi_{N-1}$. This Slater determinant can be rewritten as

$$\Psi_1 \propto \left(\prod_{1 \le i,j \le N} (z_i - z_j) \right) e^{-\sum_{1 \le i \le N} \frac{|z_i|^2}{4}}. \tag{1.5}$$

The many-body wavefunction Ψ_1 is clearly antisymmetric under exchange of two electron coordinates, as required for a spin-polarized wavefunction for electrons. As required by this antisymmetry, the wavefunction vanishes whenever two electrons are at the same spot.

It is reasonable to assume that the ground state with interactions can be constructed from LLL wavefunctions if the Coulomb interaction is weak compared to the inter-Landau-level spacing $\hbar\omega_c$ and the Zeeman energy. The effect of the Coulomb interaction will be to penalize wavefunctions which allow two electrons to approach each other. In zero magnetic field in two dimensions, it is known that at low density and temperature the electron ground state with Coulomb interactions is a "Wigner crystal" and has long-range crystalline order at zero temperature. In a strong magnetic field, the ground state for some densities is an incompressible quantum liquid with a gap for bulk excitations but no conventional long-range order. A natural generalization of (1.5) with filling factor $\nu = 1/m$ is the Laughlin wavefunction [4]

$$\Psi_m \propto \left(\prod_{1 \le i,j \le N} (z_i - z_j)^m \right) e^{-\sum_{1 \le i \le N} \frac{|z_i|^2}{4}}. \tag{1.6}$$

Originally the Laughlin wavefunction for $m = 3$ was justified through numerical calculations which showed it to have a lower energy than other proposals, and a high overlap with the exact ground state for small systems studied through exact diagonalization. The wavefunction Ψ_3 has a third-order zero whenever two electron coordinates are brought together, suggesting that it will be favored for repulsive electron-electron interactions. Haldane made this connection precise by showing that the Laughlin state Ψ_3 is the exact ground state of a certain Hamiltonian with non-Coulombic interactions. [5] (Specifically, the Laughlin ground state is exact if all interaction pseudopotentials for relative angular momentum greater than $2\hbar$ vanish.) It is believed that no phase transition occurs between this parent Hamiltonian and the true Coulomb or screened-Coulomb Hamiltonian, so that the true ground state is "essentially similar" to the Laughlin state for $\nu = 1/3$ and $\nu = 1/5$. The precise definition of this similarity is that the true ground state and the Laughlin state have the same topological order. [6] For $m \geq 7$ it is thought that the Laughlin state is unstable to Wigner crystallization. [7]

The wavefunction Ψ_3 supports excitations of fractional charge $\pm e/3$. This seems nonsensical at first, since Ψ_3 was constructed as a wavefunction for indivisible charge e electrons. But consider multiplying Ψ_3 by $\prod_i z_i$. The total electron charge within a circle of large radius R around the origin is then reduced by $e/3$, so that at large distances it appears that a "quasihole" of charge $e/3$ has been added to the system at the origin. Another way to see that fractional charges really exist in the system is to consider the degeneracy of low-energy excitations when an electron is added or removed from the system. Instead of scaling with the area A as for a normal metal, the degeneracy scales with A^3 for the $\nu = 1/3$ state: the electron is "fractionalized" into three quasiparticles.

A major subject of this thesis will be how the remarkable features of bulk FQHE states are revealed at the edge. In particular, there are now many observed quantum Hall fractions beyond the Laughlin states, which are predicted to have a rich structure of quasiparticles and topological orders. There are two alternate constructions of fractional quantum Hall states beyond the Laughlin states (here we restrict ourselves to Abelian single-layer quantum Hall states). The first, due to Haldane [5] and Halperin [8], forms a "hierarchy" of odd-denominator filling fractions. Starting from a parent Laughlin state such as $\nu = 1/3$, one can imagine adding Laughlin states of quasiparticles or quasiholes to form daughter states (in this case $\nu = 2/5$ and $\nu = 2/7$) which now have different types of quasiparticle excitations. The hierarchical construction can be iterated to give daughter states of these daughter states (third-level hierarchy states), and so on. Rather than discuss the various approximate wavefunctions proposed for daughter states, their important universal features affecting edge excitations will be described in detail in Chapter 2.

1.3 Experiments at the edge

The only gapless excitations of an incompressible quantum Hall state are localized at the edge. For this reason, measurements on the edge provide the most sensitive probe

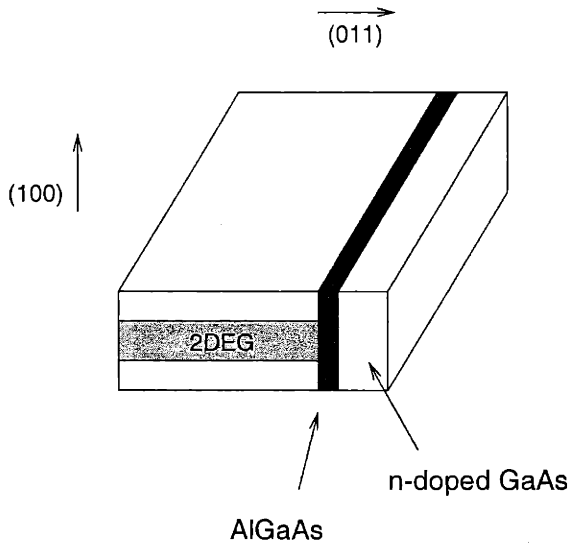

Figure 1-1: Cleaved-edge overgrowth technique to create a sharply defined edge for the 2DEG. Tunneling conductance into the edge is measured through the AlGaAs barrier.

of the rich structures believed to exist in bulk quantum Hall states. In the following two sections, we explain how the edge properties are connected to the topological orders of the bulk quantum Hall state, and why the edge is of interest in its own right as a model one-dimensional system. Now we discuss a beautiful experimental technique, cleaved-edge overgrowth, developed to create a sharp potential barrier at the edge of a quantum Hall droplet. [9] The resulting density profile for the electrons in the lowest Landau level is much sharper than that obtained by electrostatic potentials on gates relatively far from the 2DEG layer, the usual way of defining the droplet edges. The reason why cleaved-edge overgrowth is such a valuable technique is that the non-Fermi-liquid properties of quantum Hall edges are more visible in a sharp edge than a smooth one. Here a sharp edge is one in which the density variation scale $\nabla n/n$ is of order the magnetic length ℓ. In a smooth edge, the density profile can become quite complicated as a result of the Coulomb interaction; this phenomenon is known as edge reconstruction.

Figure 1-1 shows a cleaved-edge overgrowth [10] sample schematically. The 2DEG is cleaved along the (011) crystal axis, and overgrown with a thin layer (90-250 Å) of $Al_{0.1}Ga_{0.9}As$, followed by a 5000 Å layer of GaAs. The band mismatch between the 2DEG and thin layer creates a sharp potential barrier of height about 100 meV. This barrier creates a much sharper edge than possible using the metallic gates which define the other edges of the 2DEG.

It was predicted by Wen [11] that tunneling into the $\nu = 1/3$ Laughlin state would show a strongly nonlinear behavior: $I \propto V^3$, where I is the tunneling current and V the voltage difference between the tunneling lead and sample edge. The reasons for this prediction are discussed in the following sections. For a $\nu = 1$ edge, the Fermi-liquid-like result $I \propto V$ is observed. A nonlinear curve $I \propto V^\alpha$ for small V for the $\nu = 1/3$ edge was observed [12, 13], but with exponent $\alpha \approx 2.7$ rather than 3. The

striking difference in the experimental results for $\nu = 1/3$ and $\nu = 1$ is confirmation that the strong correlations of FQHE states are manifested at the edge.

As the tunneling current increases, the power-law behavior eventually ceases and the differential conductance becomes approximately constant. This asymptotic conductance probes different aspects of edge physics than the weak tunneling power-law behavior, and is discussed in the second part of this thesis. It is believed that in all current experiments on tunneling into cleaved-edge overgrowth samples, there are multiple tunneling points, with different tunneling amplitudes. This does not modify the weak tunneling power-law behavior, but does affect the asymptotic conductance. Here we will consider only the case of a single tunneling junction; it is not too difficult to extend single-junction results to many tunneling junctions. Another type of experiment which we will occasionally refer to measures the temperature dependence of the linear-response conductance.

1.4 Edge states, bosonization, and Luttinger liquids

Our goal in this section is to motivate the description of a clean, sharp quantum Hall edge by a free bosonic one-dimensional field theory. The integer quantum Hall state $\nu = 1$ and the Laughlin states $\nu = 1/m$ have, in the Chern-Simons effective theory for FQHE states described in the next section, a single "condensate" in the bulk, and as a result have a single bosonic branch of excitations at the edge. Edges of more complicated states with multiple condensates have several bosonic modes at the edge. We start in this section with the edge of the $\nu = 1$ integer quantum Hall state, which can be understood from a noninteracting picture, and then consider how this picture can be generalized to more complex states.

Consider the effect of a rotationally symmetric confining potential on the LLL eigenstates near the edge (Fig. 1-2). The degeneracy of the eigenstates is split by the potential, with eigenstates of larger radius gaining more energy. In this simple noninteracting picture, the number of electrons fixes the Fermi level beyond which the states are unoccupied in the many-electron ground state. We will show that the spectrum of the fermionic system shown in Fig. 1-2 can be written in terms of *bosonic* operators. The amazing equivalence between fermionic and bosonic systems in one spatial dimension, which goes by the name of "bosonization," holds well beyond this specific noninteracting example. In fact, the utility of bosonization for quantum Hall states and other one-dimensional problems is that some interacting fermionic systems become free systems in the bosonic language. This important property will be discussed in more detail below. Here we will try to give some intuitive understanding of why bosonization works by counting excitations in a simple case. Chapter 2 includes a summary of results from bosonization which are required for the rest of this thesis.

The lowest-energy excited state, with excitation energy equal to the interlevel separation (E in Fig. 1-2), is obtained by moving the outermost electron one state outward. Note that the potential is assumed approximately linear near the edge of

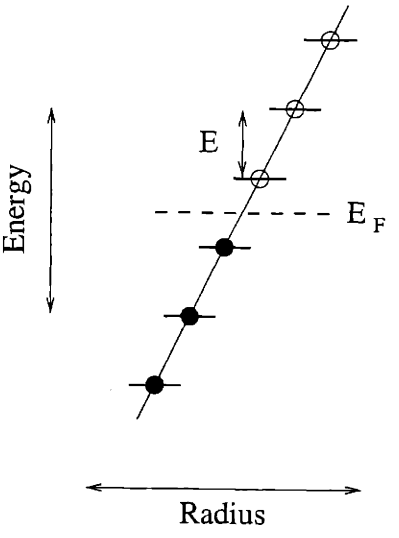

Figure 1-2: Energy levels near the edge for noninteracting $\nu = 1$ state in a rotationally symmetric potential. Solid circles indicate occupied levels and open circles vacant levels in the ground state.

the sample. There are two degenerate states of energy $2E$: one formed by moving the outermost electron two levels outward, and one formed by moving the outermost two electrons one level outward each.

Now let us define a set of bosonic operators $b_m, b_m^\dagger$, $m = 1, 2, \ldots$. The effect of $b_m^\dagger$ on a many-electron state in the occupancy number basis is to move the outermost m electrons one level outward. (These operators conserve the total number of fermions and can be taken to have bosonic mutual statistics.) The operators b_m move the outermost m electrons one level inward if possible and annihilate states where this operation would put two electrons on top of each other. Writing the ground state as $|0\rangle$, the excited state of energy E is $b_1^\dagger|0\rangle$, and the two excited states of energy $2E$ are $(b_1^\dagger)^2|0\rangle$ and $b_1^\dagger|0\rangle$. A moment's thought shows that the entire spectrum is reproduced by the Hamiltonian

$$H = E \sum_{m=1}^{\infty} (m b_m^\dagger b_m). \tag{1.7}$$

This Hamiltonian describes a single branch of edge modes all propagating in the same direction: each mode of angular momentum $m\hbar$ carries energy Em. The chiral boson action which reproduces this Hamiltonian when discretized is

$$S = \frac{1}{4\pi} \int dx\, dt\, \partial_x \phi (\partial_t \phi - v \partial_x \phi). \tag{1.8}$$

Here $v = EL/\hbar$ is simply the physical velocity of the edge excitations, with L the length of the edge. Note that the kinetic part of the action is universal (i.e., has no sample-dependent constants), while the potential part contains v, which depends on the details of the confining potential producing the edge.

The original electronic operators do not appear in the action (1.8), but in order

to calculate the electron correlation functions we need the relation

$$\psi_e^\dagger = \chi \exp(i\phi). \tag{1.9}$$

Here χ is a "Klein factor" or cocycle required to give the right-hand side the correct statistics; it is equivalent to the Jordan-Wigner string which appears in one-dimensional lattice spin models. The Klein factors do not affect the calculations to be done in this thesis, so we will omit them henceforth. The local electronic density is given by $\rho(x) = \frac{1}{2\pi}\partial_x \phi(x)$, and the electron creation operator satisfies (shown in Chapter 2)

$$\left[\rho(x), e^{i\phi(y)}\right] = \delta(x-y). \tag{1.10}$$

The action (1.8) describes not only the $\nu = 1$ edge, but also the $\nu = 1/m$ edge, even though the $\nu = 1/m$ state only exists in the presence of strong electron-electron interactions. There are several ways to derive a chiral boson action at the edge for FQHE states. For states with a single bulk condensate such as the Laughlin states, one can consider the low-energy edge excitations in the classical limit as hydrodynamic ripples on the edge of the Hall droplet. The ripples move in the direction of the classical $\mathbf{E} \times \mathbf{B}$ drift at the edge, and quantizing the ripples leads again to a chiral boson description. A more sophisticated derivation [14] motivates the edge action for a general quantum Hall state by the requirement that the bulk and edge effective theories together satisfy gauge invariance. The edge action derived in this way inherits its universal features from the bulk quantum Hall theory, such as the number of modes in each direction and their relative statistics.

Before considering how tunneling experiments probe edge structure, we now explain why bosonic actions similar to (1.8) are of interest in other condensed-matter problems. Our understanding of clean metals in two and three dimensions is based upon Landau's notion of a Fermi liquid. In one sentence, the Fermi-liquid idea is that the low-energy excitations of a real metal can be put in one-to-one correspondence with those of a free Fermi gas, despite the strong repulsive Coulomb interactions between electrons. The stability of low-energy fermionic excitations results from the Pauli principle and simple geometry: the lifetime of a quasiparticle excitation of small energy E scales with E^{-2} in three dimensions because there is only a small amount of phase space (determined by energy and momentum conservation and the Pauli principle) available for decay by particle-hole pair creation.

In one dimension even weak repulsive interactions are enough to destabilize the Fermi liquid. We mentioned above that even interacting quantum Hall edges can be described by free bosonic Lagrangians; the same is true for the nonchiral (i.e., left-right symmetric) problem of electrons in one-dimensional wires. The nonexistence of a Fermi liquid (other than free fermions) in one dimension results because, after linearizing at the Fermi surface, energy conservation and momentum conservation are redundant, and hence the quasiparticle decay rate does not diverge as the quasiparticle approaches the Fermi surface. The generic state of interacting one-dimensional electrons is referred to as the Luttinger liquid [15, 16, 17], which has a free bosonic description but not a free fermionic description. Luttinger-liquid properties have been difficult to observe experimentally, however, because of the tendency of electrons in

one dimension to localize in the presence of even weak disorder. Quantum Hall edges have thus been studied in their own right as model one-dimensional interacting systems, which show Luttinger-liquid behavior (the prevailing model of edge structure is referred to as the chiral Luttinger liquid) but are relatively insensitive to disorder.

1.5 Tunneling into quantum Hall edges

The simplest understanding of tunneling current into an edge at a given energy is as a measurement of the electronic density of states in the edge at that energy. As we show in this section, the low-voltage scaling $I \propto V^\alpha$ at zero temperature is determined by the scaling dimension of the most relevant electron operator along the edge.

The scaling dimension of an operator is half the power of t in its correlation function:

$$\begin{aligned} \langle e^{im\phi(x,t)} e^{-im\phi(0,0)} \rangle &= e^{m^2 \langle \tilde{\phi}(x,t)\tilde{\phi}(0,0)\rangle - m^2 \langle \tilde{\phi}_j(0,0)\tilde{\phi}_j(0,0)\rangle} \\ &\propto (x+ivt)^{m^2}. \end{aligned} \tag{1.11}$$

Here we have switched to imaginary time and the scaling dimension of the operator $O_m = \exp(im\phi)$ is $\Delta = m^2/2$. The correlation function is calculated from the free action (1.8).

The relation between scaling dimensions and tunneling conductance can be understood simply from the RG equation for the flow of a tunneling amplitude. Suppose that at some starting energy scale the tunneling amplitude coupled to O_m is t. The scaling dimension Δ of O_m determines the RG flow t:

$$\frac{dt}{d\ell} = (1-2\Delta)t. \tag{1.12}$$

Then we expect that at low temperature T the effective amplitude t and the linear-response conductance G scale as $T^{2\Delta-1}$. At zero temperature, the energy scale is set by the voltage V, and the current is

$$I = \int_0^V dV' \frac{dI}{dV}(V') \propto V^{2\Delta}. \tag{1.13}$$

It is also possible to derive the current scaling by deriving the electron DOS as a Fourier transform of the correlation function, but the RG picture will be useful later on in our treatment of random hopping at the edge.

In a general quantum Hall edge, there are many vertex operators (i.e., exponentials of bosonic operators) which carry electron charge, and the physical electron operator is expected to be a linear combination of all of these with unknown coefficients. The tunneling exponent $I \propto V^\alpha$ is clearly determined by the most relevant operator (that which has the lowest value of Δ) for the smallest voltage, but at finite voltage one could envisage a crossover to a less relevant operator with a larger coefficient. Another caveat is that the experimentally measurable tunneling is sensitive only to electronic states which are extended or propagating, for the following reason. Tunneling into a single localized state in the absence of interactions will not give a macroscopic current, as once the state becomes occupied by an electron there is no way for that electron to leave the state and allow another electron to tunnel in.

1.6 Outline of results

Now we are in a position to state the main results of this thesis. The first part (Chapters 2 through 5) reviews the chiral-Luttinger-liquid model of edge states and examines how edge structure determines the nonlinear tunneling conductivity $I \propto V^{\alpha}$. In states such as $\nu = 2/3$ with edge modes propagating in both directions, some form of impurity scattering, modelled theoretically by random hopping of quasiparticles between edge modes, is necessary for α to take universal values. [18, 19] When random hopping is relevant in the $\nu = 2/3$ case studied by Kane, Fisher, and Polchinski (KFP), it drives the system to a unique fixed point where the system can be solved exactly by "gauging away" the disorder. One special feature of this fixed point is that only one edge mode carries charge; the other mode is electrically neutral, so the fixed point shows charge-neutral separation.

We develop a technique to study random hopping in a general Abelian edge, not just the $\nu = n/(2n \pm 1)$ states studied previously. An important result is that edges with neutral modes traveling in both directions, such as $\nu = 5/7$, have several physically different edge phases with different values of the tunneling exponent α. All these phases show spin-charge separation but differ in how they break the symmetries of the kinetic part of the Lagrangian (Chapter 4). Our technique enables a complete classification of the effects of disorder on Abelian principal hierarchy states. The results of this classification are summarized in Table 5.1 and Fig. 5-1 of Chapter 5.

There is an interesting form of agreement between this theory for incompressible quantum Hall states and a composite-fermion (CF) theory [20] for compressible quantum Hall states. The CF theory predicts a continuous curve for tunneling exponent α as a function of filling fraction ν, for compressible states; at incompressible fractions, we find that exactly one phase has tunneling exponent α which lies on the CF curve (Fig. 5-1). Chapter 6 uses a perturbative RG technique to calculate the flows of random hopping operators and justify the flow diagrams found in previous chapters.

The second part of this thesis (Chapters 7 through 9) describes strong tunneling between edges, when the low-voltage power-law relationship between I and V no longer applies. Tunneling between two Laughlin states such as $\nu = 1/3$ shows a crossover between two fixed points as a function of applied voltage. The low-voltage or weak-coupling fixed point can be thought of as weak electron tunneling and is understandable by the methods of the first part. The strong-coupling fixed point describes quasiparticle tunneling between two edges of the same quantum Hall bar. For tunneling between more complicated edge states, the strong-coupling behavior provides a probe of edge structure which is relatively independent of the weak-tunneling probe. We develop a formalism to describe strong-coupling fixed points in the chiral Luttinger liquid model and apply it to a number of examples.

The experimentally relevant correlation functions for electronlike operators across the junction can be calculated from this framework, and have a simple "image-charge" description when the tunneling problem is folded onto the half-line. We present a solvable model in which interactions between edges give a continuous variation with interaction strength of effective tunneling charge and the $I - V$ curve. This suggests that once interactions between edges are considered, nonuniversal features can appear

in tunneling properties and the identification of effective tunneling charge becomes more difficult. We end with a brief summary of our conclusions and of open problems for future work.

Chapter 2

The chiral-Luttinger-liquid model of quantum Hall edge states

2.1 Chern-Simons effective theory of FQHE states

The topological orders associated with bulk quantum Hall states can be understood by constructing a low-energy theory. The theory is "low-energy" in the same sense as the Ginzburg-Landau theory of a fully gapped superconductor: even though the bulk is gapped, there is a nontrivial response to an applied electromagnetic field. In this section we review the Chern-Simons effective theory for the bulk degrees of freedom, and . The effective theory we use is in the pure Chern-Simons form of Wen [6], which is related to the earlier formalism of Read [21] and Zhang *et al.* [22] by a duality transformation.

For a Laughlin state, the response of the particle number current J_μ to an applied field is fixed by $\sigma_{xx} = 0$, $\sigma_{xy} = \frac{\nu e^2}{h}$:

$$e\delta J_\mu = \frac{\nu e^2}{h}\epsilon^{\mu\gamma\lambda}\partial_\gamma \delta A_\lambda. \tag{2.1}$$

Here μ, γ, λ are spacetime indices $(0, 1, 2)$ and the electron charge is e. We seek to find a Lagrangian whose equation of motion is (2.1). Current conservation is automatically satisfied if we write J_i as the curl of a $U(1)$ gauge field a_i (now $\hbar = 1$):

$$J_\mu = \frac{1}{2\pi}\epsilon^{\mu\gamma\lambda}\partial_\gamma a_\lambda. \tag{2.2}$$

Then for $\nu = 1/m$ the effective Lagrangian is

$$L = -\frac{m}{4\pi}\epsilon^{\mu\gamma\lambda}a_\mu\partial_\gamma a_\lambda + \frac{e}{2\pi}\epsilon^{\mu\gamma\lambda}A_\mu\partial_\gamma a_\lambda. \tag{2.3}$$

We briefly review the properties of this effective Lagrangian to gain some understanding of how it captures the physics of the Laughlin states. The above Lagrangian supports excitations of fractional charge $\pm\frac{e}{m}$. Interchanging identical quasiparticles of charge $\frac{e}{m}$ gives a statistics angle $\theta = \pi/m$, so these quasiparticles have fractional

statistics in addition to fractional charge. In more complicated hierarchical states, there are several types of quasiparticles with different relative statistics. That is, for each pair of quasiparticles the wavefunction gains some phase when the two quasiparticles are moved around one another, and this phase may vary with the type of quasiparticle. We now give the Chern-Simons Lagrangian for a general Abelian quantum Hall state. (The terminology "Abelian" means that the total statistics from a given exchange process can be described simply by an angle, or an element of the Abelian group $U(1)$.)

The Chern-Simons action for a state with n condensates contains n bosonic fields a_i:

$$L = -\frac{1}{4\pi} K^{ij} \epsilon^{\mu\gamma\lambda} a^i_\mu \partial_\gamma a^j_\lambda + \frac{e}{2\pi} \epsilon^{\mu\gamma\lambda} t^i A_\mu \partial_\gamma a^i_\lambda. \tag{2.4}$$

Here K is a symmetric integer $n \times n$ matrix which contains information about the relative statistics of the quasiparticles. The integer charge vector $\mathbf{t}$ contains the electromagnetic charges of the different quasiparticle types: a quasiparticle of type i carries charge $q = eK^{-1}_{ij} t_j$. The filling fraction is $nu = \mathbf{t}^T K^{-1} \mathbf{t}$. We will now give some examples of K matrices for the simplest fractional quantum Hall states.

The integer quantum Hall state $\nu = n$ has $K = I_n$ (the $n \times n$ identity matrix) and $\mathbf{t} = (1, \ldots, 1)$. Thus at the effective theory level this state is simply n decoupled copies of the $\nu = 1$ state, which has $K = (1)$ and $\mathbf{t} = (1)$. Below we will see that the same picture applies at the edge. The Laughlin states $\nu = 1/m$ have $K = (m)$, $\mathbf{t} = (1)$. The simplest hierarchical FQHE states are $\nu = \frac{2}{5}$ and $\nu = \frac{2}{3}$. The $\nu = 2/5$ state is obtained from the $\nu = 1/3$ state by condensing a gas of quasiparticle excitations:

$$K = \begin{pmatrix} 3 & 1 \\ 1 & 2 \end{pmatrix}, \quad \mathbf{t} = (1, 0). \tag{2.5}$$

The meaning of the above matrix is that there are two Chern-Simons fields which have nontrivial relative statistics since the off-diagonal elements are nonzero. The 2 on the diagonal means that the gas of quasiparticle excitations have bosonic statistics. The off-diagonal elements are nonzero because in this basis (the Haldane basis [5]) the quasiparticles are sensitive to an effective magnetic field from the original fermions, but not directly coupled to the electromagnetic field.

Another simple hierarchy state, whose edge will be of great interest below, is the $\nu = \frac{2}{3}$ state. In the basis we will generally be using

$$K = \begin{pmatrix} 1 & 1 \\ 1 & -2 \end{pmatrix}, \quad \mathbf{t} = (1, 1). \tag{2.6}$$

Here the -2 on the diagonal means that we have condensed quasiholes rather than quasiparticles, giving a state with filling fraction lower than the original $\nu = 1$ state. A more transparent basis is

$$K = \begin{pmatrix} 1 & 0 \\ 0 & -3 \end{pmatrix}, \quad \mathbf{t} = (1, 1). \tag{2.7}$$

This is equivalent to the previous form under a simple $SL(2, Z)$ redefinition of the boson fields. This diagonal form shows that the $\nu = 2/3$ state can be interpreted as

a $\nu = 1/3$ Laughlin state of holes in a $\nu = 1$ IQHE state of electrons. The K matrix for the $\nu = 2/3$ state turns out to have profound consequences for the structure of the edge of this state.

The $\nu = 2/3$ and $\nu = 2/5$ states are both principal hierarchy states, which means that the daughter state $\nu = 2/5$ is constructed from the lowest-energy excitations of the parent $\nu = 1/3$ state, and similarly for $\nu = 2/3$. The most robust fractional quantum Hall states are principal hierarchy states, although non-principal states such as $\nu = 4/5$ do exist. The K matrix of a principal hierarchy state in the Haldane basis has all diagonal elements equal to ± 2, and all elements immediately above and below the diagonal equal to 1. We will see in Chapter 3 of this thesis how important differences emerge at the edge between principal hierarchy states and non-principal states. The most robust states lie in the "main sequence" $\nu = n/(2n \pm 1)$ where all the diagonal elements aside from the first are the same. That is, in a main-sequence state all elements are either $+2$ (for $\nu = 2/5, 3/7, 4/9, \ldots$) or -2 (for $\nu = 2/3, 3/5, 4/7, \ldots$). An example of a principal hierarchy state which is not on the main sequence but is observed experimentally is $\nu = 5/7$, which has diagonal elements $(1, -2, 2, -2)$.

Every odd-denominator fraction can be obtained as the filling fraction of some (many-level) hierarchy state, but this may seem problematical as only certain fractions are observed. However, the prediction of the hierarchy picture that whenever a daughter state is observed, all of its parent states must also be observed, seems to be correct. An alternate "composite fermion" picture of some FQHE states was developed by Jain [23], which explains the main-sequence FQHE states as IQHE states of composite fermions. It is currently believed that for main-sequence states the composite-fermion and hierarchy constructions have finite overlap in the thermodynamic limit and have the same topological orders (and hence same K matrices). In the next section we discuss the low-energy edge theory and its relationship to the bulk Chern-Simons theory.

2.2 The effective theory of the edge

Edges of quantum Hall systems are described by a chiral Luttinger liquid (χLL) theory related to the topological orders of the bulk quantum Hall state. We introduce the theory for a clean edge and diagonalize it to obtain scaling dimensions of impurity scattering operators. For a derivation of the theory from the bulk Lagrangian the reader is referred to [14]. Before discussing the physical content of the χLL description, we introduce some needed formalism. The χLL action in imaginary time for a clean edge of a QH state characterized by the matrix K contains $n = \dim K$ bosonic fields ϕ_i and has the form [11]

$$S_0 = \frac{1}{4\pi} \int dx\, d\tau \, [iK_{ij}\partial_x \phi_i \partial_\tau \phi_j + V_{ij}\partial_x \phi_i \partial_x \phi_j] \tag{2.8}$$

where, as in the rest of this chapter, the sum over repeated indices is assumed. K is a symmetric integer matrix and V a symmetric positive matrix. K gives the topological properties of the edge: the types of quasiparticles and their relative statistics. V, the

velocity matrix, is positive definite so that the Hamiltonian is bounded below. The charges of quasiparticles are specified by an integer vector $\mathbf{t}$ and the filling factor is $\nu = t_i(K^{-1})_{ij}t_j$.

The quasiparticle density of type i is given by $\rho_i(x) = \frac{1}{2\pi}\partial_x\phi_i(x)$. Now we find the commutation relations of the ϕ fields. In the $\nu = 1$ case, we want the operator $\psi^\dagger = e^{i\phi}$ to change the local density by 1:

$$\left[\rho(x), e^{i\phi(y)}\right] = \delta(x-y). \tag{2.9}$$

This is satisfied if the commutator of ϕ fields has the nonlocal form

$$[\phi(x), \phi(y)] = -i\pi\mathrm{sgn}(y-x). \tag{2.10}$$

Our sign convention is that positive x along the edge (right-moving) is the direction of the classical $\mathbf{E}\times\mathbf{B}$ drift and of propagation for the single-mode $\nu = 1$ and $\nu = 1/m$ edges. The generalization of (2.10) to a multicomponent edge is

$$[\phi_i(x), \phi_j(y)] = -i\pi K^{-1}_{ij}\mathrm{sgn}(y-x). \tag{2.11}$$

This implies for the densities

$$[\rho_i(x), \rho_j(y)] = -\frac{i}{2\pi}K^{-1}_{ij}\delta'(y-x). \tag{2.12}$$

One simple and powerful prediction of the chiral Luttinger liquid model is that the number and directionality of edge modes is determined by the K matrix of the bulk Chern-Simons effective theory. The number of right-moving modes is equal to the number of positive eigenvalues of K, and the number of left-moving modes equal to the number of negative eigenvalues. For example, the $\nu = 2/3$ state is predicted to have one mode traveling in each direction, which has been verified by numerical diagonalization of small systems for the spin-polarized [24] and spin-unpolarized [25] cases. Experiments to count the number of modes are difficult because often one or more modes is neutral and difficult to observe directly. The bulk of this thesis is devoted to finding the predictions of the chiral-Luttinger-liquid model for more feasible experiments, such as tunneling $I-V$ measurements.

There are major differences between chiral edges (all modes propagate in the same direction) and nonchiral edges (at least one mode in each direction). In chiral edges all scaling dimensions are universal, in that they depend only on K and not on V, and so are the same for all samples of a given edge. In nonchiral edges scaling dimensions and associated tunneling properties are sensitive to V. As mentioned in the Introduction, impurity scattering (modeled by random hopping of quasiparticles) is necessary to understand tunneling measurements in nonchiral edges. In the remainder of this chapter we introduce random hopping of quasiparticles and show how scaling dimensions of quasiparticle creation and annihilation operators are calculated.

Scattering by spatially random quenched impurities is described by the action

$$S_1 = \int dx\, d\tau\, [\xi(x)e^{im_j\phi_j} + \xi^*(x)e^{-im_j\phi_j}] \tag{2.13}$$

Here ξ is a complex random variable and $[\xi(x)\xi^*(x')] = D\delta(x-x')$, with D the (real) disorder strength. The integer vector $\mathbf{m}$ describes how many of each type of quasiparticle are annihilated or created by the operator $O_{\mathbf{m}} = \exp(im_j\phi_j)$. For a real system all charge-neutral scattering operators m_j are expected to appear, but most of these will be irrelevant in the RG sense as discussed in the following. The condition for charge-neutrality is $t_i(K^{-1})_{ij}m_j = 0$. The random variables $\xi_{\mathbf{m}}$ for different scattering operators $O_{\mathbf{m}}$ may be uncorrelated or correlated depending on the nature of the physical impurities causing the scattering.

Now consider the correlation functions of these scattering operators with respect to the clean action S_0. For integer vectors $\mathbf{m}$, define the function $K(\mathbf{m}) \equiv m_i(K^{-1})_{ij}m_j$. $K(\mathbf{m})$ governs the topological part of the correlation function of the scattering operator $O_{\mathbf{m}}$ as follows: the correlation function is, ignoring cutoffs,

$$\begin{aligned} G(x,\tau) &= \langle e^{im_j\phi_j(x,\tau)}e^{-im_j\phi_j(0,0)}\rangle \\ &\propto (\textstyle\prod_{k=1}^{n^+}(x+iv_k^+\tau)^{-\alpha_k})(\prod_{k=1}^{n^-}(x-iv_k^-\tau)^{-\beta_k}). \end{aligned} \tag{2.14}$$

Here n^+ and n^- are the numbers of positive and negative eigenvalues of K, and $v_k^\pm$, α_k, β_k are nonnegative real numbers which depend on V and K. However, $\sum_{k=1}^{n^+}\alpha_k - \sum_{k=1}^{n^-}\beta_k = K(\mathbf{m})$ independent of V. Setting all velocities $v_k^\pm = 1$ and introducing $z = x + i\tau$,

$$\langle e^{im_j\phi_j(x,\tau)}e^{-im_j\phi_j(0,0)}\rangle \propto \frac{1}{z^{K(\mathbf{m})}}\frac{1}{|z|^{2\Delta(\mathbf{m})-K(\mathbf{m})}} \tag{2.15}$$

with $K(\mathbf{m})$ assumed positive. $\Delta(\mathbf{m}) = (\sum_{k=1}^{n^+}\alpha_k + \sum_{k=1}^{n^-}\beta_k)/2$ is the scaling dimension of the operator $\exp(im_j\phi_j)$.

2.3 The electron and quasiparticle lattices

In addition to the edge action, we need to fix which vertex operators $O_{\mathbf{m}}$ are allowed by the requirements of charge quantization and mutual locality. There are two classes of vertex operators which will be needed in what follows. The first type are those operators which can be generated by applying one or more electron creation or annihilation operators at the edge. Any product of two operators in this class is itself in this class, so the vectors $\mathbf{n}$ associated to operators in this class form a lattice:

$$O_{\mathbf{n}} = e^{i\mathbf{n}\cdot\phi}, \quad \mathbf{n} \in \Gamma_c. \tag{2.16}$$

The lattice Γ_c is the set of integral linear combinations of some basis of $n = \dim K$ vectors. Some $O_{\mathbf{n}}$ add charge to the edge and others transfer electrons or quasiparticles between different edge branches but are neutral overall. The charge and the statistics of $O_{\mathbf{n}}$ are given by

$$Q = \mathbf{n}^T K^{-1}\mathbf{q}, \quad \theta = \pi\mathbf{n}^T K^{-1}\mathbf{n}. \tag{2.17}$$

The vectors in Γ_c satisfy

$$\begin{aligned} \mathbf{n}^T K^{-1} \mathbf{n}' &= \text{integer}, \\ \mathbf{n}, \mathbf{n}' &\in \Gamma_c. \end{aligned} \tag{2.18}$$

Thus the charge excitations in Γ_c are bosons or fermions with trivial mutual statistics. These vertex operators can appear in the Hamiltonian if they have bosonic statistics. In many cases, the lattice Γ_c is generated by electron operators, so we will refer to Γ_c as the E-lattice (although Γ_c sometimes contains operators that transfer quasiparticles between different branches).

The quasiparticle operators are also labeled by points in a lattice, Γ_q:

$$\Gamma_q = \{\mathbf{n} | \mathbf{m}^T K^{-1} \mathbf{n} = \text{integer, for all } \mathbf{m} \in \Gamma_c\} \tag{2.19}$$

We will call this lattice the quasiparticle lattice or Q-lattice. Note that the Q-lattice Γ_q is the dual lattice in K^{-1} of the E-lattice Γ_c. The condition (2.19) arises from the requirement that quasiparticle operators be local with respect to electron operators [14]. Physically, the quasiparticle operators are relevant for tunneling between two quantum Hall edges separated not by vacuum but by a quantum Hall state which is capable of supporting fractionally charged quasiparticles.

From the definition of the E-lattice, we see that $\Gamma_c \subset \Gamma_q$. Since we are going to discuss many lattices in this thesis, it will be convenient to use matrices to describe lattices. We will say a lattice Γ is described by a matrix M if the column vectors of the matrix are a basis for the lattice. We will denote such a lattice as $\Gamma = \text{Latt}(M)$. Also we will use $W\Gamma$ to denote the transformed lattice of Γ by W: $W\Gamma \equiv \text{Latt}(WM)$. Under this notation, we can write the E-lattice $\Gamma_c = \text{Latt}(C)$, where the k by k matrix C satisfies $C^T K^{-1} C =$ integral matrix. The Q-lattice is then

$$\Gamma_q = \text{Latt}(K(C^T)^{-1}). \tag{2.20}$$

2.4 Boost coordinates

The scaling dimensions of the various operators in the edge theory are functions of V, an $n \times n$ matrix. Much of the physics of a disordered edge depends on V only through the scaling dimensions of various operators. In this section we introduce a coordinate system which greatly simplifies the calculation of scaling dimensions. The scaling dimension of an operator determines whether that operator is relevant in the RG sense when added to the clean action S_0. The operator is relevant with a uniform coefficient when $\Delta(\mathbf{m}) < 2$, relevant with a spatially random coefficient when $\Delta(\mathbf{m}) < 3/2$, and relevant at a point (with a δ-function coefficient) when $\Delta(\mathbf{m}) < 1$. For the random case this follows from the leading-order RG flow equation for disorder strength D, [26]

$$\frac{dD}{dl} = (3 - 2\Delta)D. \tag{2.21}$$

It is thus useful to write V in a way which isolates the parts of V which affect $\Delta(\mathbf{m})$ so that scaling dimensions depend on as few parameters as possible.

As mentioned in the introduction, the tunneling conductance exponent α in $I \propto V^\alpha$ is determined by the scaling dimension of the most relevant electronlike operator. The two-terminal conductance in units of e^2/h is given by twice the scaling dimension $\Delta(\mathbf{t})$ of the charge operator as a consequence of the Kubo formula. [18] This is the conductance measured with ideal contacts; a kinetic theory model for nonideal tunnel-junction contacts gives a different nonuniversal value. [27] So a simple way to calculate scaling dimensions in complicated edges will be quite useful to understand experimentally relevant properties.

Equation 2.14 is obtained by simultaneously diagonalizing K and V by a basis change $\phi_i = M_{ij}\tilde{\phi}_j$. Suppose M_1 brings K to the pseudo-identity $I(n^+, n^-)$, i.e.,

$$M_1^{\mathrm{T}} K M_1 = I_{n^+,n^-} = \begin{pmatrix} I_{n^+} & 0 \\ 0 & -I_{n^-} \end{pmatrix}. \tag{2.22}$$

Basis changes preserve the number of positive and negative eigenvalues of a matrix ("Sylvester's law of inertia"). Now consider another basis change M_2 which will diagonalize V and preserve the pseudo-identity: $M_2 \in SO(n^+, n^-) \Rightarrow M_2^{\mathrm{T}} I(n^+, n^-) M_2 = I(n^+, n^-)$, introducing the proper pseudo-orthogonal group $SO(m, n)$. The real positive symmetric matrix $V' \equiv M_1^{\mathrm{T}} V M_1$ can be written as $(M_2^{-1})^{\mathrm{T}} V_D M_2^{-1}$ for some diagonal matrix V_D and some $M_2 \in SO(n^+, n^-)$. The entries in V_D are all positive and are the $v_k^{\pm}$ from (2.14), with (v^+, v^-) corresponding to (positive, negative) eigenvalues of K.

Since V_D and $I(n^+, n^-)$ are diagonal, the correlation functions in the basis $\tilde{\phi} = (M_1 M_2)^{-1}\phi$ are trivial:

$$\begin{aligned} \langle e^{i\tilde{\phi}_j(x,\tau)} e^{-i\tilde{\phi}_j(0,0)} \rangle &= e^{\langle \tilde{\phi}_j(x,\tau)\tilde{\phi}_j(0,0)\rangle - \langle \tilde{\phi}_j(0,0)\tilde{\phi}_j(0,0)\rangle} \\ &\propto \frac{1}{x \pm i v_j \tau} \end{aligned} \tag{2.23}$$

where the sign depends on whether $\tilde{\phi}_j$ appears with -1 or $+1$ in $I(n^+, n^-)$. Going back to the original fields ϕ, we obtain

$$K^{-1} = M_1 M_2 I_{n^+,n^-} M_2^{\mathrm{T}} M_1^{\mathrm{T}} = M_1 I_{n^+,n^-} M_1^{\mathrm{T}}, \tag{2.24}$$

$$V_D = M_2^{\mathrm{T}} M_1^{\mathrm{T}} V M_1 M_2. \tag{2.25}$$

Let us define a matrix Δ through

$$\begin{aligned} I &= M_2^{\mathrm{T}} M_1^{\mathrm{T}} (2\Delta)^{-1} M_1 M_2 \\ \Rightarrow \quad 2\Delta &= M_1 M_2 M_2^{\mathrm{T}} M_1^{\mathrm{T}}. \end{aligned} \tag{2.26}$$

The positive definite matrix Δ gives the scaling dimension of the operator $O_{\mathbf{m}}$: $\Delta(\mathbf{m}) = m_i \Delta_{ij} m_j$. Note that under the basis change $\phi_i = M_{ij}\tilde{\phi}_j$, the vector $\mathbf{m}$ transforms to preserve $\tilde{m}_i \tilde{\phi}_i = m_i \phi_i = m_i M_{ij} \tilde{\phi}_j$, so $\tilde{\mathbf{m}} = M^{\mathrm{T}}\mathbf{m}$. Thus the functions $K(\mathbf{m})$ and $\Delta(\mathbf{m})$ are basis-invariant.

The scaling dimensions are independent of the $n = n^+ + n^-$ velocities in V_D, as expected on physical grounds. M_1 depends only on K, not on V, so all possible matrices

Δ for a given edge are obtained as M_2 ranges over $SO(m,n)$ with M_1 fixed. We now introduce a parameterization of M_2 in which only n^+n^- coordinates affect Δ. The physical picture is that the scaling dimensions are independent of the velocities of the eigenmodes and also of the interactions between modes going in the same direction; the scaling dimensions are only affected by interactions between counterpropagating modes. Thus of the $n(n+1)/2$ free parameters in V, n correspond to velocities of eigenmodes, $(n^+(n^+-1)+n^-(n^--1))/2$ to same-direction interactions, and n^+n^- to opposite-direction interactions.

The study of a nonchiral edge with several branches of excitations is thus feasible if one is willing to concentrate on edge properties and renormalization-group flows determined by the scaling dimensions of various operators. There are interesting physical phenomena which are not determined solely by scaling dimensions, such as the equilibration of velocities of modes moving in the same direction by interchannel hopping (which does not affect the conductance). But the effects of disorder on the commonly measured physical properties can be obtained from studying only the n^+n^- parameters of V which affect scaling dimensions, rather than the $n(n+1)/2$ needed for a complete description of the theory. This is apparent in the study of an $n=2$ case ($\nu=2/3$)[18]: the velocity matrix has the form

$$V=\begin{pmatrix} v_1 & v_{12} \\ v_{12} & 3v_2 \end{pmatrix} \tag{2.27}$$

with one branch in each direction, and the conductance and the structure of the RG flow are found to depend only on the combination $c=2v_{12}(v_1+v_2)^{-1}/\sqrt{3}$.

The separation of V comes about because every element M in $SO(m,n)$ can be written as a product of a symmetric positive matrix B and an orthogonal matrix R, both of which are in $SO(m,n)$. This is a generalization of the familiar decomposition of a Lorentz transformation (an element of $SO(3,1)$) into a boost (a symmetric positive matrix) and a rotation (an orthogonal matrix). For all examples in this thesis $m=1$ or $n=1$ and this decomposition follows easily from the parameterization of boost matrices given below. More details are in Appendix A. Writing $M_2=BR$,

$$2\Delta = M_1M_2M_2^{\mathrm{T}}M_1^{\mathrm{T}} = M_1BRR^{\mathrm{T}}B^{\mathrm{T}}M_1^{\mathrm{T}} = M_1B^2M_1^{\mathrm{T}}. \tag{2.28}$$

So Δ is independent of R and depends only on the n^+n^- parameters in B. B can be written

$$B=\exp\begin{pmatrix} \mathbf{0} & b \\ b^{\mathrm{T}} & \mathbf{0} \end{pmatrix} \tag{2.29}$$

for some $n^+\times n^-$ matrix b.

For a maximally chiral edge, the boost part B is just the identity matrix, so the scaling dimension of every operator $\exp(im_j\phi_j)$ is independent of V, and in particular the conductance $\sigma=2\Delta(t)=K(t)=\nu$. For nonchiral edges, nonuniversal values of the conductance are possible with $2\Delta(t)\geq\nu$ and equality if and only if the velocity matrix is charge-unmixed. This is a special case of the general property $2\Delta(\mathbf{m})\geq|K(\mathbf{m})|$ for all integer vectors $\mathbf{m}$ (with equality if and only if the V_{1j} vanish in the basis with $\mathbf{e}_1\parallel\mathbf{m}$ and K^{-1} diagonal). Consequently the scattering term $\exp(im_j\phi_j)$

can only be relevant if $|K(\mathbf{m})| \leq 3$. The scattering operator must have bosonic commutation relations so the three possibilities are $K(\mathbf{m}) = 2, 0, -2$. If a null vector exists with $K(\mathbf{m}) = 0$, the edge is not T-stable. Operators with $|K(\mathbf{m})| = \pm 2$ are necessary if the impurities are to drive the edge state to a fixed point. The next step is to calculate which velocity matrices make the scattering terms $\xi(x)\exp(im_j\phi_j) + \xi^*(x)\exp(-im_j\phi_j)$ relevant.

The possible matrices Δ for a given edge can be studied simply by calculating $2\Delta = M_1 B^2 M_1^{\mathrm{T}}$ for all boosts B. For a two-component edge with one branch propagating in each direction, there is just one boost parameter. For a three-component edge, there are two parameters, and the scaling dimensions of various operators can be plotted on the plane as functions of these two parameters. For $SO(1,m)$ a useful parameterization of boosts as a function of momentum coordinates $(p_1, \ldots, p_m)$ is [28]

$$\begin{aligned} B_{11} &= \gamma = \sqrt{1+p^2}, \quad B_{1i} = B_{i1} = p_{i-1}, \\ B_{ij} &= \delta_{ij} + p_{i-1}p_{j-1}(\gamma - 1)/p^2 \end{aligned} \tag{2.30}$$

where $2 \leq i, j \leq m+1$. It is convenient to work with dimensionless momentum $\mathbf{p} = \gamma \mathbf{v}$ because of the singularity at $v = c = 1$ in the velocity coordinates. However, in Chapter 3 we mention an advantage of the velocity coordinates for certain edges. Permuting indices gives a version appropriate for $SO(m,1)$.

For a given edge it is now possible to search for all possibly relevant neutral operators ($|K(\mathbf{m})| = 2$) and then calculate where in the space of boost parameters each operator is relevant. The rest of this section describes a few technical details needed to carry out this program. The search for $|K(\mathbf{m})| = 2$ operators is done on a computer: there is a finite p-adic test for whether an integer quadratic form takes the value zero, [29] but we know of none to determine all vectors for which an integer quadratic form takes a particular nonzero value. It will be useful to consider basis changes not in $SL(n,Z)$ which bring K^{-1} to diagonal form, so that the locality condition is no longer that $\mathbf{m}$ be an integer vector. The local operators in the new theory are the transforms of integer vectors in the original theory. The advantage of such a basis change $K^{-1} \to OK^{-1}O^{\mathrm{T}}$, $\mathbf{m} \to O^{\mathrm{T}^{-1}}\mathbf{m}$ which makes K^{-1} diagonal and brings the charge vector $\mathbf{t}$ to the first basis vector $\mathbf{e_1}$ is that some of the boost parameters can be interpreted as the strength of mixing of the charge mode with neutral modes. Then the charge-unmixed velocity matrices will be exactly those with these boost parameters equal to zero. Table 3.1 of Chapter 3 summarizes the possible parameter spaces for all nonchiral edges with four or fewer components.

For each operator with $|K(\mathbf{m})| = 2$, there is some velocity matrix which gives that operator scaling dimension $2\Delta(\mathbf{m}) = 2$: this follows from choosing M_1 in (2.24-2.26) to make $\mathbf{m}$ one of the basis vectors and choosing M_2 so that all parameters rotating $\mathbf{m}$ into other basis vectors are zero. The operation of changing bases distorts the phase diagram nonlinearly but preserves its topology and produces the same set of possible scaling matrices Δ. The sign of $K(\mathbf{m})$ will affect the dimension of the subset of matrices V which make $\exp im_j\phi_j$ maximally relevant. In the next chapter we use the boost coordinate system to classify all disordered Abelian quantum Hall edges.

Chapter 3

Classification of disordered Abelian edge states

The method described in the previous section greatly simplifies the analysis of a nonchiral edge of several condensates. In particular it allows us to determine in which regions of the space of velocity matrices V a particular impurity scattering operator $\exp(im_j\phi_j)$ is relevant, and hence determine the phase diagram of the edge state. We find that the edge of a single quantum Hall state can have different phases, with transitions between phases caused by changes in V. We also find that only a special class of edge states (principal hierarchy states) have enough $|K(\mathbf{m})| = 2$ impurity scattering operators to ensure that the conductivity is driven to the quantized value. The phase diagrams for this class of edge states show remarkable symmetries absent in the phase diagram of a general edge. In Chapter 4 these symmetries are shown to reflect broken symmetries of the K matrix.

All the examples are in the hierarchy of quantum Hall states. [5, 8] Hierarchical states have tridiagonal K matrices with all off-diagonal matrix elements equal to 1 and $K_{11} = l$ an odd integer, $K_{ii} = n_i$ even for $i = 2, \ldots, \dim K$. The matrix will often be given simply by its diagonal elements $(l, n_2, \ldots)$. The charge vector is $\mathbf{t} = (1, 0, \ldots, 0)$. The number of modes moving opposite the direction of the charge mode is equal to the number of negative elements on the main diagonal. States with all $|n_i| = 2$ are called principal states and are the most stable states at each level of the hierarchy.

First we study the edges of all hierarchy states at second level ($\dim K = 2$) and show that the principal hierarchy states are all similar to the $\nu = 2/3$ state studied by KFP. The states which are not principal have no relevant random operators and are thus unaffected by weak impurity scattering. In particular, for these states elastic impurity scattering alone is insufficient to give edge equilibration at low temperature.

A rich variety of behavior is possible for $\dim K = 3$ states, where the two neutral modes can move in the same direction (opposite the charge mode) or in opposite directions (cf. Table 3.1). The principal hierarchy state of $\dim K = n$ with all neutral modes in the same direction flows to an $SU(n) \times U(1)$ fixed point which is the only point where conductance is quantized. The charge mode satisfies a $U(1)$ Kac-Moody algebra, and the $n - 1$ neutral modes satisfy an $SU(n)$ Kac-Moody algebra.

Table 3.1: Possible nonchiral edge types for dim $K \leq 4$. For dim $K = 5$ there are no principal hierarchy states and for dim $K > 5$ no states at all which are T-stable and have neutral modes in both directions.

dim K	Mode directions (charge always $\rightarrow$)	Example	Boost parameters	Boost parameters with charge mode unmixed
2	$\begin{matrix}1\rightarrow\\1\leftarrow\end{matrix}$	$\nu = 2/3$	1	0
3	$\begin{matrix}2\rightarrow\\1\leftarrow\end{matrix}$	$\nu = 5/3$	2	1
	$\begin{matrix}1\rightarrow\\2\leftarrow\end{matrix}$	$\nu = 3/5$	2	0
4	$\begin{matrix}3\rightarrow\\1\leftarrow\end{matrix}$	$\nu = 12/31$	3	2
	$\begin{matrix}2\rightarrow\\2\leftarrow\end{matrix}$	$\nu = 12/17$	4	2
	$\begin{matrix}1\rightarrow\\3\rightarrow\end{matrix}$	$\nu = 4/7$	3	0

The highly symmetric phase diagram for the $SU(3)$ case is shown not to describe the simplest few non-principal states.

For the dim $K = 3$ case with neutral modes in both directions, conductance is quantized along a line in the phase diagram, and for the principal hierarchy states we find an infinite number of fixed points along this line corresponding to the infinite number of possibly relevant random operators. There are two different types of fixed points which correspond to two measurably different phases. A few results on the dim $K = 4$ cases are also presented. No principal hierarchy edges with dim $K > 4$ are topologically stable except those with all neutral modes in the same direction. [30]

3.1 Edges with dim $K = 2$

The K matrix in the hierarchy basis has the form

$$K = \begin{pmatrix} l & 1 \\ 1 & n \end{pmatrix}, \quad \mathbf{t} = (1, 0) \tag{3.1}$$

with l odd and n even. For the state to be nonchiral, $n < 0$. A quick calculation shows that if $\mathbf{m} = (m_1, m_2)$ is a charge-neutral $K(\mathbf{m}) = -2$ operator (there are no charge-neutral $K(\mathbf{m}) = 2$ operators), ${m_1}^2 = -2/n$ which has the solutions $m_1 = \pm 1$ if $n = -2$ and no integer solution otherwise. Hence for principal hierarchy states ($n = -2$) there is one complex-conjugate pair of possibly relevant operators labeled by $\mathbf{m} = \pm(1, -2)$, while for other hierarchy states there are no relevant random operators.

For a dim $K = 2$ state there is a single boost parameter p and a single value of this parameter that makes V charge-unmixed. It remains to show that this value is

exactly the value which gives the scattering operator $\exp(im_j\phi_j)$ its minimum scaling dimension $\Delta = 1$. In the basis of $\mathbf{t} = (1,0)$ and $\mathbf{m} = (1,-2)$, K^{-1} is diagonal with elements $(\nu, -2)$ and the scaling dimension matrix is

$$\begin{aligned} 2\Delta &= \begin{pmatrix} \sqrt{\nu} & 0 \\ 0 & \sqrt{2} \end{pmatrix} B^2 \begin{pmatrix} \sqrt{\nu} & 0 \\ 0 & \sqrt{2} \end{pmatrix} \\ &= \begin{pmatrix} \sqrt{\nu} & 0 \\ 0 & \sqrt{2} \end{pmatrix} \begin{pmatrix} \sqrt{1+p^2} & p \\ p & \sqrt{1+p^2} \end{pmatrix} \begin{pmatrix} \sqrt{\nu} & 0 \\ 0 & \sqrt{2} \end{pmatrix}. \end{aligned} \tag{3.2}$$

The conductance $2\Delta(t)$ is $\nu\sqrt{1+p^2}$ and the scaling dimension $\Delta(\mathbf{m})$ is $\sqrt{1+p^2}$. So $\Delta(\mathbf{m}) = 1$ exactly at the charge-unmixed point ($p = 0$), as required. The region of attraction of this fixed point is determined by the equation $\Delta(\mathbf{m}) \leq 3/2$ giving $-\sqrt{5}/2 \leq p \leq \sqrt{5}/2$ for $\nu = 2/3$.

Now we briefly outline the exact solution at the fixed point found by KFP which also shows the stability of the fixed point under RG transformations. Let the elementary fields in the basis defined above be the charge mode ϕ_ρ and neutral mode ϕ_σ. At the fixed point,

$$K = \begin{pmatrix} \nu & 0 \\ 0 & -2 \end{pmatrix}, \quad V = \begin{pmatrix} v_\rho & 0 \\ 0 & 2v_\sigma \end{pmatrix}. \tag{3.3}$$

The three operators $\partial_x\phi_\sigma, \exp(i\phi_\sigma), \exp(-i\phi_\sigma)$ all have scaling dimension 1 and satisfy an $SU(2)$ algebra. The action at the fixed point is

$$\begin{aligned} S &= \int_{x,\tau} [\frac{\nu\partial_x\phi_\rho}{4\pi}(i\partial_\tau + v_\rho\partial_x)\phi_\rho \\ &+ \frac{2\partial_x\phi_\sigma}{4\pi}(-i\partial_\tau + v_\sigma\partial_x)\phi_\sigma + (\xi(x)e^{i\phi_\sigma} + \text{h.c.})], \end{aligned} \tag{3.4}$$

obtained by substituting the fixed point K and V into (2.8,2.13). Now the fixed point action can be written in terms of a two-component Fermi field by introducing an auxiliary bosonic field χ which does not affect physical quantities: $\psi_1 = \exp[i(\chi + \phi_\sigma)/\sqrt{2}]$, $\psi_2 = \exp[i(\chi - \phi_\sigma)/\sqrt{2}]$. The clean part of the action is diagonal in the components while the impurity term becomes a hermitian combination of raising and lowering operators, $\psi_1^\dagger\psi_2$ and $\psi_2^\dagger\psi_1$, with random coefficients. The impurity term is then eliminated by a local $SU(2)$ gauge transformation which preserves the clean part of the action. The clean part of the action is just the action for free chiral fermions.

When the system is near but not at the fixed point, there is a weak coupling $V_{\rho\sigma}\partial_x\phi_\rho\partial_x\phi_\sigma$ between the charged and neutral modes. The scaling dimension of this term in the original action is 2 so the operator is marginal with a uniform coefficient. However, the $SU(2)$ rotation of $\partial_x\phi_\sigma$ gives this term a random coefficient and makes it irrelevant. According to this picture, once V falls into the basin of attraction of the fixed point, i.e., $|p| <= \sqrt{5}/2$ in (3.2), it flows to the fixed point $p = 0$ with K and V given by (3.3). Since the boost part of V is uniquely determined at the fixed point, many physical properties are uniquely determined, such as the conductance $\sigma = \nu e^2/h$. The same technique of fermionization followed by a gauge transformation solves the $SU(n) \times U(1)$ fixed point described below.

3.2 Three-branch edges, parallel neutral modes

Such edges have both neutral modes antiparallel to the charge mode (line 3 of Table 3.1). There is a single charge-unmixed point in the boost coordinates of Chapter 2. In the hierarchy representation such edges have K matrix $(l, -n_1, -n_2)$. The principal hierarchy edges of this type are $\nu = 3/5$ with $K = (1, -2, -2)$, $\nu = 3/11$ with $K = (3, -2, -2)$, and so forth. The principal hierarchy edges with n condensates and all neutral modes antiparallel to the charge mode have an $SU(n)$ symmetry ($n = \dim K$) in their K matrix $(l, -2, \ldots, -2)$, as first pointed out by Read. [21] The filling fraction is $\nu = n/(n(l+1) - 1)$. Kane and Fisher showed [19] that each of these edges has a fixed point with a charge field ϕ_ρ of dimension $\nu/2$ and a set of $n-1$ dimension 1 neutral fields ${\phi_\sigma}^i$ obeying an $SU(n)$ algebra. There are $n-1$ roots of $SU(n)$ which correspond to the $n-1$ operators $\partial_x {\phi_\sigma}^i$. Now we obtain the phase diagram for the $n = 3$ case, which is easily generalized to $n > 3$.

Any neutral operator $O_{\mathbf{m}}$ for these edges has negative $K(\mathbf{m})$ because all neutral modes travel opposite the direction of charge. There must be $(n^2-1)-(n-1) = n(n-1)$ operators with $K(\mathbf{m}) = -2$ in order to obtain the complete $SU(n)$ algebra (here $\mathbf{m}$ and $-\mathbf{m}$ are counted independently). For $\nu = 3/5$ this requires 6 such operators which in the hierarchy basis are labeled by $\mathbf{m} = \pm(0, 1, -2), \pm(1, -2, 1), \pm(1, -1, -1)$. Now the technique of Chapter 2 can be used to find when these operators become relevant and thus the region of attraction of the fixed point. For this case the procedure is described in detail for the sake of clarity; for subsequent cases some intermediate steps will be skipped.

The basis $\{(1,0,0),(0,1,-2),(2,-3,0)\}$ brings K^{-1} to diagonal form with elements $(3/5, -2, -6)$. The above six operators with $K(\mathbf{m}) = -2$ become $\pm(0,1,0)$, $\pm(0,1/2,1/2)$, $\pm(0,1/2,-1/2)$. At the fixed point point, V is also diagonal in the new basis $\{\phi_\rho, \phi_1, \phi_2\}$, and $\exp(i\phi_\rho)$ has scaling dimension $\nu/2 = 3/10$, $\exp(i\phi_1)$ scaling dimension 1, and $\exp(i\phi_2)$ scaling dimension 3, so that a neutral operator $\exp(im_1\phi_1 + im_2\phi_2)$ has scaling dimension ${m_1}^2 + 3{m_2}^2$. Let D be the diagonal matrix with diagonal elements $(\sqrt{3/5}, \sqrt{2}, \sqrt{6})$, which are the square roots of twice the scaling dimensions of the basis fields at the fixed point. Using the boost parameters (p_1, p_2), $\gamma = \sqrt{1 + {p_1}^2 + {p_2}^2}$, to parameterize non-diagonal V, we find the scaling dimension matrix in the basis $\{\phi_\rho, \phi_1, \phi_2\}$ is

$$2\Delta = D \begin{pmatrix} \gamma & p_1 & p_2 \\ p_1 & 1 + \frac{{p_1}^2(\gamma-1)}{{p_1}^2+{p_2}^2} & \frac{p_1 p_2(\gamma-1)}{{p_1}^2+{p_2}^2} \\ p_2 & \frac{p_1 p_2(\gamma-1)}{{p_1}^2+{p_2}^2} & 1 + \frac{{p_2}^2(\gamma-1)}{{p_1}^2+{p_2}^2} \end{pmatrix}^2 D \tag{3.5}$$

From this equation it is apparent that for $p_1 = p_2 = 0$ (a diagonal V in the new basis) all six operators have scaling dimension equal to 1, and this is the only charge-unmixed point since if p_i is nonzero the charge mode is partly mixed with the ith neutral mode. Fig. 3-1 shows the scaling dimension of the possibly relevant operators as functions of (p_1, p_2). The scaling dimension of $(0,1,0)$ is independent of p_2 so its contours are exactly vertical. Note that such a plot can be drawn without any information about the fixed point.

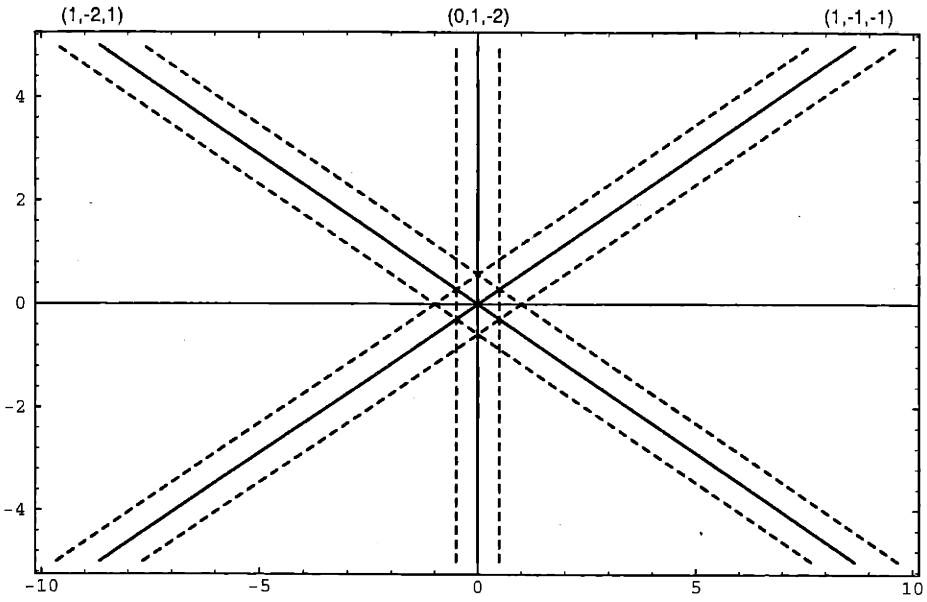

Figure 3-1: Plot of scaling dimension of the three $|K(\mathbf{m})| = 2$ operators for $\nu = 3/5$ edge as functions of boost parameters (p_1, p_2). The charge-unmixed point is the origin. Dashed lines indicate when operators become marginal ($\Delta(\mathbf{m}) = 3/2$) and solid lines indicate when operators become maximally relevant ($\Delta(\mathbf{m}) = 1$).

The qualitative interpretation of RG flows from Fig. 3-1 is quite simple and will be justified in Chapter 6. Each relevant scattering operator causes the velocity matrix to move to make the operator maximally relevant ($\Delta = 1$). If the starting velocity matrix is near the origin, all three operators are relevant and drive the velocity matrix to the origin, the only point at which all three are maximally relevant. The high symmetry of the graph reflects the $SU(3)$ symmetry of the fixed point. General three-species hierarchy states do not have this symmetry in the phase diagram and do not have enough $|K(\mathbf{m})| = -2$ operators to determine a unique fixed point. For example, the $\nu = 7/11$ state $(1, -2, -4)$ and the $\nu = 7/9$ state $(1, -4, -2)$ both have just one $K(\mathbf{m}) = -2$ operator which is maximally relevant along a line through the origin. The phase diagram is like Fig. 3-1 with only one line instead of three. Now the charge-unmixed point has an $SU(2)$ symmetry rather than an $SU(3)$ symmetry because only one impurity operator is relevant. It is not clear that the system flows to this point in the absence of long-range interactions, even if it starts near the charge-unmixed point, because other points along the maximally relevant line are also possible fixed points.

The $\nu = 15/19$ state $(1, -4, -4)$ has no $|K(\mathbf{m})| = 2$ operators at all so no stable fixed points result from the addition of weak disorder. States with no $|K(\mathbf{m})| = 2$ operators are predicted to have diverging equilibration lengths from impurity scattering as temperature is lowered since impurity scattering is never relevant. For the other type of third level hierarchical states, which have one neutral mode parallel to the charge mode, the same basic property is seen: only for principal hierarchy states are

there enough $|K(\mathbf{m})| = 2$ operators for impurity scattering to determine a discrete set of charge-unmixed fixed points.

3.3 Three-branch edges, antiparallel neutral modes

These edges have a line in the phase diagram along which the conductance is quantized, rather than a point as in the previous cases. For the principal hierarchy states, there are infinitely many $|K(\mathbf{m})| = 2$ operators, and these can be enumerated by a simple linear recursion relation. Examples are $\nu = 5/3$ with $K = (1, 2, -2)$, $\nu = 5/7$ with $K = (1, -2, 2)$, $\nu = 5/13$ with $K = (3, 2, -2)$, and $\nu = 5/17$ with $K = (3, -2, 2)$. These four edges all have the property that their $|K(\mathbf{m})| = 2$ operators $O_{\mathbf{m}}$ form a (vector) Fibonacci sequence: $\mathbf{m}_{n+1} = \mathbf{m}_n + \mathbf{m}_{n-1}$. The reason why these four edges have the same Fibonacci pattern is that their χLL theories have, up to a minus sign, the same neutral sector. Thus properties which depend only on neutral operators are shared by all states $K = (l, 2, -2)$ and $K = (l, -2, 2)$ independent of l. The familiar scalar Fibonacci sequence $(1, 1, 2, 3, 5, \ldots)$ has previously appeared in physics in growth models of phyllotaxis. Note that the property $\mathbf{m}_{n+1} = \mathbf{m}_n + \mathbf{m}_{n-1}$ is linear and hence independent of basis.

The $\nu = 5/3$ edge is convenient to study because of its $SL(3, Z)$ equivalence to the diagonal K matrix with elements $(1, 1, -3)$. The charge vector in this basis is $\mathbf{t} = (1, 1, 1)$. This gives the state a natural interpretation as a $\nu = 1/3$ gas of holes in two filled Landau levels. Also in this basis $K(m_1, m_2, m_3) = K(m_2, m_1, m_3)$. The $|K(\mathbf{m})| = 2$ operators in this theory are labeled by $\mathbf{m} = \pm(1, -1, 0)$, $\pm(1, 0, 3)$, $\pm(2, -1, 3)$, $\pm(3, -1, 6)$, $\pm(5, -2, 9), \ldots$ plus the same list with first and second elements exchanged. The sign of $K(\mathbf{m})$ alternates between terms in this sequence: $(1, -1, 0)$ has $K(\mathbf{m}) = 2$ (as befits hopping between two rightward-moving modes), $(1, 0, -3)$ has $K(\mathbf{m}) = -2$, and so forth. There is an important difference between $K(\mathbf{m}) = 2$ and $K(\mathbf{m}) = -2$ operators: $K(\mathbf{m}) = 2$ operators are maximally relevant along a line in the phase diagram, while $K(\mathbf{m}) = -2$ operators are maximally relevant at a single point. This happens for the same reason that the charge-unmixed region was a single point for edges with all neutral modes opposite the charge mode. In a basis with $\mathbf{m}$ an eigenvector, if there are no other eigenvectors with the same direction then every boost involves $\mathbf{m}$ and affects its scaling dimension. If there are other eigenvectors in the same direction, there is a nontrivial linear space of boosts which do not affect the scaling dimension of $O_{\mathbf{m}}$.

The scaling dimension of the first few $|K(\mathbf{m})| = 2$ operators for $\nu = 5/3$ are plotted in Fig. 3-2 as functions of boost parameters (p_n, p_c) according to

$$2\Delta = D' \begin{pmatrix} 1 + \frac{{p_c}^2(\gamma-1)}{{p_c}^2+{p_n}^2} & p_c & \frac{p_c p_n(\gamma-1)}{{p_c}^2+{p_n}^2} \\ p_c & \gamma & p_n \\ \frac{p_c p_n(\gamma-1)}{{p_c}^2+{p_n}^2} & p_n & 1 + \frac{{p_n}^2(\gamma-1)}{{p_c}^2+{p_n}^2} \end{pmatrix} D'. \tag{3.6}$$

This expression for Δ is in the basis $\mathbf{t} = (1, 1, 1)$, $\mathbf{m_1} = (1, -1, 0)$ and $\mathbf{m_2} = (1, 1, 6)$ in terms of the original basis. $\phi_\rho, \phi_1, \phi_2$ with $\phi_1 = (1, -1, 0), \phi_2 = (1, 1, 6)$ in terms of the original basis (where $K = (1, 1, -3)$). Let $\phi_\rho, \phi_1, \phi_2$ be the three boson fields in the

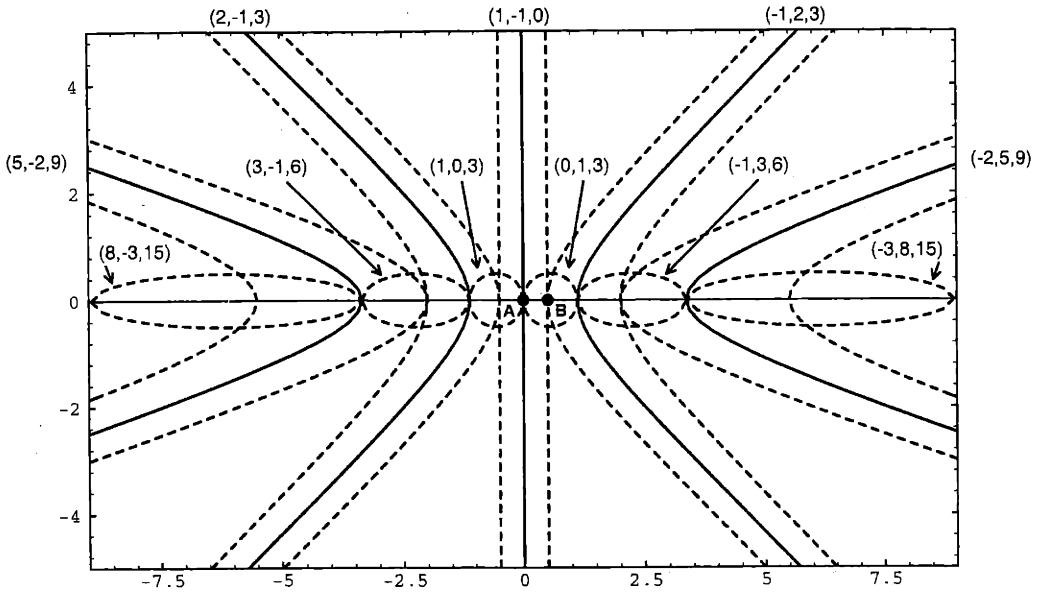

Figure 3-2: Plot of scaling dimension of the first 11 $|K(\mathbf{m})| = 2$ operators for $\nu = 5/3$ edge as functions of boost parameters (p_n, p_c). Dashed and solid lines are as in Fig. 1. The charge-unmixed line is the x-axis. At each point on the x-axis where one operator is maximally relevant, two other operators are marginal. Points A and B are examples of the two different types of fixed point.

new basis. The diagonal matrix D' has elements $(\sqrt{5/3}, \sqrt{2}, \sqrt{10})$. This expression for Δ is similar to (3.5) for $\nu = 3/5$ with two important differences: the scaling dimension of $e^{i\phi_2}$ is 5 rather than 3 at the fixed point $(p_n = p_c = 0)$, and the timelike row and column of the boost matrix correspond to ϕ_1 rather than ϕ_ρ, because now it is one of the neutral modes rather than the charge mode which has no other modes parallel to it.

In the coordinate space (p_n, p_c) (Fig. 3-2), $K(\mathbf{m}) = -2$ operators are relevant on compact regions and $K(\mathbf{m}) = 2$ operators on noncompact regions of the plane. The fixed points form lines and isolated points in Fig. 3-2, where one operator with $|K(\mathbf{m})| = 2$ is maximally relevant. For fixed points on the charge-unmixed line $p_c = 0$ (the x-axis in Fig. 3-2), there are two marginal operators with the opposite sign of $K(\mathbf{m})$. The x-coordinates of these special points are found by taking alternately the rational part and the coefficient of $\sqrt{5}$ in $((1 + \sqrt{5})/2)^n$. The theory at each of these fixed points is similar: in a basis bringing the maximally relevant operator $\exp(im_j\phi_j)$ to $\exp(i\phi_1)$, ϕ_2 can be chosen so that the marginal operators at the fixed point are $\exp(i(\phi_1 \pm \phi_2)/2)$, and $\exp(i\phi_2)$ has scaling dimension 5 rather than 3 in the $\nu = 3/5$ case. The scaling dimension of the marginal operators is then $(\Delta(\phi_1) + \Delta(\phi_2))/4 = (1 + 5)/4 = 3/2$ as required. The marginal operators cannot form an $SU(3)$ multiplet with the maximally relevant operator because their scaling dimensions are different. We have not been able to obtain an exact solution of this fixed point. Appendix B describes the leading-order RG flows along the charge-

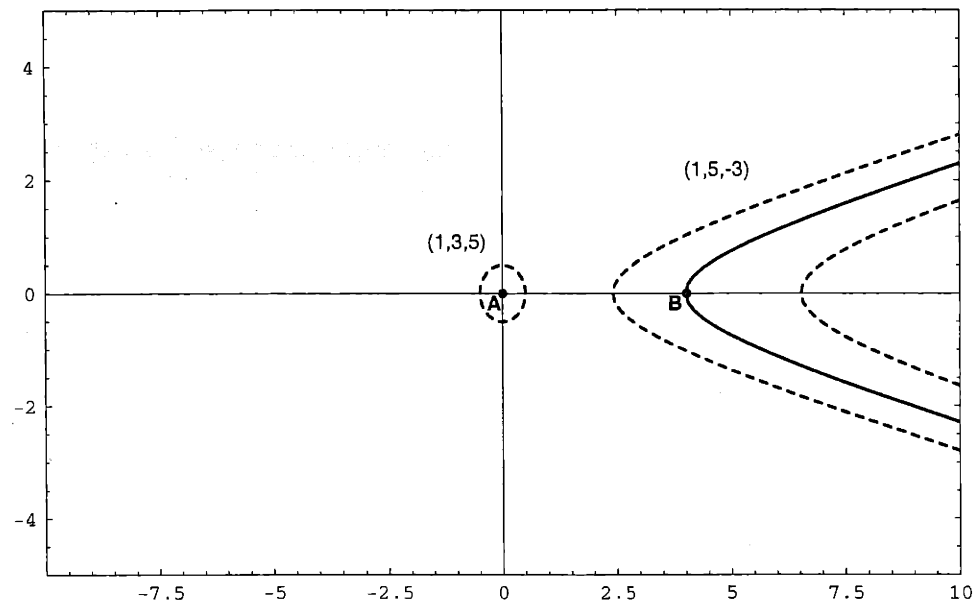

Figure 3-3: Plot of scaling dimension of the two $|K(\mathbf{m})| = 2$ operators for $\nu = 17/13$. Axes are as in Fig. 2. At most points on the charge-unmixed line, there are no relevant disorder operators. Points A and B are the two charge-unmixed fixed points.

unmixed line between points A and B and addresses the stability of the two types of fixed points. The reasons for the periodicity of Fig. 3-2 are discussed in Chapter 4.

Several dim $K = 3$ non-principal edges of this type (antiparallel neutral modes) were studied, and all were found to have too few $|K(\mathbf{m})| = 2$ operators for the system to flow to a quantized σ. The four hierarchical states with K matrices $(1,2,-4),(1,-2,4),(1,-4,2),(1,4,-2)$, $\nu = (9/5, 9/13, 9/11, 9/7)$ are not T-stable and have only one $|K(\mathbf{m})| = 2$ operator. The two states with K matrices $(1,4,-4)$ and $(1,-4,4)$, $\nu = (17/13, 17/21)$ each have a Fibonacci sequence of $|K(\mathbf{m})| = 4$ operators as well as one $K(\mathbf{m}) = 2$ and one $K(\mathbf{m}) = -2$ operator. The resulting phase diagram for $\nu = 17/13$ is shown in Fig. 3-3. Most velocity matrices near the charge-unmixed line are not affected by either $|K(\mathbf{m})| = 2$ operator. If the starting V matrix makes the $K(\mathbf{m}) = -2$ operator relevant, the system is driven by impurity scattering to the $(0,0)$ point on the charge-unmixed line. For starting points with this operator irrelevant, impurity scattering is insufficient to give edge equilibration at low temperatures.

Tuning the V matrix in the $\nu = 17/13$ state in principle allows a transition like the KFP transition for $\nu = 2/3$ to be observed, even if the system is always on the charge-unmixed line. Recall that for $\nu = 2/3$ the system has continuous, nonuniversal scaling dimensions as long as V is not too close to the charge-unmixed point. A Kosterlitz-Thouless type transition occurs when $|p| = \sqrt{5}/2$ in (3.2), and for $|p| <= \sqrt{5}/2$ the system has a universal scaling dimension matrix. In the $\nu = 17/13$ state, as V is tuned on the charge-unmixed line the scaling dimension matrix is continuously variable until one of the disorder operators becomes relevant; then V is driven to one

of the two fixed points, depending on which operator is relevant. Unfortunately the $\nu = 17/13$ state is expected to be quite difficult to observe, as it is a nonprincipal state with three condensates.

3.4 Edges with dim $K = 4$

The edges with all neutral modes opposite the charge mode have a single charge-unmixed point in the three-dimensional space of boost parameters, while the other two types of edges (Table 3.1) have a plane of charge-unmixed points. This section studies the charge-unmixed plane of four-condensate T-stable principal hierarchy states and finds a pattern with high symmetry and three different types of fixed points, two of which are exactly solvable. The states studied have $K = (l, 2, -2, 2)$ or $K = (l, -2, 2, -2)$, which were shown by Haldane to be the only dim $K = 4$ T-stable principal hierarchy states with neutral modes traveling in both directions. [30] Examples are $\nu = 12/31$ with $K = (3, -2, 2, -2)$ and $\nu = 12/17$ with $K = (1, 2, -2, 2)$.

These states behave differently away from the charge-unmixed plane but have identical structures on the plane, where each state has two neutral modes traveling in one direction and one neutral mode traveling in the opposite direction as well as a decoupled charge mode. For definiteness we study the $\nu = 12/17$ state, although all four states $\nu = 12/7$, $12/17$, $12/31$, $12/41$ have the same neutral sector. Each of these states has an infinite number of $|K(\mathbf{m})| = 2$ operators. For the $\nu = 12/17$ state, $K(\mathbf{m}) = 2$ operators are relevant on compact regions and $K(\mathbf{m}) = -2$ operators on noncompact regions of the plane. The maximally relevant points and contours are plotted in Fig. 3-4 as functions of boost parameters. The points and the intersections of the contours mark the position of fixed points. The points marked A, B, C are examples of the three different types of fixed points.

Plotting the marginal contours of the $|K(\mathbf{m})| = 2$ operators gives Fig. 3-5. Fig. 3-5a was obtained by choosing a basis to bring a point (A) of sixfold symmetry to the origin. There are also points of fourfold symmetry (B) as at the origin of Fig. 3-4 and Fig. 3-6, and points of twofold symmetry (C). There is no *a priori* reason to favor one type over the others. In the same way, Fig. 3-2 could have been drawn using a different basis to bring point B at the origin. The third type of fixed point has one operator maximally relevant and four marginal operators: these points are visible in Fig. 3-5 as the crossings of four marginal lines at the center of a marginal circle. These "double marginal" fixed points resemble the fixed points of the Fibonacci $\nu = 5/3$ state except that there are four rather than two marginal operators.

Fig. 3-6 shows a curious property of these four-condensate edges: the most relevant contours plotted as functions of "velocity" coordinates rather than "momenta" p_i in (2.30) turn out to be straight lines. Marginal contours are not straight lines. Mathematically the most relevant contours are straight because the square-root terms cancel in the equation $\Delta(\mathbf{m}) = 1$ which determines the contour, leaving only linear terms.

The complicated patterns in Fig. 3-5 have physical consequences. The sixfold symmetric points like A have three maximally relevant operators and an $SU(3)$ symmetry

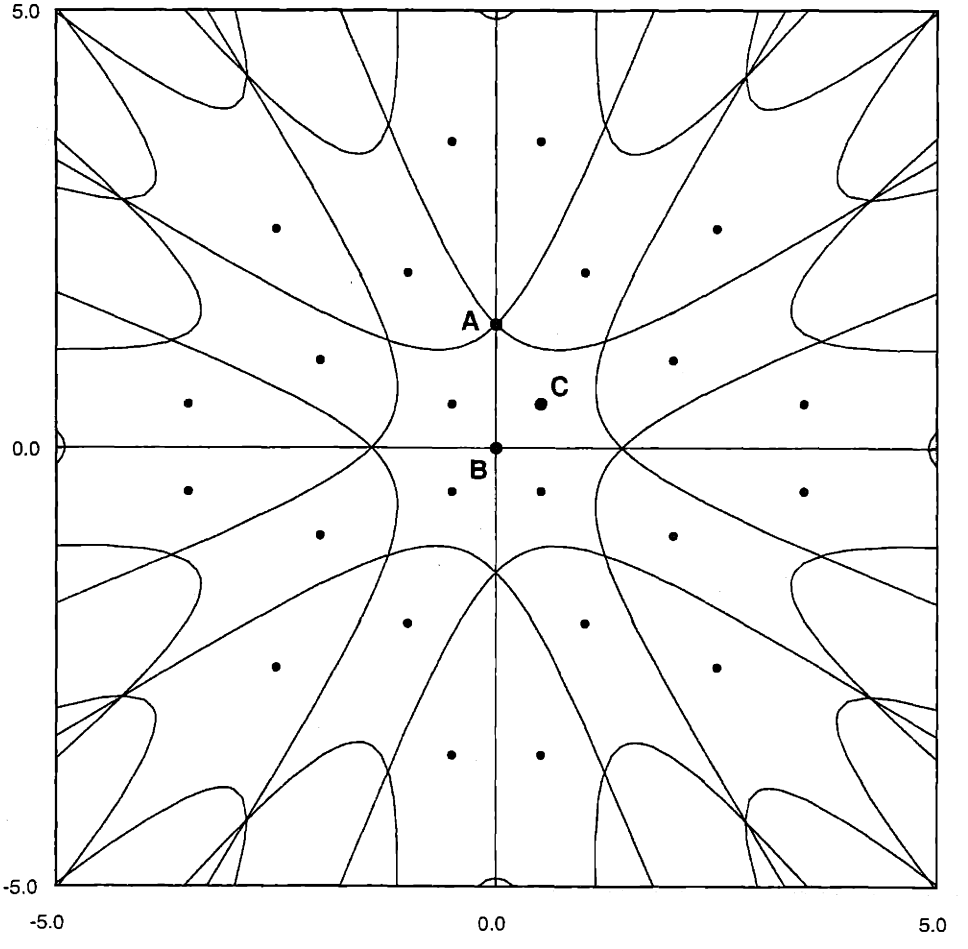

Figure 3-4: The most relevant contours of $|K(\mathbf{m})| = 2$ operators on the charge-unmixed plane of the $\nu = 12/17$ edge as functions of boost parameters (p_1, p_2). Points A, B, C are examples of the three different types of fixed points: A is an $SU(3)$ point, B an $SU(2) \times SU(2)$ point, and C a "double marginal" point. Dots are most relevant points of $K(\mathbf{m}) = 2$ operators, lines are most relevant lines of $K(\mathbf{m}) = -2$ operators.

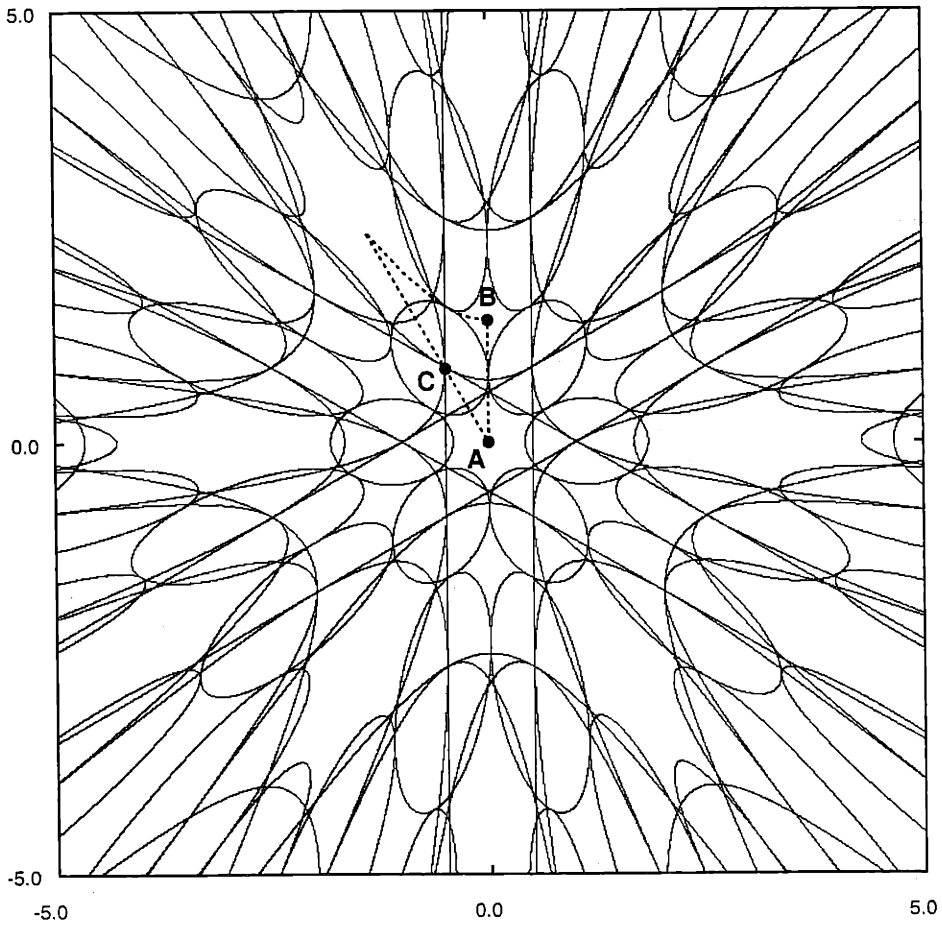

Figure 3-5: The *marginal* contours rather than the most relevant contours of $|K(\mathbf{m})| = 2$ operators for the $\nu = 12/17$ edge. The three types of fixed points are the $SU(3)$ point A at the origin, the $SU(2) \times SU(2)$ point B, and the "double marginal" point C. Here the basis was chosen to bring a point of type A to the origin, rather than B as in Fig. 4. The 75 operators shown are those most relevant at the origin.

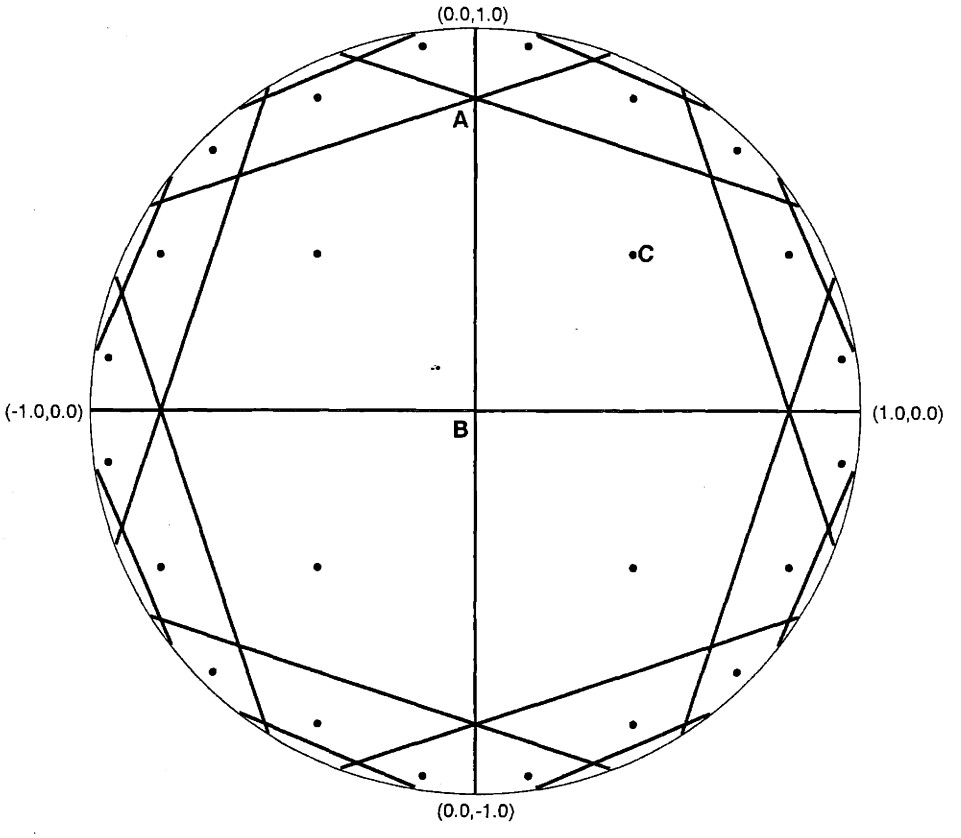

Figure 3-6: The most relevant contours of $|K(\mathbf{m})| = 2$ operators on the charge-unmixed plane of the $\nu = 12/17$ edge as functions of *"velocity"* coordinates (v_1, v_2). Plot is the same as Fig. 4 except that contours are shown as functions of "velocities" rather than "momenta". Only the 42 most relevant operators at the origin are shown because the full diagram becomes infinitely dense at the edge of the circle.

identical to that of the $\nu = 3/5$ fixed point previously studied. The fourfold symmetric points like B have two independent $|K(\mathbf{m})| = 2$ operators and an $SU(2) \times SU(2)$ symmetry which is similar to the $SU(2)$ symmetry of the $\nu = 2/3$ fixed point. The double marginal points like C are shown in Chapter 5 to give a different tunneling exponent than the roughly similar $\nu = 5/3$ fixed point. These different phases within the charge-unmixed plane are important even if quantum Hall systems necessarily have quantized conductance, as has been suggested. [30] Points A and B are stable and solvable but are shown in Chapter 5 to have different measurable properties, so a single FQH edge with impurities can have several physically different stable phases.

A complete understanding of these dim $K = 4$ states would require studying the three- or four-dimensional plots of which Fig. 3-5 is a section. One difference between the dim $K = 4$ states and the states studied up to this point is that there are small regions of the charge-unmixed plane on which only one operator is relevant, making it less certain that points not on the plane but near one of these regions would flow toward the plane as required for robust quantization. The dashed line between A and B in Fig. 3-5 passes through one such region. Some experimental properties of the dim $K = 4$ states are discussed in Section V.

Chapter 4

Symmetry restoration by disorder

This chapter discusses the effects of impurity scattering on the symmetries in the χLL theories of various edges. The restoration of symmetry by impurity scattering will be shown to explain the patterns in the phase diagrams found in Chapter 3. The χLL theory of a quantum Hall edge contains two matrices K and V and a charge vector $\mathbf{t}$ as described in Chapter 2. The integer matrix K may admit discrete symmetries, which are described by integer matrices M invertible over the integers with

$$M^{\mathrm{T}}KM = K, \quad M^{\mathrm{T}}\mathbf{t} = \mathbf{t}. \tag{4.1}$$

Most velocity matrices V do not have such symmetries. Thus a symmetry possessed by K is in general broken by the V terms in the χLL action.

One result of KFP is that impurity scattering can drive the velocity matrix to a fixed point where all the symmetries of K are symmetries of the full theory. In this chapter we show that, for the edges with infinitely many fixed points found in Chapter 3, impurity scattering sometimes restores some but not all of the symmetry of the K matrix. Because of this broken symmetry, the different fixed points are like spin-up and spin-down fixed points for an Ising ferromagnet below the transition temperature: the Ising fixed points are carried into each other by spin rotation, which is a symmetry of the starting Hamiltonian but not of the fixed points. The infinitely many impurity fixed points are carried into each other by symmetries of K which are not symmetries of V at the fixed points. The broken-symmetry structure can be very rich, as in the case of the $\nu = 12/17$ state, which has three different types of fixed points, each breaking different symmetries of K.

The matrix M in (4.1) gives a transformation $\phi_i = M_{ij}\tilde{\phi}_j$ of the bosonic fields ϕ_i under which the action is form-invariant. The discrete symmetry transformation M can reflect an underlying continuous symmetry, as in the theory of the $\nu = 2/3, 3/5, 4/7, \ldots$ states, where the discrete symmetries of the K matrix reflect an $SU(n)$ symmetry of the field theory, $n = \dim K$. [21] It is easily seen that the symmetries M of a given K matrix form a group with matrix multiplication as the group product. The key difference between edges with a single impurity fixed point and edges with infinitely many fixed points is that the the former have finite symmetry groups, while the latter have infinite symmetry groups. As examples of the two types, we find the symmetries of the $\nu = 3/5$ (finite) and $\nu = 5/3$ (infinite)

edges. The results presented for $\nu = 5/3$ also apply to the other Fibonacci-type edges: $\nu = 5/7$, $\nu = 5/13$, $\nu = 5/17$. Chapter 5 shows that the two different types of fixed points in the $\nu = 5/3$ edge have different experimentally observable properties. The $\nu = 12/17$ edge (likewise $\nu = 12/7$, $\nu = 12/31$, $\nu = 12/41$) is shown to have three different types of fixed points related by a complicated symmetry group.

The $\nu = 3/5$ state in the hierarchy basis has

$$K = \begin{pmatrix} 1 & 1 & 0 \\ 1 & -2 & 1 \\ 0 & 1 & -2 \end{pmatrix}, \quad \mathbf{t} = (1, 0, 0). \tag{4.2}$$

One way to find the symmetries of K is to start with transformations W bringing K to diagonal form and preserving $\mathbf{t}$, as were used in Chapter 3 to obtain phase diagrams. Let D be the matrix with diagonal elements $(1, -1, 1)$. If $W^{\mathrm{T}}KW$ is diagonal, then $M = WDW^{-1}$ is a symmetry of K with the property that $M^2 = I$, the identity. The effect of M is to use W to go to independent fields $\tilde{\phi}_i$, change the sign of one field, and then return to the original fields. The problem is that M is only integral for some choices of W. One hopes that by choosing different matrices W_i, one can find enough integral M_i to generate the entire group of symmetries. The M_i are improper since $\det M_i = -1$; the proper symmetry group contains only products of even numbers of M_i.

For $\nu = 3/5$ two generators found using this trick are

$$x = \begin{pmatrix} 1 & 0 & 0 \\ 0 & 1 & 0 \\ 0 & 1 & -1 \end{pmatrix}, \quad y = \begin{pmatrix} 1 & 0 & 0 \\ 1 & -1 & 1 \\ 0 & 0 & 1 \end{pmatrix}. \tag{4.3}$$

The element xy is a proper symmetry which generates a 120° rotation of Fig. 3-1, and as expected $(xy)^3 = I$. The symmetry group has six elements: three proper elements $\{I, xy, (xy)^2 = y^{-1}x^{-1}\}$ and three improper elements $\{x, y, xyx\}$. It is easy to check that these six elements are the full symmetry group G. The velocity matrix at the fixed point also has all of these symmetries. (For the sake of exactness, recall that the origin of Fig. 3-1 represents the set of all velocity matrices with certain values of the boost parameters, as described in Chapter 2. There is an additional RG flow of the other parameters in V which makes the two neutral modes have the same velocity. Without this additional flow, only the boost part of the velocity matrix would have the symmetry.)

One simple consequence of the symmetry at the $\nu = 3/5$ fixed point is that the V-dependent scaling dimension matrix Δ, which determines the scaling dimension of the operator $O_{\mathbf{m}} = \exp(im_j\phi_j)$ according to $\Delta(\mathbf{m}) = m_i\Delta_{ij}m_j$, has the same symmetries as K^{-1}: $x\Delta x^{\mathrm{T}} = y\Delta y^{\mathrm{T}} = \Delta$. Note that Δ transforms like K^{-1} rather than K so its symmetries are transposed symmetries of K. At the fixed point Δ is invariant under all symmetries of K^{-1} for any edge with all neutral modes moving opposite the charge mode, as now shown. These edges have fixed points where K^{-1} and Δ are both diagonal in some integral basis with first basis vector $\mathbf{e}_1 = \mathbf{t}$. K^{-1} has all diagonal entries negative except for the first, and $2\Delta = |K^{-1}|$ has all diagonal

entries positive. Any vector $\mathbf{m}$ with charge $q = \mathbf{t}K^{-1}\mathbf{m}$ can be written as $\mathbf{m} = a\mathbf{t}+\mathbf{n}$, where $\mathbf{n}$ has charge zero ($\mathbf{t}K^{-1}\mathbf{n} = 0$) and $a = \mathbf{t}K^{-1}\mathbf{m}/\mathbf{t}K^{-1}\mathbf{t} = q\nu^{-1}$. Now with $K(\mathbf{x}) = \mathbf{x}K^{-1}\mathbf{x}$,

$$2\Delta(\mathbf{m}) = 2\Delta(a\mathbf{t}+\mathbf{n}) = a^2K(\mathbf{t}) - K(\mathbf{n}) = \frac{q^2}{\nu} - K(\mathbf{n}). \tag{4.4}$$

Let $\mathbf{m}' = M\mathbf{m}$ be the image of $\mathbf{m}$ under a symmetry of K^{-1}. Then $2\Delta(\mathbf{m}') = q^2/\nu - K(\mathbf{n}') = q^2/\nu - K(\mathbf{n}) = 2\Delta(\mathbf{m})$, since $\mathbf{n}' = M\mathbf{n}$. Thus Δ has every symmetry of K^{-1} for any charge-unmixed fixed point in a state with all neutral modes opposite the charge mode. Broken-symmetry fixed points therefore appear only in states with neutral modes in both directions. The same argument gives that at any charge-unmixed fixed point where K and Δ are diagonal,

$$2\Delta(\mathbf{m}) \geq q^2/\nu \tag{4.5}$$

where q is the charge of $\mathbf{m}$. This inequality appears in the discussion of quasiparticles in Chapter 5.

The same technique can be used to find the symmetries of K for the $\nu = 5/3$ Fibonacci-type edge shown in Fig. 3-2. Two elements of the symmetry group are found from changing the sign of $(1,-1,0)$, which corresponds to reflecting $x \leftrightarrow -x$ in Fig. 3-2, and from changing the sign of $(0,1,3)$, which corresponds to reflecting the x-axis through the point B. The resulting matrices are

$$u = \begin{pmatrix} 0 & 1 & 0 \\ 1 & 0 & 0 \\ 0 & 0 & 1 \end{pmatrix}, \quad v = \begin{pmatrix} 1 & 0 & 0 \\ 0 & 2 & 3 \\ 0 & -1 & -2 \end{pmatrix}. \tag{4.6}$$

The difference between this case and the previous one appears when u and v are multiplied to obtain other group elements. The element $w \equiv uv$ is a proper symmetry of infinite order: $I, w, w^2, \ldots$ are all different matrices and all symmetries of K. Each application of w corresponds to translating Fig. 3-2 horizontally. The Fibonacci property $\mathbf{m}_{n+1} = \mathbf{m}_n + \mathbf{m}_{n-1}$ mentioned earlier is a consequence of symmetry under w. The powers of w and its inverse give the entire proper symmetry group, which is isomorphic to Z^+, the group of integers under addition. The full symmetry group is isomorphic to the semidirect product of Z^+ and the binary group $\{1,-1\}$.

At each fixed point Δ has a much smaller symmetry group than K. The only symmetry of Δ at a fixed point other than I is the unique reflection which changes the sign of the operator maximally relevant at the fixed point. For example, u is a symmetry of point A ($u\Delta_A u^{\mathrm{T}} = \Delta_A$) but v is not. It is apparent from Fig. 3-2 that some symmetry of K^{-1} is broken at each fixed point because neutral operators $\mathbf{m}_i$ with the same minimum scaling dimensions $K(\mathbf{m}_i) = 2$ have different actual scaling dimensions $\Delta(\mathbf{m}_i)$. The matrix $w = uv$ is a symmetry of no fixed point, but its effect is to move the system from one fixed point to the next: $w\Delta_i w^{\mathrm{T}} = \Delta_{i+1}$, where i labels fixed points *of the same type*, i.e., w never takes maximally relevant points of $K(\mathbf{m}) = -2$ operators to maximally relevant points of $K(\mathbf{m}) = 2$ operators, since w preserves K. Thus in Fig. 3-2 there is no symmetry taking point A to point B.

In Chapter 5 it is shown that the two different types of fixed points have different experimentally measurable properties.

By applying symmetries of K, the boost part of any velocity matrix can be made to lie in the region bounded by the maximally relevant lines of $(1,-1,0)$ and $(-1,2,3)$ in Fig. 3-2. This region is a "fundamental period" of the symmetries of K. However, different fixed points of the same type may correspond to experimentally different phases, even though they are related by a discrete symmetry and will have the same scaling dimensions, etc. The reason is that an experimental probe will couple nonuniversally to some combination of the original fields ϕ_i, which after applying a symmetry of K will be some different combination of the redefined fields ϕ_i'. Experiments will measure different prefactors for various quantities at different fixed points of the same type. Hence even if only points of type A are found to be stable for $\nu = 5/3$, for example, there would still be multiple edge phases with true transitions at phase boundaries. This is not true if there are *continuous* rather than discrete symmetries of the χLL system relating fixed points of the same type, since then all the fixed points are continuously connected. Such a situation occurs if the discrete symmetries of the bosonized (K,V) theory arise from continuous symmetries of the underlying fermionic Lagrangian. Stable fixed points of different types always give different phases.

Multiple-condensate edges have quite complicated symmetry groups, and it is an interesting mathematical exercise to classify these groups in terms of familiar finitely generated groups. The symmetry group of $\nu = 3/5$ found above is D_3, the triangular dihedral group, for example. Principal hierarchy states with all neutral modes opposite the charge mode have finite symmetry groups, and principal hierarchy states with neutral modes in both directions have infinite symmetry groups. Non-principal hierarchy states often have no nontrivial symmetries. Here we will be content to mention some results on the four-condensate principal hierarchy states discussed previously. The four-condensate states $\nu = 12/7,\ 12/17,\ 12/31,\ 12/41$ have three distinct types of fixed points (A, B, C in Fig. 3-5a-c). The phase diagram has sixfold symmetry about point A, fourfold symmetry about point B, and twofold symmetry about point C. It seems likely that these point symmetries are sufficient to generate the full symmetry group, which at point A is broken to a six-element subgroup and similarly for B and C. A fundamental period of the symmetry group is drawn in Fig. 3-5a. A set of generating matrices for $\nu = 12/17$ in the hierarchy basis is then

$$m_1 = \begin{pmatrix} 1 & 0 & 0 & 0 \\ 0 & 1 & 0 & 0 \\ 0 & 0 & 1 & 0 \\ 0 & 0 & 1 & -1 \end{pmatrix}, \quad m_2 = \begin{pmatrix} 1 & 0 & 0 & 0 \\ 1 & -1 & 1 & 0 \\ 0 & 0 & 1 & 0 \\ 0 & 0 & 0 & 1 \end{pmatrix},$$
$$m_3 = \begin{pmatrix} 1 & 0 & 0 & 0 \\ 0 & 1 & 0 & 0 \\ 0 & -1 & -1 & -1 \\ 0 & 0 & 0 & 1 \end{pmatrix}. \tag{4.7}$$

These m_i were obtained with the sign-flip procedure used above: for each i $\det m_i = -1$ and ${m_i}^2 = I$. The symmetries of point B are generated by m_1 and m_2,

which commute, and m_3 gives a rotation by π around point C. A sample element of order 3 is $m_1m_3m_2m_3$, and an element of infinite order is m_3m_2.

Chapter 5

Experimental consequences–weak tunneling

The conductance and other experimental properties of a quantum Hall state are affected by disorder according to the RG flows described in the preceding chapters. One important feature of the three- and four-condensate principal hierarchy states is that they can have multiple phases within the charge-unmixed subset of velocity matrices. This is different from the situation in two-condensate states and for any state with all neutral modes moving in the same direction, where the quantization of conductance occurs at a single point in boost-parameter space and no phase transitions are predicted within the charge-unmixed subset of velocity matrices.

In this chapter we first consider the $\nu = 5/3$ state and argue that experimental setups are likely to be close to point B in the phase diagram, Fig. 3-2. The $\nu = 5/7$ state probably offers the best chance for an experimentally accessible phase transition. We calculate electron and quasiparticle tunneling exponents for the different types of fixed points found in the preceding chapters and show that different phases at the same filling fraction have different temperature dependences of electron tunneling through a barrier.

The $\nu = 5/3$ state seen experimentally is likely to contain both up spins and down spins: it consists of a $\nu = 1$ state of spin-up electrons and a $\nu = 2/3$ state of spin-down electrons, or vice versa. The fully polarized state has higher energy than the mixed-spin state because some electrons lie in the second Landau level rather than the first, costing energy proportional to $\hbar\omega_c$, ω_c the cyclotron frequency. This dominates the savings in the Zeeman and Coulomb energies from polarizing the spins, at least in GaAs, where the effective g-factor and Zeeman energy are small. The fully polarized state might appear in other materials with larger g, or in tilted-field configurations which allow the Zeeman energy to be increased with ω_c constant.

In the mixed-spin $\nu = 5/3$ state, scattering between up and down spins is expected to be very weak unless magnetic impurities are added. Thus the spin-up and spin-down components are largely independent. Independent $\nu = 1$ and $\nu = 2/3$ liquids are described by point B in Fig. 3-2 because the velocity matrix which has no interactions

between the two liquids gives the scaling dimension matrix

$$2\Delta = \begin{pmatrix} 2\Delta_1 & 0 & 0 \\ 0 & & 2\Delta_{2/3} \\ 0 & & \end{pmatrix} = \begin{pmatrix} 1 & 0 & 0 \\ 0 & 2/3 & 0 \\ 0 & 0 & 2 \end{pmatrix}, \quad \mathbf{t} = (1,1,0) \tag{5.1}$$

which is brought by a change of basis to point B. It is shown below that point B has the same low-temperature tunneling conductance exponent $G \sim T^0$ as a combination of a $\nu = 1$ state ($G \sim T^0$) and $\nu = 2/3$ state ($G \sim T^2$) would have. The fixed point A is not easily interpreted as a sum of two independent edges. At A the operator $(1,-1,0)$ which hops charge between the two right-moving modes is maximally relevant, suggesting that in this phase the $\nu = 1/3$ left-moving mode pairs with a bound, $SU(2)$ symmetric combination of right-moving modes rather than with just one right-moving mode as at point B.

The $\nu = 5/7$ ground state is spin-polarized and its two edge fixed points may be more easily found experimentally than those of the $\nu = 5/3$ state. The $\nu = 5/7$ state is equivalent in K-matrix terms to a $\nu = 2/7$ gas of holes in a $\nu = 1$ state: $K_h = M^{\mathrm{T}} K' M, M^{\mathrm{T}}\mathbf{t}' = \mathbf{t}$, with $\mathbf{t}' = (1,1,0)$, $\mathbf{t} = (1,0,0)$,

$$\begin{aligned} K_h &= \begin{pmatrix} 1 & 1 & 0 \\ 1 & -2 & 1 \\ 0 & 1 & 2 \end{pmatrix}, \\ K' &= \begin{pmatrix} K_1 & 0 & 0 \\ 0 & & -K_{2/7} \\ 0 & & \end{pmatrix} = \begin{pmatrix} 1 & 0 & 0 \\ 0 & -3 & -1 \\ 0 & -1 & 2 \end{pmatrix}, \\ M &= \begin{pmatrix} 1 & 1 & 0 \\ 0 & -1 & 0 \\ 0 & 0 & 1 \end{pmatrix}. \end{aligned} \tag{5.2}$$

However, the V matrix $V_{1-2/7}$ with no interactions between the $\nu = 2/7$ holes and $\nu = 1$ electrons gives a conductance (in units of e^2/h) $\sigma = 9/7 = 1 + 2/7$ rather than $\sigma = 5/7 = 1 - 2/7$. This happens for exactly the same reason that a $\nu = 2/3$ state with velocity matrix describing $\nu = 1/3$ holes not interacting with $\nu = 1$ electrons gives a conductance $\sigma = 4/3$: the quantized value of conductance is only obtained if the edge equilibrates and all charged eigenmodes move in the same direction.

It is not difficult to find the point represented by $V_{1-2/7}$ in the $\nu = 5/7$ version of Fig. 3-2 (which looks similar but with some stretching along the y-axis): it lies on the y-axis with boost coordinates $(0, \sqrt{2/5})$. This is not a fixed point in the presence of disorder, and we expect the system to flow to a fixed point of type A or type B. Unlike in the $\nu = 5/3$ case, where type B was easily interpreted as a $\nu = 1$ state plus a $\nu = 2/3$ state with no interactions between the two, for $\nu = 5/7$ we have no simple interpretation of either phase as two independent subedges. The K matrix K_h is inequivalent to a combination of $\nu = 2/3$ and $\nu = 1/21$ because $\det K_h \neq (\det K_{2/3})(\det K_{1/21})$, so no invertible integral basis change can relate the two. Below we show that the A and B phases can be distinguished experimentally, so that measurements of a $\nu = 5/7$ sample edge would allow its phase to be determined.

Then changes in the V matrix (from changes in the gate voltages, e.g.) might drive a new type of impurity phase transition.

Before calculating tunneling properties for the various fixed points, we would like to suggest briefly an experimental approach to edge impurity scattering based on the existence of spin-polarized and spin-singlet states at $\nu = 2/3$. At $\nu = 2/3$ there is an unpolarized spin-singlet state with the same K matrix and charge vector as the well-known spin-polarized state. The polarized state is naturally interpreted as the particle-hole conjugate of the Laughlin $\nu = 1/3$ state [2], while the unpolarized state is *not* the double-layer state consisting of a spin-up $\nu = 1/3$ state and a spin-down $\nu = 1/3$ state, which has an inequivalent K matrix. The unpolarized state can be studied in tilted-spin experiments such as those of Eisenstein *et al.* [31] and appears because of the relatively low Zeeman energy in GaAs as suggested by Halperin. [32] The KFP treatment should be just as valid for the unpolarized edge as for the polarized edge because they have the same K matrix. The unpolarized edge has an exact $SU(2)$ symmetry if the Zeeman energy is ignored, however, and this symmetry has physical consequences.

Numerical results on the unpolarized edge show that at low energy there are two branches of excitations, one spin-singlet charge branch and one spin branch described by the $SU(2)$ Kac-Moody algebra. [25] This is the structure found at the KFP fixed point and different from the numerical results on the clean polarized edge, which indicate two spatially separated subedges with no special symmetry. [24, 14] It seems logical that the physical requirement of $SU(2)$ spin symmetry of the unpolarized edge forces the system to the KFP fixed point even in the absence of disorder, assuming the "hidden" $SU(2)$ symmetry is only found at the fixed point. The $SU(2)$ structure of the unpolarized edge is found in a small system (hence without RG flows) for both Coulomb and short-range interactions. The separation of the $\nu = 2/3$ edge into charge modes and neutral modes can thus be caused by (i) an exactly charge-unmixed velocity matrix, (ii) an unbroken $SU(2)$ symmetry, or (iii) random impurities. The possibility that impurities affect the polarized edge but not the unpolarized edge suggests that measurements of the edge equilibration length and tunneling conductance across the topological phase transition [33] between the two may be illuminating.

In FQH states the tunneling conductance through a point constriction in a Hall bar decreases with decreasing temperature. In the integer effect this conductance is temperature-independent. The physical electron operator is a superposition of all charge-e fermionic operators, and the low-temperature conductance is determined by the scaling dimension Δ_e of the most relevant such operator according to [34, 35]

$$G(T) \approx t^2 T^{2(2\Delta_e - 1)} \tag{5.3}$$

where t is the amplitude for the dominant tunneling process. Different fixed points in the same FQH state can have different Δ_e and different tunneling exponents. These exponents can be calculated for the marginal-type fixed points even though the electron dynamics at these points is unclear. All fixed points of the same type have the same scaling exponents but are expected to have measurably different prefactors as described in Chapter 4.

Charge-e operators $\mathbf{m}$ have $t_i K_{ij}^{-1} m_j = 1$ and scaling dimension $\Delta_e = m_i \Delta_{ij} m_j$ where Δ is the same symmetric matrix calculated in Chapter 3. Since Δ is known at each fixed point, it is simple to search for the most relevant charge-e operator. The $SU(n)$ fixed points found by Kane and Fisher for the $\nu = n/(2n-1)$ states have $2\Delta_e = 3 - 2n^{-1}$ and tunneling exponent

$$G(T) \approx t^2 T^\alpha, \quad \alpha = 4 - 4n^{-1}. \tag{5.4}$$

In Table 5.1 we list the low-temperature conductance behavior for each of the fixed points found in Chapter 3. Note that corresponding fixed points in states with the same neutral sector, such as $\nu = 5/3$ and $\nu = 5/7$, can have different tunneling exponents because the charge sectors of the two edge theories are different. The Fibonacci-type states have two possible values of the low-temperature tunneling conductance exponent, so that there is a real physical difference between the A and B phases.

The most interesting property of the results in Table 5.1 is illustrated in Fig. 5-1. For each principal hierarchy state with neutral modes in both directions, there are multiple phases with different values of the tunneling exponent. However, one phase always lies on the line obtained by the composite-fermion approach for compressible states. [20] Thus there is an interesting agreement between the chiral-Luttinger-liquid model for incompressible states and the composite-fermion result for compressible states, suggesting that similar physics is captured by the two approaches.

The level four states studied ($\nu = 12/7$, $12/17$, $12/31$, $12/41$) have three different tunneling exponents corresponding to the three different types of fixed points. For example, in the $\nu = 12/17$ state the $SU(3)$ fixed points have $\Delta_e = 7/6$ and $\alpha = 8/3$ as appear in the $SU(3)$ fixed point of the $\nu = 3/5$ state. The $SU(2) \times SU(2)$ fixed point is the same as the $SU(2)$ fixed point for $\nu = 2/3$ except that there are two charge-e operators of minimal scaling dimension rather than one. The double marginal fixed point has an operator with $\Delta_e = 11/12$ so $\alpha = 5/3$. So the three different fixed points have three different values of α: $5/3$ for the double marginal points, 2 for the $SU(2) \times SU(2)$ points, and $8/3$ for the $SU(3)$ fixed points.

Other tunneling experiments are sensitive to the most relevant quasiparticle operator at a fixed point, rather than the most relevant electron operator. One experiment sensitive to the quasiparticle scaling dimension is tunneling through a slight constriction rather than through a deep constriction as described above. [19] We have calculated the scaling dimension of the most relevant quasiparticle operators for the various fixed points. No simple patterns are observed: often two or more quasiparticle operators have nearly the same minimum scaling dimension, and the charge of the most relevant quasiparticle operator varies among different fixed points of the same edge. As an example, in the $12/17$ edge the most relevant quasiparticles at the different fixed points are: $2\Delta = 5/17$, $q = 3e/17$ at the $SU(3)$ points, $2\Delta = 6/17$, $q = 2e/17$ at the $SU(2)$ points, and $2\Delta = 43/102$, $q = e/17$ at the double-marginal points. Typically the most relevant quasiparticles have small charges, as expected from the inequality (4.5).

Time-domain experiments have so far not resolved the neutral modes in nonchiral edge states, [36] but in principle a perturbation at one contact on a sample edge

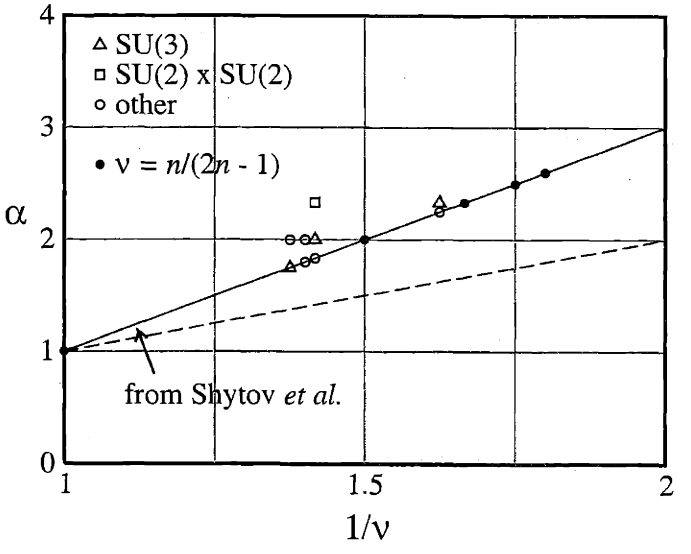

Figure 5-1: The tunneling exponent $I \propto V^{\alpha}$ for quantum Hall states in the range $1/2 < \nu < 1$. The solid line is the prediction of the compressible-state theory of Shytov, Levitov, and Halperin[20] for infinitely many channels. The dotted line is $\alpha = 1/\nu$. Solid circles are the main-sequence edges with one phase per edge, and other shapes describe fixed points of various symmetry classes in edges with multiple phases.[37] The states shown are all principal hierarchy states up to 4th level: the main-sequence states plus $\nu = 8/11, 5/7, 12/17, 8/13$.

Table 5.1: Low-temperature tunneling conductance behavior $G \sim T^{\alpha}$ for hierarchical daughter states of $\nu = 1$ (top) and $\nu = 1/3$. Only "charge-unmixed" phases (those with quantized conductance, or alternately those which can occur with long-range interactions) are shown. The different fixed points A and B for the Fibonacci-type states correspond to the labeling in Fig. 2. The phases $\nu = 12/7, 12/17, 12/31, 12/41$ have fixed lines L and three types of fixed point with $SU(2) \times SU(2)$ symmetry (abbreviated $SU(2)$ in the table), $SU(3)$ symmetry, or two independent marginal operators (DM). The tunneling exponent on the fixed lines L is nonuniversal. Note that each exponent in the lower table is given by $\alpha_{1/3} = 4 + \alpha_1$ where α_1 is the exponent of the state in the upper table at the same position in the hierarchy. The pattern continues to lower filling fractions: daughter states of $\nu = 1/5$ have filling fractions between $1/8 < \nu < 1/4$ and tunneling exponents $8 \leq \alpha \leq 12$, e.g.

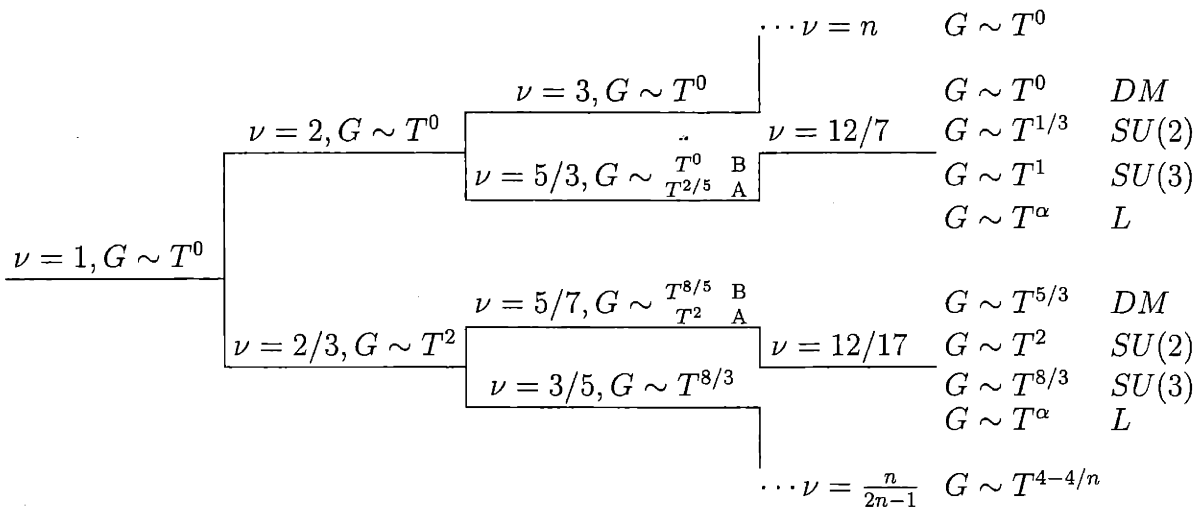

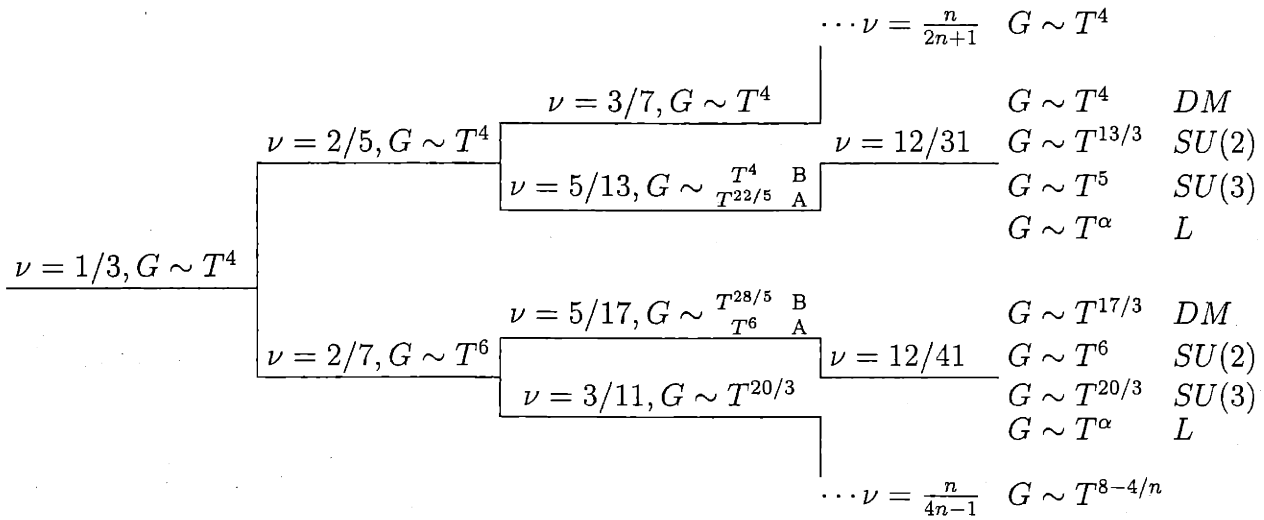

should excite propagating charged and neutral modes observable at another contact. Such an experiment might reveal whether the neutral modes in the Fibonacci-type states $\nu = 5/3, 5/7, 5/13, 5/17$ propagate or are localized. The measurement of edge equilibration lengths might also give interesting results: measurements on the edge of the $\nu = 4/5$ edge, which has no $|K(\mathbf{m})| = 2$ operators and hence no KFP-type instability, could show another type of equilibration mechanism (such as inelastic scattering from phonons) with a different temperature dependence.

Chapter 6

Renormalization group flows in edges with random hopping

In the χLL theory, the edge of a bulk QH state with n condensates is described by two symmetric $n \times n$ matrices, K and V. The integer matrix K is determined by the bulk QH state and is the same for all samples of a given edge. The positive matrix V contains non-universal velocities and interaction strengths which are expected to vary from sample to sample. In this chapter, we study the RG flow of the V matrix in the presence of impurity scattering toward fixed points [18, 19, 37] which describe an equilibrated edge..

The RG calculation is given in some detail in an appendix because there are several new features not present in similar treatments of the 2D classical XY model [49, 50] and 2D melting, [51] as well as 1D disordered quantum electrons. [26] Calculations on 1D quantum disordered systems differ from those on classical 2D systems in that quenched disorder is random in space but constant in time, so the two spacetime dimensions enter asymmetrically. The chirality of the χLL is responsible for the differences between our results and previous results on disordered electrons in 1D: correlation functions in a χLL depend on $x + ivt$ rather than just the magnitude $x^2 + v^2t^2$, and the operators of interest can have nonzero "conformal spin" (difference of right- and left-moving dimensions). One of the resulting RG equations disagrees with a result previously obtained by Kane, Fisher, and Polchinski. [18] We outline our results before proceeding to the calculation

In a maximally chiral edge, such as IQHE edges or $\nu = 2/5$, whether a given impurity operator (i.e., type of impurity scattering) is relevant depends only on K, not on V. For IQHE edges and also for the main-sequence chiral FQHE edges $\nu = 2/5, \nu = 3/7, \ldots$, there are relevant impurity operators which decouple the charge mode from the neutral mode(s). The charge mode must decouple and the neutral mode velocities must equilibrate for the system to flow to the $U(1) \times SU(n)$ fixed point ($n = \dim K$), where the impurity scattering can be "gauged away." [18, 19] The $U(1) \times SU(n)$ symmetry possessed by K for these edges [21] is generically broken by V, but restored if V flows to a decoupled charge mode (the $U(1)$) and $n - 1$ neutral modes with identical velocities (the $SU(n)$). To our knowledge it has not previously been shown that general initial conditions flow toward this fixed point for chiral edges.

The charge mode velocity is *not* required to equal the neutral mode velocity, since the disorder drives V to be diagonal in a basis where no disorder operator couples charged and neutral modes. There remain operators which couple the neutral modes to each other; thus although to leading order in the disorder strength the neutral mode velocities do not flow together, it seems clear that the eventual strong-disorder fixed point will have equal neutral mode velocities but a possibly different charge mode velocity. We find that the fixed point is only stable if the charge mode has greater velocity than the neutral modes.

The main-sequence *nonchiral* FQHE edges $\nu = 2/3, 3/5, \ldots$ have similar $U(1) \times SU(n)$ fixed points. Impurity scattering now can be either relevant or irrelevant, depending on V, and if it is irrelevant the system will not flow to the fixed point. For $\nu = 2/3$ KFP used a perturbative calculation for weak disorder to find the basin of attraction of the fixed point [18]; this calculation is similar to ours, although we find a slight disagreement (Appendix B). The flow to the fixed point has a much more pronounced effect on some observable quantities than in the chiral case: away from the fixed point, conductance and tunneling properties are nonuniversal. The differences between chiral and nonchiral edges result because scaling dimensions of vertex operators are independent of V (fixed by K) in chiral edges but depend on V in nonchiral edges.

The edge theory of each daughter state of $\nu = 1$ in the hierarchy is essentially the same as that of the corresponding daughter state of $\nu = 1/3, 1/5, \ldots$. Every principal hierarchy state, chiral or not, with neutral modes parallel to each other has a single solvable charge-decoupled fixed point in the presence of disorder. Edges with neutral modes traveling in both directions, such as $\nu = 5/3$ and $\nu = 5/7$, can have infinitely many fixed points of several different types. [37] The RG shows how for all of these fixed points the charge mode decouples, while the neutral modes can reach different equilibria, with consequences for tunneling experiments. The fixed points not solvable by the KFP method have disorder operators which frustrate each other at the fixed point.

The χLL action in imaginary time for a clean edge of a QH state characterized by the matrix K contains $n = \dim K$ bosonic fields ϕ_i: [11]

$$S_0 = \frac{1}{4\pi} \int dx\, dt\, [iK_{ij}\partial_x\phi_i\partial_t\phi_j + V_{ij}\partial_x\phi_i\partial_x\phi_j], \tag{6.1}$$

where the sum over repeated indices is assumed. K is a symmetric integer matrix and V a symmetric positive matrix. K gives the topological properties of the edge: the types of quasiparticles and their relative statistics. V, the velocity matrix, is positive definite so that the Hamiltonian is bounded below. The electromagnetic charges of quasiparticles are specified by an integer vector $\mathbf{t}$ and the filling factor is $\nu = t_i(K^{-1})_{ij}t_j$.

Now a term representing quenched random impurity scattering is added to the action:

$$S_1 = \int dx\, dt\, [\xi(x)e^{im_j\phi_j} + \xi^*(x)e^{-im_j\phi_j}] \tag{6.2}$$

Here ξ is a complex random variable and $\langle\langle \xi(x)\xi^*(x')\rangle\rangle = D\delta(x - x')$, with D the (real) disorder strength. The integer vector $\mathbf{m}$ describes how many of each type of

quasiparticle are annihilated or created by the operator $O_{\mathbf{m}} = \exp(im_j\phi_j)$. For a real system all charge-neutral scattering operators m_j are expected to appear, but most of these will be irrelevant in the RG sense. The condition for charge-neutrality is $t_i(K^{-1})_{ij}m_j = 0$. The random variables $\xi_{\mathbf{m}}$ for different scattering operators $O_{\mathbf{m}}$ may be uncorrelated or correlated depending on the nature of the physical impurities causing the scattering.

The clean action (6.1) is quadratic and hence does not flow under RG transformations. Adding impurities (6.2) causes the V matrix in (6.1) to flow, and in some cases the flow is to a new type of strong-disorder fixed point. [18, 19, 37] Here we will quickly review the diagonalization of the clean action to find the eigenmodes $\mathbf{a}_i$ and their velocities v_i, and then find the RG flows for two-mode edges with a single impurity operator. Then a general edge with several modes and impurity operators is considered.

Let M_1 be some matrix which brings K to the pseudo-identity I_{n^+,n^-}: $K^{-1} = M_1 I_{n_+,n_-} {M_1}^T$. Then V can be brought to a diagonal matrix $V_D = {M_2}^T {M_1}^T V M_1 M_2$, where M_2 is an element of the group $SO(n^+, n^-)$ so that M_2M_1 still takes K to the pseudo-identity. The point of these transformations is that the action is now diagonal in the basis $\tilde{\phi} = (M_1M_2)^{-1}\phi$, so the correlation functions are simple:

$$\begin{aligned} \langle e^{i\tilde{\phi}_j(x,t)} e^{-i\tilde{\phi}_j(0,0)} \rangle &= e^{\langle\tilde{\phi}_j(x,t)\tilde{\phi}_j(0,0)\rangle - \langle\tilde{\phi}_j(0,0)\tilde{\phi}_j(0,0)\rangle} \\ &\propto (x \pm iv_jt)^{-1} \end{aligned} \tag{6.3}$$

where the sign depends on whether $\tilde{\phi}_j$ appears with -1 or $+1$ in $I(n^+, n^-)$. The vertex operator $O_{\mathbf{m}}$ described by the integer vector $\mathbf{m}$ has correlation function

$$\langle e^{im_j\phi_j(x,t)} e^{-im_j\phi_j(0,0)} \rangle = \prod_{j=1}^{n} (x \pm iv_jt)^{-{c_j}^2} \tag{6.4}$$

with $m_j\phi_j = c_j\tilde{\phi}_j$. The total scaling dimension of $O_{\mathbf{m}}$ is $\Delta(\mathbf{m}) = \sum c_j^2/2$, which is bounded below by $K(\mathbf{m})/2 \equiv \mathbf{m}K^{-1}\mathbf{m}/2$. The impurity term S_1 containing $O_{\mathbf{m}}$ with a random coefficient is relevant if $\Delta(\mathbf{m}) < 3/2$; the corresponding marginal value for a uniform coefficient is 2, and for a δ-function coefficient 1.

Appendix B calculates the change in the correlation function of $O_{\mathbf{m}}$ under an infinitesimal RG transformation induced by the impurity term S_1. Here we find the change in the underlying V matrix required to produce the new correlation function. The K matrix is unchanged as it is "topological" (it does not enter the Hamiltonian). The V matrix flow has a simple interpretation, valid for any number of edge modes traveling in either direction. Each impurity operator $\mathbf{m}$ drives V to become diagonal in the basis with $\mathbf{m}$ an eigenvector. This automatically minimizes the scaling dimension of $O_{\mathbf{m}}$ in a nonchiral edge. In cases where there are more impurity operators than independent eigenvectors, so that not all impurity operators can simulatenously be eigenvectors, the impurity operators frustrate each other.

Both $\nu = 2$ and $\nu = 2/5$ have a single $K(\mathbf{m}) = 2$ operator which is always relevant. In the basis $\mathbf{e}_1 = \mathbf{t}$, $\mathbf{e}_2 = \mathbf{m}$,

$$K^{-1} = \begin{pmatrix} \nu & 0 \\ 0 & 2 \end{pmatrix}, \qquad K^{1/2} = \begin{pmatrix} 1/\sqrt{\nu} & 0 \\ 0 & 1/2 \end{pmatrix}$$

$$V = K^{1/2} R \begin{pmatrix} v_1 & 0 \\ 0 & v_2 \end{pmatrix} R^{-1} K^{1/2}. \tag{6.5}$$

with R a two-by-two rotation matrix by some angle θ. Note that all V are obtained by considering θ in the interval $[0, \pi)$. Now $\alpha = 2\sin^2\theta$ and $\beta = 2\cos^2\theta$ are the exponents appearing in the correlation function of the impurity operator: $\langle O_{\mathbf{m}}(x,t) O^\dagger_{\mathbf{m}}(0,0)\rangle = (x + iv_1 t)^{-\alpha}(x + iv_2 t)^{-\beta}$, $\alpha + \beta = 2$. Then to first order in disorder strength, the diagonal velocities v_1 and v_2 are unchanged, and (Appendix B)

$$\frac{d\alpha}{d\ell} = -\frac{8\pi D \alpha\beta}{(v_1 - v_2) v_1{}^{\alpha-1} v_2{}^{\beta-1}}. \tag{6.6}$$

Since $d\alpha = 2\sin(2\theta) d\theta = 2\sqrt{\alpha\beta}\, d\theta$,

$$\frac{d\theta}{d\ell} = -\frac{4\pi D \sin(2\theta) v_1 v_2}{(v_1 - v_2) v_1{}^{2\sin^2\theta} v_2{}^{2\cos^2\theta}}. \tag{6.7}$$

There are two fixed points of this equation, with $\theta = 0$ stable and $\theta = \pi/2$ unstable for $v_1 > v_2$, and vice versa for $v_1 < v_2$. The stable fixed point always corresponds to neutral mode velocity less than charge velocity (Fig. 6-1a).

We can summarize the effect of the disorder operator in the comoving case simply: it rotates V so that $\mathbf{m}$ becomes an eigenvector. Since $\mathbf{m}$ is neutral ($\mathbf{m}K^{-1}\mathbf{t} = 0$) the other eigenvector is driven to the charge vector. The idea that impurity operators drive V to make themselves eigenvectors is quite general. The case of two *countermoving* modes (e.g., $\nu = 2/3$) with a $K(\mathbf{m}) = -2$ disorder operator is similar in form. The rotation matrix R in (6.5) is replaced by a boost matrix B,

$$B = \begin{pmatrix} \cosh\tau & \sinh\tau \\ \sinh\tau & \cosh\tau \end{pmatrix}, \tag{6.8}$$

and the exponents in the correlator are $\alpha = 2\sinh^2\tau$, $\beta = 2\cosh^2\tau$, $\alpha - \beta = -2$, $\alpha + \beta = 2\Delta(\mathbf{m})$. The flow equation for τ is then

$$\frac{d\tau}{d\ell} = -\frac{4\pi D \sinh(2\tau) v_+ v_-}{(v_+ + v_-) v_+^{2\sinh^2\tau} v_-^{2\cosh^2\tau}}. \tag{6.9}$$

Here v_+ and v_- are the (positive) velocities of the right- and left-moving modes. Now there is only one fixed point, at $\tau = 0$ (Fig. 6-1b), which is the solvable fixed point found by KFP. [18]

Now we consider a general edge with several modes and impurity operators. To first order in disorder strength, the effects of each impurity operator add independently. Scaling dimensions $\Delta(\mathbf{m})$ of vertex operators $O_{\mathbf{m}}$ are independent of V in chiral edges, depending only on K: $2\Delta(\mathbf{m}) = \mathbf{m}K^{-1}\mathbf{m} = K(\mathbf{m})$. In a nonchiral edge this holds as an inequality: $2\Delta(\mathbf{m}) \geq K(\mathbf{m})$, with equality only if V is diagonal in a basis with $\mathbf{m}$ an eigenvector. Since most experimentally relevant quantities are determined by scaling dimensions, it is useful to isolate which parts of V affect scaling dimensions. The matrix M_2 used above to diagonalize V while preserving the

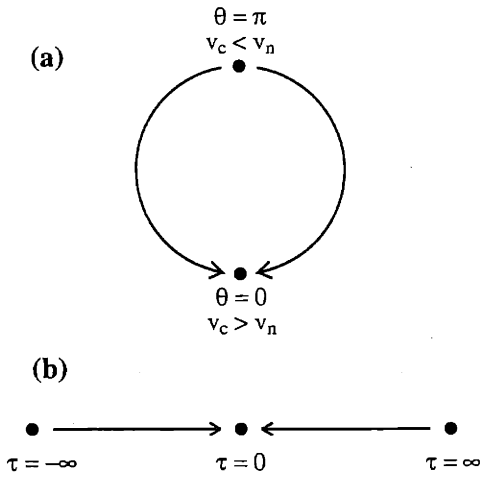

Figure 6-1: Schematic RG flows for two-mode (a) chiral and (b) nonchiral edges. The same idea applies to main-sequence edges with more than two modes: the chiral case has one stable ($v_c > v_n$) and one unstable ($v_c < v_n$) fixed point, while the nonchiral case has one stable fixed point independent of v_c, v_n.

pseudo-identity I_{n^+,n^-} is an element of $SO(n^+, n^-)$. It can be decomposed $M_2 = BR$ into a product of a 'boost', a symmetric matrix, and a rotation, an orthogonal matrix, each elements of $SO(n^+, n^-)$. [37] The $n(n+1)/2$ free parameters in the symmetric positive matrix V are now taken as n eigenvelocities (the elements of V_D), n^+n^- "boost parameters" (which correspond to interactions between oppositely directed modes), $n^+(n^+-1)/2$ rotation parameters between right-movers, and $n^-(n^--1)/2$ rotation parameters between left-movers. Only the n^+n^- boost parameters affect scaling dimensions because, introducing the matrix Δ_{ij} via $2\Delta(\mathbf{m}) = \mathbf{m}_i\Delta_{ij}\mathbf{m}_j$,

$$\Delta = M_1 BRR^T B^T {M_1}^T = M_1 B^2 {M_1}^T. \tag{6.10}$$

For each pair of comoving modes appearing in the correlation function, there is an infinitesimal change in the rotational part R, and for each pair of countermoving modes, there is an infinitesimal change in the boost part B.

Given an impurity operator $O_{\mathbf{m}}$ and initial $V(\ell)$, we need to find $V(\ell + d\ell)$ which gives the changes to the correlation function calculated in Appendix B. However, there is an important issue not present in the two-mode case: there are more free parameters in V than exponents in the correlation function, so V is not uniquely determined without additional assumptions. We assume that each term in Appendix B coupling two modes affects only the components of V between those two modes. We will also write the flow equations for the components of V directly, rather than introducing a parametrization as we did above in terms of θ or τ, because for multi-mode edges such parametrizations become quite complicated.

Suppose that rescaling by $d\ell$ changes the V matrix from $(M_1M_2)^{-1T}V_D(M_1M_2)^{-1}$ to

$$V(\ell + d\ell) = (M_1M_2N)^{-1T}V_D(M_1M_2N)^{-1}. \tag{6.11}$$

Note that V does not flow if the eigenmodes have the same velocity, so that V_D is a multiple of the identity. Here N is an element of $SO(n_+, n_-)$ differing only by order $d\ell$ from the identity. The fields which diagonalize $V(\ell + d\ell)$ are $\phi' = (M_1M_2N)^{-1}\phi = N^{-1}\tilde{\phi}$. Now let c_i be the components of the disorder operator in the $\tilde{\phi}$ basis which diagonalizes $V(\ell)$: $m_i\phi_i = c_j\tilde{\phi}_j$. The exponents appearing in the correlation function, whose flow is calculated in Appendix B, are $\alpha = {c_1}^2$, $\beta = {c_2}^2$, etc.

Now we are ready to construct N. For each pair of countermoving modes i and j, N has an infinitesimal rotation angle $d\theta_{ij} = -d\theta_{ji}$, and for each pair of comoving modes i and j, a boost $d\tau_{ij} = d\tau_{ji}$. For an edge with two right-movers and one left-mover, e.g.,

$$N = \begin{pmatrix} 1 & -d\theta_{12} & d\tau_{13} \\ d\theta_{12} & 1 & d\tau_{23} \\ d\tau_{13} & d\tau_{23} & 1 \end{pmatrix}. \tag{6.12}$$

Then for a disorder operator $O_{\mathbf{m}}$ with projections c_i and strength D,

$$\begin{aligned} d\theta_{ij} &= -\frac{4\pi c_i c_j v_i v_j D\, d\ell}{(v_i - v_j)\prod_i {v_i}^{c_i{}^2}}; \\ d\tau_{ij} &= -\frac{4\pi c_i c_j v_i v_j D\, d\ell}{(v_i + v_j)\prod_i {v_i}^{c_i{}^2}}. \end{aligned} \tag{6.13}$$

Note that the c_i can have either sign and must change sign in the vicinity of a fixed point, as above in the two-mode case. Substituting N in (6.11) gives the desired RG flow equation for the components of V. The condition for a fixed point is simple: $N^TV_DN = V_D$. Hence for any chiral edge (N a pure rotation), if all velocities are the same the system is at a fixed point.

The simplest multicomponent edges are the IQHE edges $\nu = n$ and chiral main-sequence edges $\nu = n/(2n+1)$. The behavior of these is similar to the $\nu = 2$ case discussed in detail above: the stable fixed point has charge and neutral mode velocities $v_c > v_n$. The neutral mode velocities are expected to equalize while the charge mode remains different, because there are always hopping operators connecting the different neutral modes, while there is no hopping connecting the charge mode to the neutral modes. As a result there is no stable fixed point unless the neutral velocities are the same.

For the $\nu = 3$ case we can demonstrate the similarity to the $\nu = 2$ case by an explicit calculation. Parametrize the rotation part R of V as $R = R_{23}(\theta_1)R_{12}(\theta_2)R_{23}(\theta_3)$, where $R_{ij}(\theta)$ is the rotation by θ in the $i-j$ plane; then in a basis with $\mathbf{e}_1 = \mathbf{t}$, the charge mode is decoupled if $\theta_2 = 0$. The flow equation for θ_2, with $v_2 = v_3 = v_n$, is

$$\frac{d\theta_2}{d\ell} = \frac{-4\pi v_c v_n \sin(2\theta_2)}{(v_c - v_n)} \times \left[\frac{\cos^2\theta_1(4D_1 + D_2 + D_3)}{4{v_c}^{2\cos^2\theta_1\sin^2\theta_2}{v_n}^{2(\sin^2\theta_1 + \cos^2\theta_1\cos^2\theta_2)}}\right.$$

$$+\frac{3\sin^2\theta_1(D_2+D_3)}{4{v_c}^{2\sin^2\theta_1\sin^2\theta_2}{v_n}^{2(\cos^2\theta_1+\sin^2\theta_1\cos^2\theta_2)}}\Bigg] \tag{6.14}$$

where $D_{1\ldots3}$ are the strengths of the 3 hopping operators. This is of the same form as (6.7) since the quantity in brackets is clearly positive. Henceforth we will not write out the flow equations but just discuss the qualitative behavior.

The nonchiral main-sequence edges $\nu = 2/3,\ 3/5,\ldots$ have solvable stable $U(1) \times SU(n)$ fixed points if all the neutral mode velocities are equal and the charge mode is decoupled. The charge mode does indeed decouple in the perturbative RG equations since each impurity operator reduces the scaling dimension of $\mathbf{t}$ toward its minimum ν, which is only attained when the charge mode is decoupled. Once the charge mode is decoupled, the neutral modes behave exactly as in the chiral case, except that the fixed point is stable even if the neutral mode velocity is greater than the charge mode velocity.

In the edges $\nu = 5/3$ or $\nu = 5/7$, which have neutral modes in both directions, there are an infinite number of possibly relevant impurity operators. [37] However, near each of the possible fixed points there are only three relevant operators. Unlike the case with all neutral modes in the same direction, to first order in disorder strength there is no stable fixed point for V, even if the neutral mode velocities are equal. The mathematical difference is that, now that the modes move in opposite directions, the impurity operators cause infinitesimal boosts which do not disappear when the velocities are equal, unlike infinitesimal rotations. The fixed points in these edges have marginal operators not present for the KFP-type fixed points and seem to be of a different type, and their strong-disorder behavior and stability is not well understood.

There are several four-component edges, such as $\nu = 12/17$ and $\nu = 12/31$, which have solvable, $SU(n)$ symmetric fixed points of the KFP type as well as fixed points with marginal operators similar to the $\nu = 5/3$ and $\nu = 5/7$ edges. The picture of equilibration differs depending on the fixed point. The solvable $SU(2) \times SU(2)$ fixed points found in these edges can have all three neutral mode velocities different (since there is a basis where no relevant hopping operator couples neutral modes), while the $SU(3)$ fixed points have to have two neutral mode velocities equal in order to be solvable. However, as discussed in the introduction the fixed point accessible by the composite-fermion approach [20] is the one with marginal operators present, even though this is the only one of the three fixed points whose stability is doubtful. [37]

Chapter 7

Boundary conditions and tunneling

7.1 Strong and weak tunneling fixed points

Until this point, we have considered tunneling into edge states in the limit where the tunneling current is small and can be calculated perturbatively. That is, we can calculate the current by perturbing around a decoupled fixed point where no tunneling occurs. In the remainder of this thesis we will discuss other strongly coupled fixed points which appear in the quantum Hall edge system when tunneling is no longer weak. Our goal in this chapter is to outline a general formalism for treating tunneling fixed points of quantum Hall edges, which is justified in the next chapter.

As an illustrative example we start with tunneling between two edges of the same Laughlin state $\nu = 1/3$. This problem was solved exactly by Fendley, Ludwig, and Saleur [38]: the crossover between weak and strong fixed points can be calculated using a mapping onto the boundary sine-Gordon model previously shown to be integrable. [39] For a general edge this integrability technique fails, but we will show that the fixed points of the tunneling problem can still be understood and give the most essential information.

Quasiparticle tunneling at finite temperature across a slight constriction in a single $\nu = 1/3$ quantum Hall bar becomes stronger and stronger as the temperature is lowered (quasiparticle tunneling is "relevant" in renormalization-group language) until the constriction becomes large and the system can be described as weak electron tunneling between two separated $\nu = 1/3$ edges. The crossover between these two fixed points can also be driven by applying a voltage across the junction at zero temperature. The relevance of quasiparticle tunneling follows from the scaling dimension $\Delta_q = 1/3$ of quasiparticle tunneling: for point tunneling an operator of dimension $\Delta = 1$ is marginal, $\Delta \leq 1$ relevant, and $\Delta \geq 1$ irrelevant. At the decoupled fixed point, the scaling dimension of electron tunneling is $\Delta_e = 3$, so the tunneling is irrelevant and the fixed point is stable. The junction conductance is $\frac{e^2}{3h}$ for the strongly coupled fixed point, when the system is a Hall bar at filling $\nu = 1/3$, and zero at the weak-coupling fixed point, when the two edges are decoupled.

In a moment we will present a method for determining tunneling fixed points in the chiral Luttinger liquid model. First, however, we give a relatively model-independent

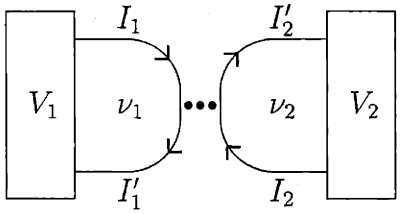

Figure 7-1: Schematic geometry for point tunneling between quantum Hall states.

picture of the strong and weak coupling fixed points for tunneling between two quantum Hall edges, which comes from considering the power dissipated at the tunneling junction. A simple argument shows that an upper bound on the conductance through a junction between FQH edges follows from the assumption that only one mode on each edge couples to the electric potential. In the χLL theory, this assumption holds in the presence of either unscreened Coulomb interactions or random hopping at the edge, for both chiral and nonchiral edges. Since in experiments the Coulomb interaction is screened only at moderate distances, and impurities are present, we assume separation of charge and neutral modes on each edge. The currents labeled in Fig. 7-1 are $I_1 = \nu_1 V_1, I_2 = \nu_2 V_2, I_1' = \nu_1 V_1', I_2' = \nu_2 V_2'$ (here $\frac{e^2}{h} = 1$). Current and energy conservation at the junction give

$$\nu_1(V_1 - V_1') + \nu_2(V_2 - V_2') = 0 \tag{7.1}$$

$$\nu_1(V_1^2 - V_1'^2) + \nu_2(V_2^2 - V_2'^2) = 2P. \tag{7.2}$$

Here P is the power dissipated at the junction. In terms of the two-terminal conductance $g = I_t/(V_1 - V_2) = I_t/V$,

$$P = g^2 V^2 \left[\frac{1}{g} - \frac{{\nu_1}^{-1} + {\nu_2}^{-1}}{2}\right]. \tag{7.3}$$

The dissipated power is zero for $g = 0$ or $g = \sigma_{hm} = 2\nu_1\nu_2/(\nu_1 + \nu_2)$, and positive for intermediate values; energy conservation forbids values $g \geq \sigma_{hm}$. The dissipated power can go into excitations of the oscillator modes of the outgoing edges [40]. The currently known fixed points for tunneling between quantum Hall edges all have zero dissipation at zero temperature except in the presence of exactly marginal operators (as in tunneling between $\nu = 1$ states). We thus conjecture that, unless marginal tunneling operators are present, the conductance saturates for large $V_1 - V_2$ at the value σ_{hm}.

Now we show how this asymptotic conductance and many other experimentally relevant results can be calculated by considering "boundary conditions" in a chiral Luttinger liquid. If tunneling occurs at a single point (say $x = 0$), the one-dimensional edge can be "folded" from the whole line to the half-line $0 \leq x < \infty$ with the tunneling junction at the boundary $x = 0$. The tunneling at $x = 0$ is a boundary interaction in the theory, and away from $x = 0$ the system is free. One renormalization-group fixed point of this system is the free fixed point where no tunneling occurs. This

corresponds to a certain boundary condition at $x = 0$ on the fields of the theory. A different boundary condition corresponds to strong tunneling, and has different scaling dimensions for the fields of the theory than the first fixed point.

We start by considering a tunneling junction at $x = 0$ between two edges described by K-matrices K_1 and K_2. Then the combination of the two edges can be described by a single K-matrix

$$K = \begin{pmatrix} K_1 & 0 \\ 0 & K_2 \end{pmatrix}. \tag{7.4}$$

To describe the possible fixed points of the tunneling junction as boundary conditions, we can fold the edge in $(-\infty, 0)$ on top of the edge in $(0, \infty)$ by introducing $2k$ fields $\tilde{\phi}_a$ on $(0, \infty)$:

$$\begin{aligned} \tilde{\phi}_a(x) &= \phi_a(x) \\ \tilde{\phi}_{k+a}(x) &= -\phi_a(-x) \\ x > 0 \qquad & \qquad a = 1, .., k. \end{aligned} \tag{7.5}$$

The resulting edge is described by $(\tilde{K}, \tilde{\mathbf{q}}, \tilde{\Gamma}_c, \tilde{\Delta})$:

$$\begin{aligned} \tilde{K} &= \begin{pmatrix} K & 0 \\ 0 & -K \end{pmatrix} \\ \tilde{\Delta} &= \begin{pmatrix} \Delta & 0 \\ 0 & \Delta \end{pmatrix} \\ \tilde{\Gamma}_c &= \Gamma_c \oplus \Gamma_c \\ \tilde{\mathbf{q}} &= \begin{pmatrix} \mathbf{q} \\ \mathbf{q} \end{pmatrix}. \end{aligned} \tag{7.6}$$

The edge is terminated at $x = 0$. Now the problem of the different fixed points of a tunneling junction becomes a problem of different ways that the edge $(\tilde{K}, \tilde{\mathbf{q}}, \tilde{\Gamma}_c, \tilde{\Delta})$ can terminate at $x = 0$. More precisely, each fixed point of the tunneling junction corresponds to a way in which the edge $(\tilde{K}, \tilde{\mathbf{q}}, \tilde{\Gamma}_c, \tilde{\Delta})$ terminates. The boundary conditions found below will also apply to the problem of an edge termination even if $\tilde{K}$ is not constructed from a tunneling problem. There are a number of interesting physical predictions which result [41], which we will not discuss here.

We find that the edge $(\tilde{K}, \tilde{\mathbf{q}}, \tilde{\Gamma}_c, \tilde{\Delta})$ can be terminated consistently (Chapter 8) if there is a $2k$ by k matrix B that satisfies

$$\begin{aligned} & B^T \tilde{K}^{-1} B = 0, \\ & \det(B^T B) \neq 0 \\ & \Gamma_B \equiv \mathrm{Latt}(B) \subset \tilde{\Gamma}_{c0} \end{aligned} \tag{7.7}$$

where $k = \dim(\tilde{K})/2$ and

$$\tilde{\Gamma}_{c0} = \{\mathbf{n} | \mathbf{n} \in \tilde{\Gamma}_c, \mathbf{n}^T \tilde{K}^{-1} \mathbf{n} = \text{even}\} \tag{7.8}$$

(i.e., the points in $\tilde{\Gamma}_{c0}$ describe the bosonic vertex operators). The physical meaning of the first two conditions is that there are k vectors of length $2k$ (the columns of the

matrix B) which are null in the indefinite quadratic form K^{-1}, orthogonal in K^{-1}, and linearly independent. Previously Haldane [30] described charge-neutral null vectors of K^{-1} as "topological instabilities," which allow oppositely directed edge modes to localize each other and drop out of the low-energy theory; thus condition (7.7) is that there be k independent topological instabilities orthogonal in K^{-1}. (We have relaxed the condition of charge-neutrality in order to include situations involving coupling to a superconductor.) In order for B to exist, $\tilde{K}$ must have the same number of positive and negative eigenvalues (the edge has the same number of right-moving and left-moving branches).

If more than one B exists, then the edge $(\tilde{K}, \tilde{\mathbf{q}}, \tilde{\Gamma}_c, \tilde{\Delta})$ can be terminated in more than one way. In other words, the boundary at $x = 0$ can have more than one fixed point. These different fixed points will be referred as different terminations of the edge.

For a termination labeled by the matrix B, the fields $\tilde{\phi}$ satisfy the following boundary conditions at the termination point

$$B^T \tilde{\phi} = 2\pi \mathbf{n}, \quad \mathbf{n} = \text{integral vectors.} \tag{7.9}$$

Note that ϕ can satisfy different boundary conditions even for a single type of termination labeled by B.

The allowed charge excitations (vertex operators) at the boundary are labeled by points in a k-dimensional lattice Γ_{q_B} (called the boundary Q-lattice):

$$\Gamma_{q_B} = \tag{7.10}$$
$$\text{Latt}\left(\tilde{K}B(B^TB)^{-1} - \frac{1}{2}B(B^TB)^{-1}B^T\tilde{K}B(B^TB)^{-1}\right)$$

The boundary quasiparticle operators have the form $V_{\mathbf{l}}^b = e^{i\mathbf{l}^T\tilde{\phi}}$, $\mathbf{l} \in \Gamma_{q_B}$. The scaling dimension of $V_{\mathbf{l}}^b$ is given by

$$h^b(\mathbf{l}) = \mathbf{l}^T\tilde{K}^{-1}B(B^T\tilde{\Delta}B)^{-1}B^T\tilde{K}^{-1}\mathbf{l} \tag{7.11}$$

This is one of the main results of this chapter.

In the above discussion of termination points, we have ignored any symmetry properties and the related selection rules. In particular, the boundary condition characterized by B may not conserve electric charge. As a result, a boundary vertex operator may not carry a definite electric charge. In order for the termination labeled by B to conserve the electric charge, we must require the B matrix to satisfy

$$B^T\tilde{K}^{-1}\tilde{\mathbf{q}} = 0 \tag{7.12}$$

For the charge conserving termination points, the electric charge of a boundary vertex operator $V_{\mathbf{l}}^b$ is found to be

$$Q = \tilde{\mathbf{q}}^T\tilde{K}^{-1}\mathbf{l} \tag{7.13}$$

For a general termination described by B, there are k combined charges that are conserved near the boundary. Their densities are given by

$$\rho_a = B_{ba}\partial_x\tilde{\phi}_a/2\pi \tag{7.14}$$

The boundary operator V_1^b carries definite values of these k combined charges:

$$\mathbf{Q} = B^T \tilde{K}^{-1} \mathbf{l} \tag{7.15}$$

7.2 An example: junction between two Laughlin states

The case of tunneling between two Laughlin states has been treated previously in the absence of intermode interactions by several authors [35, 38, 42, 40]. Here we will show how the known results for the two fixed points are recovered in our framework, and in Chapter 9 consider interaction effects. A new result even in the absence of interactions is the information found below about the lattice of charged boundary operators. For definiteness we consider the case of tunneling between $\nu = 1$ and $\nu = 1/3$ states which has attracted the most attention. The $\nu = 1$ edge can serve as a model for a metallic contact, since at $\nu = 1$ the edge is a Fermi liquid. At weak coupling between the two edges, the most relevant neutral operator tunnels an electron between the two edges, with scaling dimension 2; at strong coupling the most relevant neutral operator has scaling dimension $\frac{1}{2}$. This neutral operator can be interpreted as tunneling between different minima of the boundary cosine interaction in the sine-Gordon model, or as quasiparticle tunneling in an effective model of two $\nu = \frac{1}{2}$ edges.

With no intermode interactions, we have

$$\tilde{K} = \begin{pmatrix} m_1 & 0 & 0 & 0 \\ 0 & -m_1 & 0 & 0 \\ 0 & 0 & m_2 & 0 \\ 0 & 0 & 0 & -m_2 \end{pmatrix}, \quad \tilde{\mathbf{q}} = \begin{pmatrix} 1 \\ 1 \\ 1 \\ 1 \end{pmatrix}$$

$$\tilde{\Delta} = \begin{pmatrix} 1/m_1 & 0 & 0 & 0 \\ 0 & 1/m_1 & 0 & 0 \\ 0 & 0 & 1/m_2 & 0 \\ 0 & 0 & 0 & 1/m_2 \end{pmatrix}. \tag{7.16}$$

Fixed point A (weak coupling) is described by

$$B = \begin{pmatrix} 1 & 0 \\ 1 & 0 \\ 0 & 3 \\ 0 & 3 \end{pmatrix}. \tag{7.17}$$

The meaning of this B matrix is that the incoming and outgoing $\nu = 1$ edges are joined continuously to each other, and similarly for the incoming and outgoing $\nu = 1/3$ edges. The boundary Q-lattice is

$$\Gamma_{q_B} = \mathrm{Latt}\left(\begin{pmatrix} \frac{1}{2} & 0 \\ -\frac{1}{2} & 0 \\ 0 & \frac{1}{2} \\ 0 & -\frac{1}{2} \end{pmatrix} \right). \tag{7.18}$$

A general boundary operator $O_{\mathbf{l}}$ with $\mathbf{l} = l_1(\frac{1}{2}, -\frac{1}{2}, 0, 0) + l_2(0, 0, \frac{1}{2}, -\frac{1}{2})$, l_1 and l_2 integers, has electric charge $Q_{\mathbf{l}} = l_1 + l_3/2$ and scaling dimension ${l_1}^2/2 + {l_2}^2/6$. The most relevant neutral boundary operator has $(l_1, l_2) = (1, -3)$ and scaling dimension 2, as expected for electron tunneling at weak coupling.

Fixed point B (strong coupling) is described by

$$B = \begin{pmatrix} 2 & 1 \\ 1 & 1 \\ 0 & 1 \\ 3 & 1 \end{pmatrix}. \tag{7.19}$$

The meaning of the first column of B is that two incoming electrons become one outgoing electron and three outgoing $q = \frac{1}{3}$. quasiparticles. In the boundary sine-Gordon language, this corresponds to pinned (Dirichlet) boundary condition on the neutral mode. The second column is simply the charge vector, indicating that overall charge is conserved across the junction. The boundary Q-lattice is

$$\Gamma_{q_B} = \mathrm{Latt}\left(\begin{pmatrix} \frac{3}{10} & -\frac{1}{10} \\ \frac{3}{10} & -\frac{4}{5} \\ -\frac{7}{10} & \frac{3}{2} \\ -\frac{7}{10} & \frac{3}{5} \end{pmatrix} \right). \tag{7.20}$$

A general boundary operator $O_{\mathbf{l}}$ with $\mathbf{l} = l_1(\frac{3}{10}, \frac{3}{10}, -\frac{7}{10}, -\frac{7}{10}) + l_2(-\frac{1}{10}, -\frac{4}{5}, \frac{3}{2}, \frac{3}{5})$ has charge $Q = l_2$ and scaling dimension ${l_1}^2/2 - 3l_1l_2/2 + 3{l_2}^2/2$. The most relevant neutral boundary operator has $(l_1, l_2) = (1, 0)$ and scaling dimension $\frac{1}{2}$, as expected.

Chapter 8

Correlation functions in bounded Luttinger liquids

8.1 Correlations with boundary

We start by introducing a certain basis for K and $\mathbf{t}$ which simplifies the calculation of correlation functions. The collective modes that propagate along the edge can be described by several density operators $\rho_a(x)$, which satisfy the algebra (Chapter 2)

$$[\rho_a(x), \rho_b(y)] = \frac{i}{2\pi}(K^{-1})_{ab}\delta'(x-y) \tag{8.1}$$

where K is a symmetric integral matrix that characterizes an Abelian edge. The total electric density is a sum of ρ_a weighted by a charge vector q^a:

$$\rho_e = q^a \rho_a. \tag{8.2}$$

For all the cases of interest here, we can choose the symmetric basis in which $q^a = 1$. In the following we will work in this symmetric basis, where there are $\dim(K)$ different electron operators

$$\psi_e^b(x) = e^{in_e^{ab}\phi_a(x)} \tag{8.3}$$

where $\mathbf{n}_e^b$ is the b^{th} column of K: $n_e^{ab} = K^{ab}$. An multi-electron operator has a form $e^{in_e^a\phi_a(x)}$ with $\mathbf{n}_e$ belonging to a lattice Γ_e, which will be called the electron lattice. The lattice $\Gamma_e = \mathrm{Latt}(K)$, since Γ_e is generated by the column vectors of K.

The charge fluctuations created by the electron operators can also be described by the ϕ fields in the Lagrangian. Now the ϕ fields no longer satisfy periodic boundary conditions, but instead

$$\phi_a(L) = \phi_a(0) + 2\pi N_a \tag{8.4}$$

where N_a are integers. In fact, the above ϕ describe excitations created by $\prod_b(\psi_e^b)^{N_b}$ from the neutral ground state.

In general, the (multi-)electron operators do not represent all possible "charge" excitations. The most general charge excitations are created by

$$\psi_c(x) = e^{in_c^a\phi_a(x)} \tag{8.5}$$

where $\mathbf{n}_c$ are integral vectors belonging to a lattice Γ_c (which will be called the E-lattice). The general charge excitations contain all excitations created by the electron operators, and thus $\Gamma_e \subseteq \Gamma_c$. The general charge excitations can also include excitations that transfer fractional charges between different edge branches, but have integer overall charge.

The E-lattice Γ_c must satisfy certain conditions. Since $\psi_c(x)$ all carry integral charges (which can be zero), the vectors in Γ_c satisfy

$$\mathbf{q}^T K^{-1} \mathbf{n}_c = \text{integer} \tag{8.6}$$

The operators $\psi_c(x)$ are also mutually local; that is

$$(\mathbf{n}_c')^T K^{-1} \mathbf{n}_c = \text{integer} \tag{8.7}$$

for any $\mathbf{n}_c$ and $\mathbf{n}_c'$ in Γ_c. This condition implies that $\Gamma_c \subseteq \text{Latt}(K^{-1})$. Just like the electron operators, the excitations created by $\psi_c = e^{i\mathbf{n}_c \cdot \phi}$ are described by ϕ that satisfy the boundary condition

$$\phi(L) = \phi(0) + 2\pi K^{-1} \mathbf{n}_c \tag{8.8}$$

We can also use the above to define the periodicity conditions of the ϕ field. We take ϕ and ϕ' to be equivalent if

$$\phi = \phi' + 2\pi K^{-1} \mathbf{n}_c \tag{8.9}$$

for some $\mathbf{n}_c \in \Gamma_c$.

Now we add a tunnel junction or termination to the system. In what follows it is assumed that in the junction case the edge has been folded onto the half-line as in Chapter 7, so that one set $(\tilde{K}, \tilde{\mathbf{q}}, \tilde{\Gamma}_c, \tilde{\Delta})$ describes both incoming and outgoing edges, with a total of $2k$ bosonic fields. In the presence of tunneling between different edge branches at $x = 0$, the Lagrangian contains a term

$$\mathcal{L}_t = \sum_I t_I \delta(x) e^{\mathbf{n}^I \cdot \phi} + h.c. \tag{8.10}$$

where t_I is the (real) tunneling strength, and the integral vectors $\mathbf{n}^I$ are points in the Γ_c lattice which also satisfy

$$(\mathbf{n}^I)^T \tilde{K}^{-1} \mathbf{n}^I = \text{even}. \tag{8.11}$$

(Thus $e^{i\mathbf{n}^I \cdot \phi}$ are bosonic operators.) If electric charge is conserved at the boundary, $\mathbf{n}^I$ should also satisfy

$$\mathbf{q}^T K^{-1} \mathbf{n}^I = 0 \tag{8.12}$$

so that $e^{i\mathbf{n}^I \cdot \phi}$ represents a neutral operator. For the time being, we will not impose the above charge-conservation condition.

The Lagrangian density on the half-line is given by

$$\mathcal{L} = -\frac{1}{4\pi} \left((\tilde{K})^{ab} \tilde{\phi}_a \partial_t \partial_x \tilde{\phi}_b - (\tilde{V})^{ab} \tilde{\phi}_a \partial_x^2 \tilde{\phi}_b \right) \tag{8.13}$$

We also need to specify what are the allowed charge excitations, in addition to the Lagrangian (8.13). This can be achieved by specifying the periodicity conditions of the $\tilde{\phi}$ fields:

$$\tilde{\phi} \sim \tilde{\phi}' = \tilde{\phi} + 2\pi \tilde{K}^{-1} \mathbf{n}_c \tag{8.14}$$

where $\mathbf{n}_c$ are vectors in the lattice $\tilde{\Gamma}_c$.

To completely define our system on the half-line, we need to include boundary conditions at $x = 0$. First let us consider the boundary condition in Hamiltonian language. We will start with the following type of boundary conditions, specified by a collection of vectors B_I^a with $I = 1, ..., k$:

$$B_I^a \tilde{\phi}_a(0) = 0, \quad \text{forallI} \tag{8.15}$$

Since we are looking for critical points, we would like to study boundary conditions that are invariant under scaling, suggesting the form (8.15). However, the above form is inconsistent with the periodicity conditions on $\tilde{\phi}$. It turns out that (8.15), although sufficient to determine the correlation functions of vertex operators, must be improved (later in this chapter) in order to determine the lattice of allowed boundary quasiparticle operators.

Since $\tilde{\phi}_a(x)$'s do not commute with each other, the above boundary conditions are self-consistent only if

$$[B_I^a \tilde{\phi}_a(x), B_J^b \tilde{\phi}_b(y)] = 0, \quad \text{forallI, J.} \tag{8.16}$$

This implies that the vectors that characterize the boundary condition must satisfy

$$B^T \tilde{K}^{-1} B = 0, \quad \det(B^T B) \neq 0 \tag{8.17}$$

where B is the $2k$ by k matrix formed by B_J^a. Note that two different B matrices, B_1 and B_2, specify the same boundary condition in the sense of (8.15) if they are related by

$$B_1 = B_2 U, \quad U \in L(k) \tag{8.18}$$

where U is an $k \times k$ invertible real matrix U. In this case we say B_1 and B_2 are "weakly" equivalent

$$B_1 \sim B_2. \tag{8.19}$$

In the Lagrangian language, the above boundary condition on the fields $\tilde{\phi}$ corresponds to $B^T \tilde{\phi}(0) = 0$. Only for certain choices of B can the operator $\mathcal{K} = (\tilde{K})^{ab} \partial_t \partial_x - (\tilde{V})^{ab} \partial_x^2$ be hermitian. We will show that the condition on B that makes $\mathcal{K}$ hermitian is nothing but (8.17). To see this, we first note that

$$\int dx dt \tilde{\phi}_2^T \mathcal{K} \tilde{\phi}_1 = \int dx dt \tilde{\phi}_1^T \mathcal{K} \tilde{\phi}_2 + \int dt (\partial_t \tilde{\phi}_2^T K \tilde{\phi}_1)_{x=0} \tag{8.20}$$

Thus $\mathcal{K}$ is hermitian if B is such that

$$\tilde{\phi}_a \tilde{K}^{ab} \tilde{\phi}_b' = 0 \tag{8.21}$$

for all $\tilde{\phi}$, $\tilde{\phi}'$ that satisfy $B^T\tilde{\phi} = B^T\tilde{\phi}' = 0$. Let us choose a basis that the vectors in the null space of B have the form $\tilde{\phi}^T_{null} = (0, ..., 0, a, ..., b)$, i.e., the first k elements are zero. In this basis, by (8.21) $\tilde{K}$ has the form

$$\tilde{K} = \begin{pmatrix} K_0 & K_1 \\ K_1^T & 0 \end{pmatrix}, \tag{8.22}$$

and B has the form

$$B = \begin{pmatrix} B_1 \\ 0 \end{pmatrix} \tag{8.23}$$

where K_1 and B_1 are invertible. Since $\tilde{K}^{-1}$ has the form

$$\tilde{K}^{-1} = \begin{pmatrix} 0 & K_1^{-1} \\ (K_1^T)^{-1} & -(K_1^T)^{-1}K_0K_1^{-1} \end{pmatrix}, \tag{8.24}$$

thus the condition (8.21) implies the condition (8.17). We see that the hermiticity of the operator $(\tilde{K})^{ab}\partial_t\partial_x - (\tilde{V})^{ab}\partial_x^2$ also requires B to satisfy (8.17).

Let us summarize our results so far. The critical boundary conditions of an Abelian edge described by $\tilde{K}$ are characterized by a matrix B that satisfies (8.17). If such a B does not exist, then the edge state described by $\tilde{K}$ cannot be terminated at a point. If such a B does exist, then we can consistently impose a boundary condition $B^T\tilde{\phi} = 0$ and terminate the edge state at $x = 0$ (provided that B satisfies some other conditions that will be discussed later). If more then one inequivalent B exists, then the edge can be terminated in more than one way (the tunneling junction has more than one fixed point).

Now the question is when B exists. First, from (8.22) we see that the signature of $\tilde{K}$ must be zero in order for B to exist. Since $\tilde{K}$ is invertible, we can write $\tilde{K}$ as

$$\tilde{K} = \tilde{K}_{1/2}^T \begin{pmatrix} I_{k\times k} & 0 \\ 0 & -I_{k\times k} \end{pmatrix} \tilde{K}_{1/2}. \tag{8.25}$$

We see that B always exists for the above $\tilde{K}$. A generic B that satisfies (8.17) can be written as

$$B = \begin{pmatrix} 1 \\ T_0^T \end{pmatrix} \tilde{K}_{1/2}, \quad T_0T_0^T = I. \tag{8.26}$$

Thus B exists if and only if $\tilde{K}$ has a vanishing signature (there are as many incoming modes as outgoing modes). In this case the different boundary conditions are labeled by an element in the $O(k)$ group.

Next we would like to calculate the correlation functions of the fields $\tilde{\phi}$ in the presence of the boundary. First we choose a basis in which both $\tilde{K}$ and $\tilde{V}$ are diagonal (this can always be done [14]):

$$\tilde{K} = \begin{pmatrix} I & 0 \\ 0 & -I \end{pmatrix} \equiv \Sigma_3, \quad \tilde{V} = \begin{pmatrix} v_R & 0 \\ 0 & -v_L \end{pmatrix} \equiv \tilde{V}_{diag} \tag{8.27}$$

The block v_R has positive diagonal elements which are the velocities of right movers, while v_L has negative diagonal elements which are the velocities of left movers. Thus

the velocity for each branch is given by $v_a = (\Sigma_3 \tilde{V}_{diag})_{aa}$. In this basis a generic B is equivalent to a simple form:

$$B \sim \begin{pmatrix} I \\ T_0^T \end{pmatrix}, \quad T_0 T_0^T = I \tag{8.28}$$

Let $G_{0,ab}(x,t)$ be the correlation of $\tilde{\phi}_a(x,t)$ and $\tilde{\phi}_b(0)$ in the absence of the boundary: $G_{0,ab}(x,t) = \left\langle \tilde{\phi}_a(x,t)\tilde{\phi}_b(0) \right\rangle_0$. The correlation satisfies a linear equation

$$\frac{1}{2\pi}\left(-\tilde{K}^{ac}\partial_{x_1}\partial_t + \tilde{V}^{ac}\partial_x^2\right) G_{0,cb}(x,t) = \delta_{ab}\delta(x)\delta(t) \tag{8.29}$$

Since $\tilde{K}$ and $\tilde{V}$ are diagonal in the present basis, the above can be rewritten as

$$\begin{aligned} &\frac{1}{2\pi}\left(-\tilde{K}^{aa}\partial_x\partial_t + \tilde{V}^{aa}\partial_x^2\right) G_{0,aa}(x,t) = \delta(x)\delta(t) \\ &a = 1, ..., \dim \tilde{K}. \end{aligned} \tag{8.30}$$

We notice that the pair (a,x) is simply a label of the $\tilde{\phi}$ field. We can choose another label $(a,\tilde{x})$ to eliminate the velocities and further simplify the above equation. The two sets of labels are related by

$$(a,x) = (a, \tilde{V}^{aa}\tilde{x}) \tag{8.31}$$

Now the equations for $G_{0,aa}$ become

$$\begin{aligned} &\frac{1}{2\pi}\left(-\tilde{\Sigma}_3^{aa}\partial_{\tilde{x}}\partial_t + \partial_{\tilde{x}}^2\right) G_{0,aa}(\tilde{x},t) = \delta(\tilde{x})\delta(t) \\ &a = 1, ..., \dim \tilde{K} \end{aligned} \tag{8.32}$$

The correlation function with boundary, $G_{ab}(x_1,x_2,t) = \left\langle \tilde{\phi}_a(x_1,t)\tilde{\phi}_b(x_2,0) \right\rangle$, satisfies according to (8.15)

$$B^T G(0,x_2,t) = G(x_1,0,t)B = 0, \tag{8.33}$$

and

$$\begin{aligned} &\frac{1}{2\pi}\left(-\tilde{K}^{ac}\partial_{x_1}\partial_t + \tilde{V}^{ac}\partial_{x_1}^2\right) G_{cb}(x_1,x_2,t) \\ = \;& \delta(x_1 - x_2)\delta(t) \end{aligned} \tag{8.34}$$

for $x_1, x_2 > 0$. In the diagonal basis and in terms of the new label $(a,\tilde{x})$, the above equation becomes

$$\frac{1}{2\pi}\left(-\tilde{\Sigma}_3\partial_{\tilde{x}_1}\partial_t + \partial_{\tilde{x}_1}^2\right) G(\tilde{x}_1,\tilde{x}_2,t) = \delta(\tilde{x}_1 - \tilde{x}_2)\delta(t) \tag{8.35}$$

for $\tilde{x}_1, \tilde{x}_2 > 0$.

The boundary condition $B^T\tilde{\phi} = 0$ can be rewritten for B in the form (8.28) as

$$\tilde{\phi}_a(0^+,t) = -\sum_{b=1}^{k}(T_0)_{ab}\tilde{\phi}_{b+k}(0^+,t), \quad a = 1,\ldots,k. \tag{8.36}$$

It simply connects the right moving fields $\tilde{\phi}_a$ to the left moving fields $\tilde{\phi}_{a+k}$, $a = 1, .., k$, through an orthogonal matrix T_0. With this understanding, we find that G_{ab} is given by

$$\begin{aligned} G_{ab}(\tilde{x}_1, \tilde{x}_2, t) &= \left\langle \tilde{\phi}_a(\tilde{x}_1, t)\tilde{\phi}_b(\tilde{x}_2, 0)\right\rangle \\ &= \left(G_0(\tilde{x}_1 - \tilde{x}_2, t) - G_0(\tilde{x}_1 + \tilde{x}_2, t)T\right)_{ab} \end{aligned} \tag{8.37}$$

where $T = \begin{pmatrix} 0 & T_0 \\ T_0^T & 0 \end{pmatrix}$.

Note that by restricting to boundary conditions described in terms of the real bosonic fields, we are ignoring possible symmetries not present at the Abelian K-matrix level. For instance, if there are two incoming $\nu = 1$ edges described by Fermi fields ψ_i, there could be a unitary $U(2)$ rotation at $x = 0$ rather than the orthogonal rotation described above. As an example of the meaning of the orthogonal matrix T_0, consider the case of tunneling between $\nu = 1/3$ and $\nu = 1$ states discussed in Chapter 8. The rescaled basis is $K = \mathrm{diag}(1, 1, -1, -1)$, and the tunneling operator is $\exp(i(\phi_1 - \sqrt{3}\phi_2)) + \mathrm{h.c.}$. The matrix T_0 for strong tunneling is

$$T_0 = \begin{pmatrix} \frac{1}{2} & \frac{\sqrt{3}}{2} \\ \frac{\sqrt{3}}{2} & -\frac{1}{2} \end{pmatrix}, \tag{8.38}$$

which is the same as the matrix mapping incoming quasiparticles to outgoing quasiparticles in Sandler *et al.* [43]. For instance, two incoming electrons on the $\nu = 1$ edge become one outgoing electron on the $\nu = 1$ edge and three charge $e/3$ quasiparticles on the $\nu = 1/3$ edge.

From the symmetry of the equation for G_0, we see that, as a function of $\tilde{x}$, the matrix function $G_0(\tilde{x}, t)$ satisfies

$$TG_0(\tilde{x}, t)T = G_0(-\tilde{x}, t) \tag{8.39}$$

Using (8.39) and $B^T T = B^T$, we can check that the above G satisfies (8.33). Certainly, G also satisfies the equation (8.35).

To obtain the correlation function in the original basis and in terms of the original labeling (a, x), we need to start with the explicit form of G_0: $G_0(\tilde{x}, t) = -\ln(\Sigma_3\tilde{x} - t)$. After replacing the label $(a, \tilde{x})$ by $(a, x/|v_a|)$, we find (no summation over repeated indices)

$$\begin{aligned} G_{ab}(x_1, x_2, t) &= \left\langle \tilde{\phi}_a(x_1, t)\tilde{\phi}_b(x_2, 0)\right\rangle \\ &= -\ln((\Sigma_3)_{aa}(x_1/|v_a| - x_2/|v_b|) - t)\delta_{ab} \\ &\quad + \ln((\Sigma_3)_{aa}(x_1/|v_a| + x_2/|v_b|) - t)(T^T)_{ab}. \end{aligned} \tag{8.40}$$

If $\tilde{K}$, $\tilde{V}$ and the boundary condition B in the original basis are given by

$$\begin{aligned} &\tilde{K} = W^T\Sigma_3 W, \quad \tilde{V} = W^T\tilde{V}_{diag}W, \\ &B \sim W^T \begin{pmatrix} I \\ T_0^T \end{pmatrix} \end{aligned} \tag{8.41}$$

then the correlation function in the original basis can be obtained from the transformation $\tilde{\phi} \to W^{-1}\tilde{\phi}$, $\tilde{K} = \Sigma_3 \to (W^T)\Sigma_3 W$, $\tilde{V} = \tilde{V}_{diag} \to (W^T)\tilde{V}_{diag}W$, $B = \begin{pmatrix} I \\ T_0^T \end{pmatrix} \to W^T \begin{pmatrix} I \\ T_0^T \end{pmatrix}$, and $G \to W^{-1}G(W^T)^{-1}$:

$$\begin{aligned} & G_{ab}(x_1, x_2, t) = \\ & -\sum_{cd}(W^{-1})_{ac} \ln((\Sigma_3)_{cc}(\frac{x_1}{|v_c|} - \frac{x_2}{|v_d|}) - t)\delta_{cd}(W^T)^{-1}_{db} \\ & +\sum_{cd}(W^{-1})_{ac} \ln((\Sigma_3)_{cc}(\frac{x_1}{|v_c|} + \frac{x_2}{|v_d|}) - t)T_{cd}(W^T)^{-1}_{db}. \end{aligned} \tag{8.42}$$

The above result for the correlations of $\tilde{\phi}$ allows us to calculate the correlation functions of vertex operators $O_{\mathbf{l}}$ by exponentiation. Consider an operator $V_{\mathbf{n}} = e^{in^a\tilde{\phi}_a}$. Far away from the boundary ($x \gg |v|t$), the operator has a correlation which is determined by G_0 only:

$$\langle V_{\mathbf{n}}(x,t)V_{\mathbf{n}}(x,0)\rangle \sim 1/t^{g_{\mathbf{n}}} \tag{8.43}$$

where

$$g_{\mathbf{n}} = \mathbf{n}^T\tilde{\Delta}\mathbf{n} \tag{8.44}$$

and $\tilde{\Delta} = W^{-1}(W^T)^{-1}$. We can write W in a form

$$W = \begin{pmatrix} \tilde{R}_R & 0 \\ 0 & \tilde{R}_L \end{pmatrix} \tilde{B}_{st}\tilde{K}_{1/2}, \tag{8.45}$$

where $\tilde{R}_{R,L} \in O(k)$, and $\tilde{B}_{st}$ is the boost matrix of form

$$\tilde{B}_{st} = \exp\begin{pmatrix} 0 & \tilde{b} \\ \tilde{b}^T & 0 \end{pmatrix}. \tag{8.46}$$

In this parameterization of W, $\tilde{\Delta}$ depends only on $\tilde{B}_{st}$ (or the k-dimensional matrix b):

$$\tilde{\Delta} = \tilde{K}^{-1}_{1/2}\tilde{B}^{-2}_{st}(\tilde{K}^T_{1/2})^{-1}. \tag{8.47}$$

Near the boundary ($x \ll |v|t$), the correlation has a different algebraic decay

$$\langle V_{\mathbf{n}}(0,t)V_{\mathbf{n}}(0,0)\rangle \sim 1/t^{g^b_{\mathbf{n}}} \tag{8.48}$$

with

$$g^b_{\mathbf{n}} = \mathbf{n}^T\tilde{\Delta}^b\mathbf{n} \tag{8.49}$$

where from equation (8.42)

$$\tilde{\Delta}^b = W^{-1}(I - T)(W^T)^{-1}. \tag{8.50}$$

The above can be rewritten as

$$\tilde{\Delta}^b \;=\; 2K^{-1}B(B^T\tilde{\Delta}B)^{-1}B^TK^{-1} \tag{8.51}$$

Since it is invariant under $B \to BU$, (8.51) is valid for all B, not just the form $B = W^T\begin{pmatrix} I \\ T_0^T \end{pmatrix}$.

8.2 Boundary conditions compatible with periodicity conditions

In the above discussion of the boundary condition (8.15), we have not considered the problem that this condition violates the periodicity of the fields $\tilde{\phi}$. We need to take into account the periodic nature of $\tilde{\phi}$ field:

$$\tilde{\phi} \sim \tilde{\phi}' = \tilde{\phi} + 2\pi \tilde{K}^{-1} \mathbf{n}_c. \tag{8.52}$$

It is clear that the boundary condition $B^T \tilde{\phi} = 0$ is not consistent with all the periodic conditions of the $\tilde{\phi}$ field. Since $\tilde{\phi}$ and $\tilde{\phi} + 2\pi \tilde{K}^{-1} \mathbf{n}_c$ are equivalent, if $B^T \tilde{\phi} = 0$ is allowed, then $B^T(\tilde{\phi} + 2\pi \tilde{K}^{-1} \mathbf{n}_c) = 0$ should also be allowed. That is, we need to generalize the boundary condition to at least

$$B^T \tilde{\phi} = 2\pi B^T K^{-1} \mathbf{n}_c, \quad \mathbf{n}_c \in \tilde{\Gamma}_c. \tag{8.53}$$

One technical way to understand what has been done in the previous section is that we have only considered boundary conditions for the neutral excitations created by $\partial_x \tilde{\phi}$. (Here "neutral" does not mean electrically neutral, but rather conserving the zero mode of the bosonic theory.) In addition to these neutral excitations, there are also charged excitations created by vertex operators $V_{\mathbf{n}} = e^{i\mathbf{n}_c \cdot \tilde{\phi}}$, where $\mathbf{n}_c$ is a vector in the E-lattice $\tilde{\Gamma}_c$. Since the vertex operators are the primary fields of the theory, it is the vertex operators which we expect to have scale-invariant boundary conditions, rather than the bosonic fields $\tilde{\phi}$. The generalized boundary condition (8.58) can also be written as

$$e^{i\mathbf{n}^T \tilde{\phi}} = 1, \quad \mathbf{n} \in \Gamma_B, \tag{8.54}$$

where the rows of B are basis vectors of Γ_B, or

$$\Gamma_B = \mathrm{Latt}(B). \tag{8.55}$$

Strictly speaking, it is the boundary condition of the *normal-ordered* exponential which is conformally invariant, and the normal-ordered version of (8.54) has ∞ rather than 1 on the right-hand side.

To gain a better understanding of the generalized boundary condition (8.53), let us consider a physical realization of the termination of the edge. We start with an edge described by $\tilde{K}$ on $(-\infty, \infty)$. We then add the following potential term on $(-\infty, 0)$:

$$-\sum_{\mathbf{n} \in \Gamma_B} C_{\mathbf{n}} \cos(\mathbf{n} \cdot \tilde{\phi}) \tag{8.56}$$

where the k-dimensional lattice Γ_B is a sublattice of $\tilde{\Gamma}_c$. The vectors in Γ_B satisfy

$$\mathbf{n}^T \tilde{K}^{-1} \mathbf{n}' = 0, \quad \mathbf{n}, \mathbf{n}' \in \Gamma_B \tag{8.57}$$

and $C_{\mathbf{n}} > 0$ are very large, so that the potential consistently pins $\tilde{\phi}$ to the potential minima, and opens an energy gap in the region $(-\infty, 0)$. Such a potential leads to the boundary condition

$$B^T \tilde{\phi} = 2\pi \mathbf{n}, \quad \mathbf{n} \in \mathrm{Latt}(I_{k \times k}) \tag{8.58}$$

From the above discussions, we can draw two conclusions. First not all B matrices are consistent with the periodicity properties of $\tilde{\phi}$. To specify a valid termination of an edge, B not only must satisfy (8.17), the rows of B must also be in the $\tilde{\Gamma}_c$ lattice, or

$$\text{Latt}(B) \subset \tilde{\Gamma}_c \tag{8.59}$$

Second, two B matrices, B_1 and B_2, give rise to the same *generalized* boundary condition if

$$B_1 = B_2 M, \quad M \in GL(k, Z) \tag{8.60}$$

Such a pair of B matrices are regarded as equivalent:

$$B_1 \cong B_2 \tag{8.61}$$

Note that the above equivalence relation for generalized boundary condition is stronger (i.e., has smaller equivalence classes) than the equivalence relation $B_1 \sim B_2$ defined in (8.18) for the simple boundary condition $B^T\tilde{\phi} = 0$. *The equivalence classes (defined by (8.60)) of the B matrices that satisfy (8.17) and (8.59) label different terminations (or fixed points) of the edge.*

Now the question is what are the allowed vertex operators on the boundary. A boundary vertex operator has the form $V_{\mathbf{l}}^b = e^{i\mathbf{l}^T\tilde{\phi}}$, where $\mathbf{l}$ is vector in a k dimensional lattice Γ_{q_B} (called the boundary quasiparticle lattice). To determine $\tilde{\Gamma}_{q_B}$ we note that $V_{\mathbf{l}}^b$ changes one boundary condition $B^T\tilde{\phi} = 2\pi\mathbf{n}$ to another $B^T = 2\pi(\mathbf{n} + B^T\tilde{K}^{-1}\mathbf{l})$. Thus in order for $B^T\tilde{\phi} = 2\pi(\mathbf{n} + B^T\tilde{K}^{-1}\mathbf{l})$ to be an allowed boundary condition, $B^T\tilde{K}^{-1}\mathbf{l}$ must an integral vector. Also, we require that $V_{\mathbf{l}}^b$ only shift the combination $B^T\tilde{\phi}$. In particular, $V_{\mathbf{l}}^b$ does not shift the combination $\mathbf{l}'^T\tilde{\phi}$, $\mathbf{l}' \in \tilde{\Gamma}_{q_B}$. This leads to the condition $\mathbf{l}^T\tilde{K}^{-1}\mathbf{l}' = 0$ for any $\mathbf{l}$, $\mathbf{l}'$ in Γ_{q_B}. The above two conditions allows us to determine Γ_{q_B}:

$$\Gamma_{q_B} = \tag{8.62}$$
$$\text{Latt}(\tilde{K}B(B^TB)^{-1} - \frac{1}{2}B(B^TB)^{-1}B^T\tilde{K}B(B^TB)^{-1}).$$

The scaling dimension of $V_{\mathbf{l}}^b$ is given from (8.51) by

$$h^b(\mathbf{l}) = \mathbf{l}^T K^{-1}B(B^T\tilde{\Delta}B)^{-1}B^T K^{-1}\mathbf{l}. \tag{8.63}$$

In the above discussion of termination points, we have ignored any symmetry properties and the related selection rules. In particular, the boundary condition characterized by B may not conserve the electric charge. As a result, a boundary vertex operator may not carry a definite electric charge. In order for the termination labeled by B to conserve the electric charge, we must require the B matrix to satisfy

$$B^T\tilde{K}^{-1}\tilde{\mathbf{q}} = 0. \tag{8.64}$$

In this case, we find that $B^T\tilde{\phi}$, the fields that are about to be set to a constant, commute with the electric charge density operator ρ_e. For charge-conserving termination points, the electric charge of a boundary vertex operator $V_{\mathbf{l}}^b$ is found to be

$$Q = \tilde{\mathbf{q}}^T\tilde{K}^{-1}\mathbf{l}. \tag{8.65}$$

The condition (8.64) ensures the vertex operators of form $e^{\mathbf{n}_B^T\tilde{\phi}}|_{\mathbf{n}_B\in\Gamma_B}$ are all neutral, so that they can be set to one without violating the charge conservation. For a general B, the above vertex operators carry nonzero charges and setting them to one violates the charge conservation.

For a general boundary condition B, the charge is not conserved, but some other quantities may be conserved. On the edge there are $2k$ conserved currents (at low energies) $j_a = \partial_t\tilde{\phi}_a$, one for each branch. Near the boundary k combinations of the $2k$ conserved currents remain conserved. These k combinations are given by $B^T\partial_t\tilde{\phi}$. Thus a boundary operator $V^b\mathbf{l}$ carries k definite combined charges:

$$\mathbf{Q} = B^T\tilde{K}^{-1}\mathbf{l}. \tag{8.66}$$

To determine the stability of a fixed point, we also need to know which boundary operator $V_\mathbf{l}^b$ can appear in the boundary Hamiltonian. First let us discuss the corresponding issue along the edge. Along the edge, the lattice $\tilde{\Gamma}_c$ label all the mutually local operators. Some carry fermionic statistics, and thus are not allowed in the edge Hamiltonian. Only the subset described by $\tilde{\Gamma}_{c0}$ can appear in the edge Hamiltonian. ($\tilde{\Gamma}_{c0}$ is formed by all the bosonic operators in $\tilde{\Gamma}_c$.) If the charge is conserved, we further require the operators in $\tilde{\Gamma}_{c0}$ to be neutral.

On the boundary, only a subset of the boundary operators can appear in the boundary Hamiltonian. Since there is no statistics within the $0+1$ dimensional boundary, we only need to check the conservation of the k combined charges. The values of the combined charge Q_a, $a = 1, .., k$ allows us to determine which boundary operators can appear in the boundary Hamiltonian..

8.3 Image-charge picture and nonchiral fields

This section shows how the correlation functions can be calculated from a simple image-charge picture when the chiral bosonic fields are unified into nonchiral bosons, as is important for a number of applications. In particular, we find the falloff of the expectation value away from the boundary of a vertex operator $e^{i\Phi}$ pinned to 1 at the boundary, and how the two-body correlations are affected by the boundary. The correlation functions of vertex operators found earlier in this chapter are essentially quite simple: any correlation function of a vertex operator can be written as a product of exponentials of correlation functions of free chiral bosons. One subtlety is that after rescaling there may be more terms in these correlation functions than experimental points in the original problem, since fields at the same physical point become different points in the rescaled coordinates. Some additional structure appears in the correlations when the chiral fields are combined into nonchiral fields on the half-line, as in the boundary sine-Gordon model.

In practice it is useful to combine the chiral fields ϕ_i on the whole line into nonchiral bosons Φ_i defined on the half-line $x < 0$, in cases where the fields for $x > 0$ are the same as those for $x < 0$. As an example, the applicability of the integrable boundary sine-Gordon model used in [38] to determine tunneling behavior depends on the mapping to the half-line. The system on the half-line can be understood as a classical

system on the $x > 0$ half of the (x,t) plane, so that the physics known about such statistical-mechanical systems with boundaries is applicable. The technical motivation is that the theory on the half-line will be invariant at the fixed points under all the conformal generators which preserve the line $x = 0$. In what follows we show that the correlation functions of the nonchiral fields can be understood from an "image charge" picture (similar to electrostatics), and that the tunneling fixed points can be understood as "ordinary" and "extraordinary" transitions on the half-plane.

For each chiral boson field on the whole line ϕ_j, define the nonchiral field Φ_j on the half-plane $x < 0$ by $\Phi_j(z) = \phi_j(z) + \phi_j(\bar{z})$, where $z = t + ix$. (We use imaginary time t so that conformal invariance is manifest.) Note that if z has $x > 0$, $\bar{z}$ has $x < 0$ and that Φ_j has both left-moving and right-moving parts. The vertex operators $\exp(i\alpha\Phi_j)$ will have different behavior depending on whether ϕ changes sign at $x = 0$. First, with $\eta_j = \pm 1$ the sign gained by ϕ_j across $x = 0$, for nonzero α

$$\langle e^{i\alpha\Phi_j(0,t)} \rangle = \begin{cases} 0 & \eta = 1 \\ \infty & \eta = -1 \end{cases} . \tag{8.67}$$

Here and in the sequel we use the normal-ordered exponential, which has maximum value ∞ rather than 1. Also, below we will consider the case where $\Phi_j(0,t)$ is not pinned simply to 0 but to some set of values. The profile of the order parameter near the boundary can be calculated simply:

$$\begin{aligned} \langle e^{i\alpha\Phi_j(x,t)} \rangle &= \langle e^{i\alpha\phi_j(x,t)} e^{i\alpha\phi_j(-x,t)} \rangle \\ &= \begin{cases} 0 & \eta = 1 \\ (2x)^{-\alpha^2} & \eta = -1 \end{cases} . \end{aligned} \tag{8.68}$$

The above is the simplest case of the image-charge idea of Cardy [44, 45]: a correlation function of n nonchiral fields on the half-plane is expressed as a correlation of $2n$ chiral fields on the full plane. For the boundary conditions we are considering, the full-plane correlation functions are known from (8.42), so the half-plane correlation functions of Φ_j can be determined. The two-body function shows different scaling along the boundary from that in the bulk: (here index j suppressed)

$$\begin{aligned} & \langle e^{i\alpha\Phi(z_1)} e^{-i\beta\Phi(z_2)} \rangle \\ = \; & \langle e^{i\alpha(\phi(z_1)+\phi(\bar{z}_1))} e^{-i\beta(\phi(z_2)+\phi(\bar{z}_2))} \rangle \\ = \; & \begin{cases} \delta(\alpha-\beta) \left(\frac{4x_1 x_2}{|z_1 - z_2|^2 |z_1 - \bar{z}_2|^2} \right)^{\alpha^2} & \eta = 1 \\ \frac{|z_1 - \bar{z}_2|^{2\alpha\beta}}{(2x_1)^{\alpha} (2x_2)^{\beta} |z_1 - z_2|^{2\alpha\beta}} & \eta = -1. \end{cases} \end{aligned} \tag{8.69}$$

For example, in the $\eta = 1$ case, the equal-x correlation falls off as $(t_1 - t_2)^{-4\alpha^2}$ for $t_1 - t_2 \gg x$, while far from the boundary ($t_1 - t_2 \ll x$) the falloff is only as $(t_1 - t_2)^{-2\alpha^2}$, i.e., with the bulk scaling dimension. For $\eta = -1$ the correlation along the boundary is constant at long distances, with leading correction $(t_1 - t_2)^{-\alpha^2}$. The critical theory with $\eta = -1$ corresponds to the "extraordinary" transition in statistical mechanics, where the boundary is ordered (the order parameter $\exp(i\Phi)$ has nonzero expectation value) but the bulk is not, while the $\eta = 1$ theory corresponds to the "ordinary" transition.

Some aspects of the above picture change when the field $\Phi(0,t)$ is pinned to more than one value, e.g., to the minima $\Phi = 2\pi r n$, $n \in \mathbf{Z}$ of $\cos(\Phi/r)$. Now there is an additional average over $\Phi_0 = 0, \pm 2\pi r, \pm 4\pi r, \ldots$ in the correlation functions. The two-body correlation is unchanged, but the one-body correlation for $\eta = -1$ is now

$$\langle e^{i\alpha\Phi_j(x,t)} \rangle = \begin{cases} (2x)^{-\alpha^2} & \alpha = n/r,\ n \in \mathbf{Z} \\ 0 & \text{otherwise} \end{cases} , \tag{8.70}$$

which is natural as only those operators invariant under the symmetry transformation $\Phi \to \Phi + 2\pi r$ can have nonzero expectation values.

Chapter 9

Effects of short-range interactions

In this chapter we consider the effect of short-range interactions on tunneling through a point contact between two Laughlin states. In the absence of interactions, the nonlinear $I-V$ curve was found exactly by Fendley, Ludwig, and Saleur [38] via a mapping onto the integrable boundary sine-Gordon (BSG) model. First we show in the BSG formalism that a simple solvable model incorporating interactions gives a continuous renormalization of the effective fractional charge appearing in the $I-V$ characteristic. We use the BSG formalism since we will eventually be interested not only in the fixed points, which can equally well be described in the B-matrix formalism of Chapter 7, but also in the crossover. The $I-V$ curve measured in tunneling experiments in real systems, where the screened Coulomb interaction is present, will thus be sensitive in some geometries (discussed below) to nonuniversal electron-electron interactions. Our model is different from that of Pryadko *et al.* [48], which uses a long-range Coulomb interaction regularized by an opening angle at the junction.

The effective action describing tunneling between edges of two Laughlin states with filling fractions $\nu_1 = 1/m_1$, $\nu_2 = 1/m_2$ is

$$\begin{aligned} S &= S_{\text{free}} + S_{\text{tun}}, \\ S_{\text{free}} &= \frac{1}{4\pi}\int dx\, dt \sum_{ij}[K_{ij}\partial_t\phi_i\partial_x\phi_j - V_{ij}\partial_x\phi_i\partial_x\phi_j], \\ S_{\text{tun}} &= \Gamma\delta(x)(e^{im_1\phi_1 - im_2\phi_2}). \end{aligned} \tag{9.1}$$

Here the matrix K, which describes the statistics of the vertex operators $e^{in_i\phi_i}$ created from the bosonic fields, is

$$K = \begin{pmatrix} m_1 & 0 \\ 0 & -m_2 \end{pmatrix} \tag{9.2}$$

where we have taken the two edges to propagate in opposite directions. If V is diagonal the physics is independent of whether the modes are copropagating or counterpropagating, but we are interested in the case of general V in which case there are differences, as seen below. If the positive definite matrix V is diagonal, its two entries V_{11} and V_{22} are the velocities of the two modes. The off-diagonal elements of V correspond to a density-density interaction across the two edges, since the electron density is proportional to $\partial_x\phi_i$ for each mode.

The above action maps onto a boundary sine-Gordon model, with boson radius determined by the filling fractions of the original states and by the matrix V. The boundary sine-Gordon model contains one nonchiral boson (i.e., with both left and right components) on the half-line. The mapping consists of rotating the fields ϕ_1, ϕ_2 so that one new combination $\tilde{\phi}_1$ is proportional to the exponent $m_1\phi_1 - m_2\phi_2$ in $S_{\rm tun}$, while $\tilde{\phi}_2$ does not appear in $S_{\rm tun}$ and hence is free. Then folding the field $\tilde{\phi}_1$ onto the half-line and rescaling gives the action

$$S_{\rm BSG} = \int dt \int_{-\infty}^{0} dx [\frac{(\partial_x \Phi)^2}{2} + \frac{(\partial_t \Phi)^2}{2} + \cos(\beta\Phi/2)]. \tag{9.3}$$

The constant β, given for diagonal V by $\beta = \sqrt{4\pi/(\frac{1}{\nu_1} + \frac{1}{\nu_2})}$, gives the tunneling term in (9.3) the same scaling dimension $\Delta = ({m_1}^2 + {m_2}^2)/2$ as in (9.1). The velocities of the edge modes, defined as the velocities in a basis where V is diagonal, should strictly speaking be equal for this rotation of fields to be valid, but since the tunneling takes place at a point and there is no coherence along the edge, a difference in velocities should not have much effect.

In order to calculate the conductance across the tunneling junction, the effective β which appears in $S_{\rm BSG}$ needs to be determined, as well as the contribution $q_{\rm eff}$ to the current from each tunneling event. Previously only certain discrete values of β, corresponding to tunneling between Laughlin states, were thought to be physically relevant for edge tunneling. This is because a general β describes tunneling between two chiral Luttinger liquids with continuous Luttinger parameter, but only specific values of the Luttinger parameter correspond to quantum Hall states $\nu = 1/m$. The main result of this chapter is that tunneling between Laughlin states *with non-diagonal* V is described by the boundary sine-Gordon model with continuously varying β and $q_{\rm eff}$.

The model which we solve exactly has a region of constant interaction strength (between contacts V_1 and V_2 in Fig. 9-1) and zero interaction elsewhere. It is essential that the two modes in the interaction region be oppositely directed, so that the scaling dimension of the tunneling operator is affected by V. The first step is to write the positive definite matrices V and Δ in terms of a "boost" parameter τ. The advantage of doing so is that Δ is only a function of τ and not of the eigenmode velocities v_i which affect V; the boost decomposition [37] isolates the dependence of Δ on as few parameters as possible.

$$\begin{aligned} V &= K^{1/2} B \begin{pmatrix} v_1 & 0 \\ 0 & v_2 \end{pmatrix} B K^{1/2}, \\ \Delta &= K^{1/2} B \begin{pmatrix} 1 & 0 \\ 0 & 1 \end{pmatrix} B K^{1/2}, \\ K^{1/2} &= \begin{pmatrix} \sqrt{m_1} & 0 \\ 0 & \sqrt{m_2} \end{pmatrix}, \\ B &= \begin{pmatrix} \cosh\tau & \sinh\tau \\ \sinh\tau & \cosh\tau \end{pmatrix}. \end{aligned} \tag{9.4}$$

Now the scaling dimension and transferred charge of the tunneling operator can be simply expressed in terms of $\Delta(\tau)$. In the following we will specialize to the case

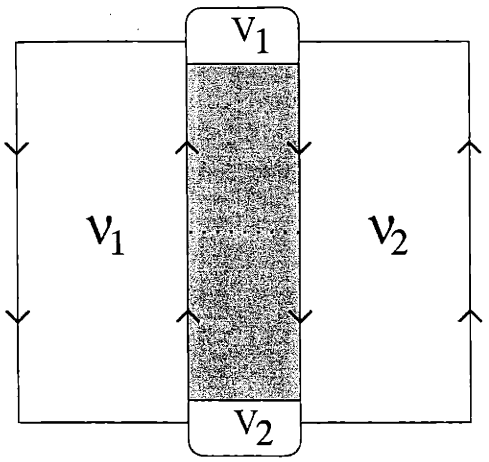

Figure 9-1: Possible experimental geometry for point tunneling between quantum Hall states ν_1 and ν_2. The density-density interaction between edges is nonzero in the shaded region, and zero elsewhere. The two contacts at voltages V_1 and V_2 are assumed to populate edge modes propagating away from the contact up to energy eV.

$m_1 = 1$, $m_2 = 3$, i.e., a $\nu_1 = 1$ edge and $\nu_2 = \frac{1}{3}$ edge propagating in opposite directions. The results generalize simply to other values of m_1 and m_2, although the boundary sine-Gordon crossover result used below requires that at most one relevant operator be present, restricting m_1 and m_2 somewhat [38].

The intuitive meaning of the effective charge transfer can be understood by considering the "charge-unmixed" point $\tau = 0$ where one of the two eigenmodes (i.e., modes which diagonalize K and V) is neutral, and one charged. Then in this basis the tunneling operator, which is neutral, is of the form $\exp(iC\phi_n) + \text{h.c.}$ for some constant C. The tunneling operator for this value of τ does not transfer any charge from one eigenmode to the other, since only one eigenmode carries charge. Hence the conductance measured across the junction is *independent* of the rate of tunneling events determined by the coefficient of the tunneling operator. The value $\tau = \log(1+\sqrt{3}/\sqrt{2})$ corresponds to decoupled $\nu = 1$ and $\nu = 1/3$ edges in the interaction region, which has been previously studied in a number of works. [35, 42, 40]

The scaling dimension of the tunneling operator $\exp(im_i\phi_i)$ is $\frac{1}{2}\mathbf{m}\Delta(\tau)\mathbf{m}$. The effective tunneling charge is determined by how far the neutral tunneling operator $\mathbf{m}$ is from being an eigenmode of the system: $q_{\text{eff}} = \frac{e}{2}\mathbf{q}\Delta\mathbf{m}$, which is zero if $\mathbf{m}$ is an eigenmode and grows as Δ moves away from the charge-unmixed point. The current measured across the two contacts of Fig. 9-1 if there is no electron tunneling across the junction (if $V_1 - V_2$ is small) is $I = (V_1 - V_2)(\frac{2}{3} + \frac{1}{2}(\sigma_1 + \sigma_2))$, where σ_1 and σ_2 are the conductances along the edges in the interaction region of Fig. 9-1. We use the identity $\sigma_1 + \sigma_2 = \mathbf{t}\Delta\mathbf{t}$ in what follows.

The total change in conductance from small V to large V is fixed by the scaling dimension of the electron tunneling operator and the effective tunneling charge. From previous work [46], it is known that if the effective tunneling charge is 1, the conductance change is $\frac{e^2}{h\Delta}$, where Δ is the scaling dimension of the electron tunneling

operator. For instance, in tunneling between two $\nu = 1/3$ states, the conductance change between no tunneling (two Hall droplets) and no backscattering (one Hall bar) is $\frac{e^2}{3h} = \frac{e^2}{h\Delta}$. In the case of interactions, e must be replaced by the effective charge transfer per tunneling event $q_{\rm eff}$. Hence for the system of Fig. 9-1,

$$\begin{aligned} \frac{h\sigma_{\max}}{e^2} &= \frac{2}{3} + \frac{\mathbf{t}\Delta\mathbf{t}}{2} = \frac{2+\cosh(2\tau)}{3}, \\ \frac{h\sigma_{\min}}{e^2} &= \frac{2}{3} + \frac{\mathbf{t}\Delta\mathbf{t}}{2} - \frac{(\mathbf{t}\Delta\mathbf{m})^2}{2\mathbf{m}\Delta\mathbf{m}} \\ &= \frac{2+\operatorname{sech}(2\tau)}{3}. \end{aligned} \tag{9.5}$$

In fact the whole conductance curve between these two values can be calculated from the mapping to $S_{\rm BSG}$. Before doing so, there is a simple check on our results which gives some insight into why the above values are natural. Assuming conservation of energy (i.e., no dissipation at the junction [47]) gives two possible values of the current: $I = (V_1 - V_2)(\frac{2}{3} + \frac{1}{2}(\sigma_1 + \sigma_2))$, corresponding to no tunneling current, and $I = (V_1 - V_2)(\frac{2}{3} + \frac{2}{9(\sigma_1+\sigma_2)})$. The two corresponding values of the conductance are exactly those in (9.5). Thus our calculation reproduces the asymptotic values of the conductance consistent with zero-dissipation fixed points.

The current-voltage characteristic can be calculated (Fig. 9-2) up to one overall constant in the energy scale, which corresponds to the initial strength of tunneling. [38] The result is, with $V = V_1 - V_2$ and $\sigma_{\max}$ as in (9.5),

$$\begin{aligned} I &= \sigma_{\max} V - I_{\rm tun}, \\ I_{\rm tun} &= \begin{cases} I^{(1)} & \text{if } V < T_B \Delta^{-1/(2-2/\Delta)} \sqrt{\Delta - 1} \\ I^{(2)} & \text{if } V \geq T_B \Delta^{-1/(2-2/\Delta)} \sqrt{\Delta - 1} \end{cases}, \\ I^{(1)} &= \frac{q_{\rm eff}^2 V}{h} \sum_{n=1}^{\infty} f_n(\Delta), \\ I^{(2)} &= \frac{q_{\rm eff}^2 V}{h\Delta} \left(1 - \sum_{n=1}^{\infty} \frac{f_n(1/\Delta)}{\Delta} \right), \\ f_n(g) &= \frac{(-1)^{n+1} \sqrt{\pi} \gamma(ng)}{2\Gamma(n)\Gamma(3/2 + n(g-1))} \left(\frac{eV}{T_B'} \right)^{2n(g-1)}. \end{aligned} \tag{9.6}$$

Here T_B is some cutoff-dependent constant which may vary with the boost parameter τ. This calculated current should be relevant as long as the interaction strength is nearly constant in the region around the tunneling junction. The details of the interaction far away from the tunneling junction should not matter as long as current is conserved in the incoming and outgoing edge branches.

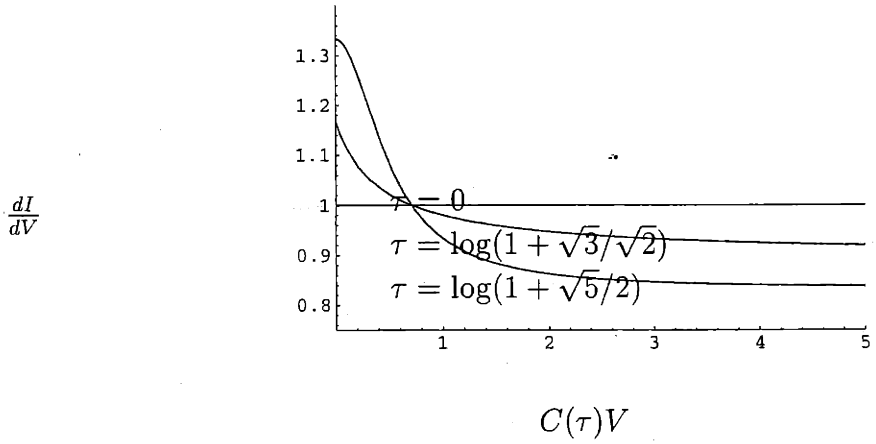

Figure 9-2: Differential conductance dI/dV in units of e^2/h versus scaled voltage $C(\tau)V$ for three different values of interaction strength (boost parameter) τ. The horizontal axis is expected to scale by a different cutoff-dependent constant $C(\tau)$ for each value of τ.

Chapter 10

Conclusions

In this chapter we summarize the main conclusions of this thesis and also mention some possible avenues for further investigation. The first part of the thesis developed a technique for studying impurity scattering in a general FQH edge and used it to find phase diagrams and experimentally measurable weak-tunneling properties for a broad class of nonchiral edges. We find that some FQH edges can have several different phases (fixed points) in the presence of randomness. These phases in general have higher symmetry at low energies and long wavelengths than the original system. Thus random edges demonstrate an interesting phenomenon of dynamical restoration of symmetries at low energies and long length scales. Different phases have different experimentally observable properties. It would be very interesting to find these phases and study transitions between them experimentally.

The transitions between phases are interesting from the point of view of Landau's symmetry breaking principle for continuous transitions: A continuous phase transition (second-order in the Ehrenfest classification) can only occur between two phases which differ in symmetry, and the symmetries of one phase are a subset of the symmetries of the other phase. This principle appears to be satisfied by all the transitions between definitely stable fixed points in the edges we study. The principle is satisfied even though the RG flows for some transitions (such as the $\nu = 2/3$ transition [18]) are similar to those in the Kosterlitz-Thouless transition, which is not clearly interpreted in terms of a broken symmetry. The symmetry breaking principle also has some implications for a possible phase transition in the $\nu = 5/3$ state, which has two types of possibly stable fixed points.

To summarize the properties of disordered edge states, two situations, with or without long-range interactions, need to be discussed separately. We have emphasized the fixed points which occur when disorder is relevant and the resulting effective interaction matrix V has decoupled charged and neutral modes. These fixed points are appropriate if the starting interactions are close enough to charge-unmixed, as for an unscreened Coulomb interaction, that disorder is relevant. For initial conditions which are not nearly charge-unmixed, all the edge modes, in general, carry some amount of charge (the edge is charge-mixed). Several different situations are illustrated by the following examples.

- The $\nu = 2/3$ edge has two phases. In one phase the edge is charge-mixed

and the two-terminal conductance σ and the exponent α of electron tunneling between two edges $\sigma_{tun} \propto T^{\alpha}$ are not universal. In the other phase the edge has an $SU(2)$ symmetry and is charge-unmixed (*i.e.* only one propagating mode, the charge mode, carries charge and other propagating modes are neutral). In this case (σ, α) take universal values $(\frac{2}{3}\frac{e^2}{h}, 2)$.

- The $\nu = 3/5$ edge has three phases, described by a fixed point (the point $(0, 0)$ in Fig. 3-1), fixed lines (the solid lines outside the hexagon bounded by the dashed lines in Fig. 3-1) and fixed planes (the region outside the region bounded by the dashed lines). This is because a point on the fixed planes does not flow as the energy is lowered, while a point between two paralell dashed lines flows to the fixed line between them and a point inside the hexagon flows to the fixed point. The fixed point has an $SU(3)$ symmetry and is charge-unmixed. $(\sigma, \alpha) = (\frac{3}{5}\frac{e^2}{h}, \frac{8}{3})$ are universal. The fixed-line and fixed-plane phases are charge-mixed and (σ, α) are not universal. But in the fixed-line phase there is an $SU(2)$ symmetry and (σ, α) and other exponents all depend on a single parameter which parametrizes the fixed line. The fixed-plane phase has no particular symmetries. We would like to point out that although the fixed-line phase in Fig. 3-1 contains six disconnected segments, this does not guarantee that there are six disconnected fixed-line phases. This is because the disconnected fixed lines may be connected in a higher-dimensional space of Lagrangians of which Fig. 3-1 is just a two-dimensional cross section. If different line segments are connected in the enlarged space, it is possible to move continuously from one segment to another without any transition. For the $\nu = 3/5$ state the higher-dimensional space results from applying the $SU(3)$ transformation on the the full Lagrangian. Note that the $SU(3)$ transformation does not change the commutators between fermions (which can be seen in the fermionic form of the Lagrangian but is not evident in the (Abelian) bosonized form), and hence leaves the Hilbert space unchanged. Acting with the $SU(3)$ generators creates off-diagonal interaction terms of the form $f(x)(\bar{\psi}_1\psi_2)(\bar{\psi}_2\psi_2)$, after we make the local $SU(3)$ transformation to remove the random hopping term between different fermions. Thus the precise form of the function $f(x)$ depends on the impurities which generate the random hopping terms. If the off-diagonal terms have precisely the variable coefficients $f(x)$, then the different fixed-line phases can be continuously connected via inclusion of such off-diagonal terms. However, in real experiments it is impossible to control the precise form of the variable coefficients $f(x)$, and the Lagrangians for experimental samples do not contain the above off-diagonal terms. Therefore for real samples all different fixed-line phases are disconnected. Similarly all fixed planes are disconnected for real samples. However, since fixed-line phases (or fixed-plane phases) all have the same symmetry, the symmetry breaking principle prohibits continuous phase transitions between two connected fixed-line phases or two connected fixed-plane phases. But there are still continuous phase transitions between a fixed-line phase and a fixed-plane phase, and a fixed-line phase and a fixed-point phase.

We would like to stress that the sequence of the phase transition: fixed-point phase $\to$ fixed-line phase $\to$ fixed-plane phase represents a sequence of symmetry breaking: $SU(3) \to SU(2) \to SU(1)$. This is consistent with the symmetry breaking principle discussed above. It appears that the symmetry breaking principle that governs the continuous transitions between clean phases in other condensed matter systems also governs the continuous transitions between disordered phases of FQH edges. All the continuous phase transitions between different disordered edge phases that we find in this thesis are related to symmetry breaking.

- The $\nu = 5/3$ edge also has three (types of) phases described by fixed points (such as B in Fig. 3-2, but not A), fixed lines (the solid lines in Fig. 3-2) and fixed planes (the region outside the region bounded by the dashed lines). Again the fixed-point phase is charge-unmixed and has universal (σ, α). The fixed-line and fixed-plane phases are charge-mixed and have non-universal (σ, α). However, here the fixed point contains two marginal operators. It is not clear whether the fixed point is stable or not (depending on whether the two marginal operators are marginally relevant or not). It is not clear if different fixed lines and fixed planes are connected or not in a higher-dimensional space. There is a continuous phase transition between the fixed-line phase (with $SU(2)$ symmetry) and fixed-plane phase (with no symmetry). We note that both the fixed-point phase and the fixed-line phase have $SU(2)$ symmetry. According to the symmetry breaking principle for continuous transition, either there is another phase separating the the fixed-point phase and the fixed-line phase, or the fixed-point phase is unstable, or the transition is first-order (discontinuous) and the first-order line does not terminate in a second-order point for any finite disorder strength. The perturbative RG in Appendix B is consistent with the last possibility.

- The $\nu = 17/13$ edge ($K = (1, 4, -4)$) again has three phases described by a fixed point, a fixed line and a fixed plane. (Fig. 3-3) However, the phase diagram is quite different from the above two. There can only be continuous phase transitions between the following phases: the fixed-point phase (with $SU(2)$ symmetry) $\Longleftrightarrow$ the fixed-plane phase (with no symmetry) $\Longleftrightarrow$ the fixed-line phase (with $SU(2)$ symmetry).

- The $K = (l, 2, -2, 2)$ and $K = (l, -2, 2, -2)$ edges are too complicated, and we will only discuss them for the case of long-range interactions.

In the presence of long-range interactions the edge is always (nearly) charge-unmixed and the two-terminal conductance always takes the quantized value $\sigma = \nu \frac{e^2}{h}$. We can restrict our discussion to the charge-unmixed subspace (the $(0, 0)$ point in Fig. 3-1 and the x-axis in Fig. 3-2 and 3). Table II gives the low-temperature tunneling exponent for all the charge-unmixed phases of principal hierarchy states. The above examples with short-range interactions can be easily modified to cover the case of long-range interactions:

- The $\nu = 2/3$ edge has only one phase which is described by a fixed point. (σ, α) take universal values $(\frac{2}{3}\frac{e^2}{h}, 2)$.

- The $\nu = 3/5$ edge has only one phase, described by a fixed point (the point $(0,0)$ in Fig. 3-1). The fixed-point phase is the same as the fixed-point phase for short-range interactions: it has an $SU(3)$ symmetry and universal $(\sigma, \alpha) = (\frac{3}{5}\frac{e^2}{h}, \frac{8}{3})$.

- The $\nu = 5/3$ edge has two (types of) phases described by A-type and B-type fixed points in Fig. 3-2. The fixed-point phases have universal α given by $\alpha = 2/5$ for A-type and $\alpha = 0$ for B-type. However both A-type and B-type fixed points contain two marginal operators, and it is not clear whether the fixed points are stable.

- The $\nu = 17/13$ edge ($K = (1, 4, -4)$) has three phases described by two fixed points (A and B in Fig. 3-3) and a fixed line (the x-axis outside the region bounded by the dashed lines). All three phases are stable. The two fixed-point phases have different universal values for the temperature exponent: $\alpha = 2$ for the A-type and $\alpha = 18/17$ for the B-type fixed-point phase. α is not universal for the fixed-line phase. The only continuous phase transitions are between one of the two fixed-point phases ($SU(2)$ symmetry) and the fixed-line phase (no symmetry).

- The $K = (l, 2, -2, 2)$ and $K = (l, -2, 2, -2)$ edges with $\nu = 12/7, 12/17, ...$ are very interesting. There are four different phases described by three types of fixed points (A, B, C in Fig. 3-4 and 5) and a fixed line (the middle segment of the dashed line connecting A and B in Fig. 3-5). Certainly there are infinitely many different disconnected A-, B-, C-type fixed points and fixed lines in Fig. 3-5, and it is not clear if all fixed points (lines) of each type are connected in a higher-dimensional space. The A-type fixed point has an $SU(3)$ symmetry, the B-type fixed point has an $SU(2) \times SU(2)$ symmetry, the fixed line and the C-type fixed point have an $SU(2)$ symmetry. The exponent α has the universal values (8/3, 2, 5/3) for the A-, B-, C-type fixed points respectively. The C-type fixed point has four marginal operators and it is not clear whether it is a stable fixed point. Among the three definitely stable phases the only possible continuous transitions are: A-type phases ($SU(3)$ symmetry) $\Longleftrightarrow$ fixed-line phase ($SU(2)$ symmetry) $\Longleftrightarrow$ B-type phases ($SU(2) \times SU(2)$ symmetry). These transitions are consistent with the symmetry breaking principle for continuous transitions. An A-type $\Longleftrightarrow$ B-type transition would violate the symmetry breaking principle and is not found in the phase diagram.

The Introduction mentioned the agreement between the χLL theory for incompressible edges and the composite-fermion theory for compressible edges, summarized in Fig. 5-1. This agreement raises the question of whether the phase which agrees with the CF theory is favored over the others at finite temperature. The phase agreeing with the CF approach has the lowest value of the tunneling exponent and has the lowest free energy at finite temperature *if* all phases are equivalent to (have the

same partition function as) clean systems, as for the solvable phases. Hence it would be worthwhile to find out whether this property holds for the currently unsolvable phases.

This question is especially important for edges such as $\nu = 12/17$, where the phase agreeing with the CF approach is the only one which cannot be solved, and hence whose stability is uncertain for strong disorder. The solvable fixed points are distinguished from unsolvable ones by having only operators which couple copropagating modes; all operators coupling counterpropagating modes are irrelevant and scale to zero. The edges with nonzero coupling between counterpropagating modes form an interesting "universality class" of one-dimensional disordered systems: they differ from ordinary one-dimensional localization by having an asymmetric left-right coupling.

In Chapter 6 and Appendix B we found the renormalization-group flows for random hopping operators on a quantum Hall edge. This extends previous results on the left-right symmetric case [26] to disorder operators of nonzero "conformal spin" $|K(\mathbf{m})|$. The flows take a simple form in the boost coordinate system, and verify that charge-neutral separation is a generic feature of principal hierarchy states once random hopping is relevant.

The main result of the second part of this thesis (Chapters 7-9) is the analysis of a large class of strong tunneling fixed points. Tunneling fixed points can be understood as conformally invariant boundary conditions once the edge-junction system is folded onto the half-line. We find the restrictions on allowable boundary conditions and the resulting correlation functions for vertex operators at the fixed points. Another result is the lattice of allowed boundary operators, both charged and neutral, for a given boundary condition. The correlation functions in the presence of a boundary can be understood through an "image-charge" picture, and take a simple form which becomes more complex when the original chiral bosons are combined into nonchiral fields as for the boundary sine-Gordon model. The two-point correlation function of a vertex operator can show different behavior (a change in scaling dimension) as the two locations are moved toward the boundary.

We solve a simplified model of how interactions between electrons on different edges affect tunneling through a point junction. Most current tunneling experiments involve multiple contacts between the two edges and variable interaction strengths along the edge, but the basic result that interactions can complicate the identification of the effective tunneling charge should still apply. The model we consider maps onto the solvable model of Fendley *et al.*with a *continuous* effective filling fraction, giving a physical realization of this result beyond the discrete cases $\nu_{eff} = 1,1/2,1/3$ known previously.

The boundary condition formalism should be able to shed some light on a few open questions. In edges with multiple modes there can be several strong-tunneling fixed points [47], which can be analyzed using our formalism. An experimentally measurable quantity which we have not touched on to this point is the shot noise, which gives information about the tunneling charges in a quantum Hall system. The finite-frequency shot noise in particular is a very useful probe of quasiparticle properties and is not yet understood for a general edge. By this point the reader will no

doubt agree that the edges of fractional quantum Hall states show an amazing variety of beautiful phenomena. It is the author's feeling that equally beautiful phenomena remain to be discovered in this seemingly simple one-dimensional system.

Appendix A

Boosts and Rotations

The decomposition of an element of $SO(m,n)$ into a product of a boost and a rotation follows in a neighborhood of the origin simply by writing the product $M = BR$ in terms of infinitesimal generators of the Lie group. If b_i are the boost generators and r_i the rotation generators, then a boost (similarly, rotation) close to the identity element contains only boost (rotation) generators:

$$BR = (1 + \epsilon_i b^i)(1 + \delta_j r^j) \approx 1 + \epsilon_i b^i + \delta_j r^j, \tag{A.1}$$

where ϵ_i and δ_j are arbitrary infinitesimal parameters. There are exactly enough free parameters to cover a neighborhood of the identity in $SO(m,n)$. Thus if the decomposition does not hold on the entire group, there must be some boundary in $SO(m,n)$ where it ceases to hold. In the next paragraph we outline a global proof of the decomposition. The details are given for $SO(m,1)$, which is the only case used in the body of this thesis.

The boost part of a given matrix M can be constructed if every symmetric positive definite element of $SO(m,n)$ has a square root within the group which is also symmetric. The square root is simple for $m = 1$ or $n = 1$, where every symmetric positive definite matrix is of the form introduced in Chapter 2 and associated with a unique velocity vector $\mathbf{v} = \mathbf{p}/\gamma$. Then the square root is the boost with velocity $\mathbf{v}' = \mathbf{v}(1 - \sqrt{1 - v^2})/v^2$, which is chosen so that the special-relativistic velocity addition formula holds: $\mathbf{v} = 2\mathbf{v}'/(1 + v'^2)$. For the general $SO(m,n)$ case, a square root can be defined by the Inverse Function Theorem within a neighborhood of the identity and analytically continued. Such a square root exists globally if every boost matrix can be written as an exponential of only boost generators, since then

$$B' = \exp\begin{pmatrix} \mathbf{0} & b \\ b^{\mathrm{T}} & \mathbf{0} \end{pmatrix}, \quad \sqrt{B'} = \exp\begin{pmatrix} \mathbf{0} & \frac{b}{2} \\ \frac{b^{\mathrm{T}}}{2} & \mathbf{0} \end{pmatrix}. \tag{A.2}$$

With a square root, the proof is simple. Given an arbitrary element $M \in SO(m,n)$, MM^{T} is symmetric and positive definite, so let $B \equiv \sqrt{MM^{\mathrm{T}}}$. It remains to show that $R \equiv B^{-1}M$ is in $SO(m,n)$ and is orthogonal:

$$\begin{aligned} RI_{m,n}R^{\mathrm{T}} &= B^{-1}MI_{m,n}M^{\mathrm{T}}B^{-1^{\mathrm{T}}} \\ &= B^{-1}I_{m,n}B^{-1^{\mathrm{T}}} = I_{m,n}, \end{aligned} \tag{A.3}$$

$$
\begin{aligned}
R^{\mathrm{T}}R &= (\sqrt{MM^{\mathrm{T}}}^{-1}M)^{\mathrm{T}}(\sqrt{MM^{\mathrm{T}}}^{-1}M) \\
&= M^{\mathrm{T}}(\sqrt{MM^{\mathrm{T}}}^{2})^{-1}M = I. \qquad \text{(A.4)}
\end{aligned}
$$

Appendix B

Perturbative Renormalization Group

This appendix uses the perturbative RG technique to study the effect of impurity scattering operators on the velocity matrix V in the chiral-Luttinger-liquid action. The K matrix does not flow and thus remains an integer matrix, which follows directly from the fact that K does not enter the Hamiltonian (i.e., it is "purely topological"). The constancy of K to leading order in D will be explicit in the results obtained below. In order to calculate the changes in V under a change in the cutoff, we expand a correlation function to first order in the disorder strength, then show that the terms proportional to the disorder strength can be interpreted as infinitesimal changes in the matrix V.

The real-space calculation is similar to previous RG calculations on 2D classical models [49, 50, 51] and 1D electrons [26]. The differences arise from the chiral nature of quantum Hall edge states. As an example, consider the correlation function of a vertex operator $O_{\mathbf{m}} = \exp(im_j\phi_j)$ in a nonchiral edge with one mode in each direction:

$$\langle O_{\mathbf{m}}(r_1)O^{\dagger}_{\mathbf{m}}(r_2)\rangle \propto (x + iv_+t)^{-\alpha}(x - iv_-t)^{-\beta} \tag{B.1}$$

with $\alpha - \beta = K(\mathbf{m})$ an even integer, $r_i = (x_i, t_i)$, $x = x_2 - x_1$ and $t = t_2 - t_1$, and (v_+, v_-) the velocities of the right and left moving modes. Unless $K(\mathbf{m}) = 0$ and $v_+ = v_-$, the correlation function has a phase as well as a magnitude.

First we treat the case of an edge with two modes, either parallel or antiparallel, and then show how the flows for an edge with more than two modes follow with no further computation.

The correlation function of an operator $O_{\mathbf{n}}$, expanded to first order in the disorder strength, is

$$\begin{aligned}
&\langle e^{in_j\phi_j(r_1)}e^{-in_j\phi_j(r_2)}\rangle_1 = \langle e^{in_j\phi_j(r_1)}e^{-in_j\phi_j(r_2)}\rangle_0 \times \\
&(1 - \int dr_3\, dr_4\, [\xi(x_3)\xi^*(x_4)\langle e^{im_j\phi_j(r_3)}e^{-im_j\phi_j(r_4)}\rangle_0]) \\
&+ \int dr_3\, dr_4\, [\xi(x_3)\xi^*(x_4)\times \\
&\qquad \langle e^{in_j\phi_j(r_1)}e^{-in_j\phi_j(r_2)}e^{im_j\phi_j(r_3)}e^{-im_j\phi_j(r_4)}\rangle_0].
\end{aligned} \tag{B.2}$$

Now carry out the disorder average $\{\xi(x)\xi^*(x')\} = D\delta(x-x')$ and consider the term with four correlation functions. Introduce $\mathbf{R} = (\mathbf{r}_3 + \mathbf{r}_4)/2, \mathbf{r} = \mathbf{r}_4 - \mathbf{r}_3$. Only configurations where the internal points $\mathbf{r}_3$ and $\mathbf{r}_4$ are near each other (i.e., separated by the cutoff a) contribute to the RG flows. [51] At this point assume for convenience that we are calculating the correlation function of the disorder operator itself ($\mathbf{m} = \mathbf{n}$). The symbol P_{12} denotes $(x + iv_+t)^{-\alpha}(x - iv_-t)^{-\beta}, x = x_2 - x_1, t = t_2 - t_1$. Because $\alpha - \beta = K(\mathbf{m})$ is even, $P_{12} = P_{21}$. The last term in (B.2) is now

$$D \int dX\, dT\, dt\, [\frac{P_{12}P_{34}P_{14}P_{23}}{P_{13}P_{24}}]. \tag{B.3}$$

The integrand is $P_{12}P_{34}\exp(g_{13} + g_{24} - g_{14} - g_{23}) \approx P_{12}P_{34}\exp(\mathbf{r}\cdot\nabla_{\mathbf{R}}(g(\mathbf{r}_1 - \mathbf{R}) - g(\mathbf{r}_2 - \mathbf{R})))$. Here $g_{ab} \equiv -\log(P_{ab}) = \alpha\log(x + iv_+t) + \beta\log(x - iv_-t)$. Disorder fixes $x = 0$ in $\mathbf{r} = (x,t)$ so the exponential is $\exp(t\partial_T(g(\mathbf{r}_1 - \mathbf{R}) - g(\mathbf{r}_2 - \mathbf{R}))) \approx 1 + t^2(\partial_T g(\mathbf{r}_1 - \mathbf{R}) - \partial_T g(\mathbf{r}_2 - \mathbf{R}))^2$. Hence we need to evaluate the following integral:

$$\begin{aligned} D \int dX\, dT\, dt\, P_{12}P_{34}[1 + t^2(&\frac{i\alpha v_+}{X - x_1 + iv_+(T - t_1)} \\ &- \frac{i\beta v_-}{X - x_1 - iv_-(T - t_1)} - \frac{i\alpha v_+}{X - x_2 + iv_+(T - t_2)} \\ &+ \frac{i\beta v_-}{X - x_2 - iv_-(T - t_2)})^2]. \end{aligned} \tag{B.4}$$

The constant term in the integrand cancels the leading term in the partition function in (B.2). When the square is expanded, products of denominators at the same point will cancel infinities arising in the calculation of products of denominators at different points, leaving a finite answer. The change of cutoff in the t integral will yield the RG equations at the end.

First consider the integrals of the α^2, β^2 terms. After rescaling the time variables by v_+, the α^2 integral is

$$\begin{aligned} &\int dX\, dT\, [\frac{1}{X + iT - x_1 - it_1}\, \frac{1}{X + iT - x_2 - it_2}] \\ &= \int dX\, dT\, [\frac{1}{z^2 - w^2}], \end{aligned} \tag{B.5}$$

with $z = X + iT, 2w = x_2 - x_1 + it_2 - it_1$. But this integral is not uniformly convergent at ∞ and thus not well-defined: for example, if $w = i$ the integral is 2π if the X integration is done first, 0 if the T integration is done first, and π if the integration is done in radial coordinates. We believe that the appropriate value of the integral (B.5) is 0, because in Minkowski space (real rather than imaginary time) the corresponding integral has integrand $(x + t - x_1 - t_1)^{-1}(x + t - x_2 - t_2)^{-1}$ and is unambiguously zero. Also, zero is the only value consistent with the fact that the randomness can be rotated away at the KFP fixed point, since at that point the RG flow of the velocity should be independent of the disorder strength.

The $\alpha\beta$ terms, give the renormalization of the scaling dimension Δ, are proportional to

$$I = \int dX\, dT\, [\frac{1}{c_-d_+} + \frac{1}{c_+d_-}],$$

$$c_\pm = X - x_1 \pm iv_\pm(T - t_1),$$
$$d_\pm = x_2 - X \pm iv_\pm(t_2 - T). \tag{B.6}$$

First do the dX integral as a contour integral. The poles of the first term are at $w_1 = x_1 + iv_-(T - t_1)$ and $w_2 = x_2 + iv_+(t_2 - T)$, and the integral vanishes unless the poles are on different sides of the real axis (likewise for the second term). Thus $T \notin [t_1, t_2]$ and we are left with

$$\begin{aligned} I &= \left(\int_{-\infty}^{t_1} dT + \int_{\infty}^{t_2} dT\right)\left[\frac{2\pi i}{y_1} - \frac{2\pi i}{y_2}\right], \\ y_1 &= x_2 - x_1 + iv_+t_2 + iv_-t_1 - i(v_+ + v_-)T, \\ y_2 &= x_2 - x_1 - iv_+t_1 - iv_-t_2 + i(v_+ + v_-)T. \end{aligned} \tag{B.7}$$

Hence

$$\begin{aligned} I &= \frac{2\pi}{v_+ + v_-}\log\left(\frac{a_1^+ a_1^- a_2^+ a_2^-}{(b^+b^-)^2}\right), \\ & a_1^\pm = x_2 - x_1 \pm i(v_+ + v_-)\infty + iv_+t_2 + iv_-t_1 \\ & a_2^\pm = x_2 - x_1 \pm i(v_+ + v_-)\infty - iv_+t_1 - iv_-t_2, \\ & b^\pm = x_2 - x_1 \pm iv_\pm(t_2 - t_1). \end{aligned} \tag{B.8}$$

The finite part of the result is independent of the order of integration, even though (B.6) is superficially even less well-defined than (B.5). The infinite part of the result is canceled by the $\alpha\beta$ terms in (B.4) with denominators at the same point. The dt integral is

$$\begin{aligned} \int_{-\infty}^{\infty} dt\, t^2 P_{34} &= 2\int_a^\infty dt\,[t^2(\frac{1}{iv_+t})^\alpha(\frac{1}{-iv_-t})^\beta] \\ &= i^{K(\mathbf{m})}\frac{2}{{v_+}^\alpha {v_-}^\beta}\int_a^\infty dt\, t^{2-(\alpha+\beta)}. \end{aligned} \tag{B.9}$$

The dependence on $K(\mathbf{m})$ here is an artifact of our using the unfortunate convention (B.1), when in fact the proportionality constant in front alternates sign as $|K(\mathbf{m})| = 0, 2, 4, \ldots$ to keep the correlation function positive when its argument is on the time axis. The effective scaling dimension Δ_{eff} after re-exponentiating the perturbation to the correlation function is

$$2\Delta_{\text{eff}} = 2\Delta - \frac{4(4\pi)\alpha\beta D}{(v_+ + v_-){v_+}^{\alpha-1}{v_-}^{\beta-1}}\int_a^\infty \frac{dt}{t^{\alpha+\beta-2}}. \tag{B.10}$$

By the usual process of changing the cutoff $a \to a\exp(\ell)$ we obtain the RG equations

$$\begin{aligned} \frac{dD}{d\ell} &= (3 - 2\Delta)D \\ \frac{d\Delta}{d\ell} &= -\frac{8\pi D(\Delta^2 - K(\mathbf{m})^2/4)}{(v_+ + v_-){v_+}^{\alpha-1}{v_-}^{\beta-1}}. \end{aligned} \tag{B.11}$$

These equations match those found by Kane, Fisher, and Polchinski for the $|K(\mathbf{m})| = 2$ operator in the $\nu = 2/3$ state. However, as mentioned above we find no term which renormalizes the velocities to first order in D.

Now consider the case of two comoving modes. The simplest example is the IQHE state $\nu = 2$, which has a relevant impurity operator hopping electrons from one mode to the other. The correlation function P_{12} of an impurity operator $O_{\mathbf{n}} = \exp(in_j\phi_j)$ has the form $(x+iv_1t)^{-\alpha}(x+iv_2t)^{-\beta}$, with (v_1, v_2) the velocities of the two eigenmodes and $\alpha+\beta = K(\mathbf{n})$ an even integer. Expanding the correlation function in the disorder strength and then evaluating the disorder average as before gives the correction to the correlation function:

$$\begin{aligned} D\int dX\, dT\, dt\, P_{12}P_{34}[1 + t^2(&\frac{i\alpha v_1}{X - x_1 + iv_1(T - t_1)} \\ &+\frac{i\beta v_2}{X - x_1 + iv_2(T - t_1)} - \frac{i\alpha v_1}{X - x_2 + iv_1(T - t_2)} \\ &-\frac{i\beta v_2}{X - x_2 + iv_2(T - t_2)})^2]. \end{aligned} \tag{B.12}$$

Expanding the square gives terms with both denominators at the same point, which cancel infinities appearing elsewhere in the calculation, and terms with both denominators having the same velocity, which were previously argued to be zero (and in any event cannot cause the two velocities to flow toward each other, since each term only involves one velocity). The result is

$$\begin{aligned} &\alpha\beta v_1v_2P_{12}\int dX\, dT\, [\frac{1}{X - x_1 + iv_1(T - t_1)}\times \\ &\frac{1}{X - x_2 + iv_2(T - t_2)} + (v_1 \leftrightarrow v_2)]\int dt\, t^2P_{34} \\ &= \frac{4\pi\alpha\beta v_1v_2P_{12}\int dt\, t^2P_{34}}{v_1 - v_2}\log[\frac{x_2 - x_1 + iv_1(t_2 - t_1)}{x_2 - x_1 + iv_2(t_2 - t_1)}]. \end{aligned} \tag{B.13}$$

Thus α and β are changed but not $\alpha + \beta = K(\mathbf{m})$. The velocities of the eigenmodes are unaltered, and the RG flows are

$$\begin{aligned} \frac{dD}{d\ell} &= (3 - \alpha - \beta)D = (3 - K(\mathbf{m}))D \\ \frac{d\alpha}{d\ell} &= -\frac{d\beta}{d\ell} = -\frac{8\pi D\alpha\beta}{(v_1 - v_2)v_1{}^{\alpha-1}v_2{}^{\beta-1}}. \end{aligned} \tag{B.14}$$

The singular denominator when $v_1 = v_2$ is acceptable because at $v_1 = v_2$, only $\alpha + \beta$ is well-defined, not α and β separately.

The generalization to a case with two modes and more than one impurity operator is simple: the contributions to the RG flow equations for the velocity matrix from each impurity operator add, since to leading order the impurity operators are independent.

Extending the calculation to an edge with more than two modes is quite simple. In the expansion of the square term in (B.4), each pair of modes gives one term. If the two modes move in opposite directions, the term lowers the total scaling dimension as in (B.11); if the two modes move in the same direction, the term maintains the total scaling dimension as in (B.14). Each term preserves $K(\mathbf{m})$ separately. For explicitness, consider the case of an edge with two right-movers and one left-mover,

which is relevant to the $\nu = 3/5$ edge. Then the correlation function has the form $(x + iv_1 t)^{-\alpha}(x + iv_2 t)^{-\beta}(x - iv_- t)^{-\gamma}$, and the RG flows for the exponents are

$$\begin{aligned}
\frac{d\alpha}{d\ell} &= -\frac{8\pi D\alpha\beta v_1 v_2}{(v_1 - v_2)v_1{}^{\alpha}v_2{}^{\beta}v_-{}^{\gamma}} - \frac{8\pi D\alpha\gamma v_1 v_-}{(v_1 + v_-)v_1{}^{\alpha}v_2{}^{\beta}v_-{}^{\gamma}} \\
\frac{d\beta}{d\ell} &= \frac{8\pi D\alpha\beta v_1 v_2}{(v_1 - v_2)v_1{}^{\alpha}v_2{}^{\beta}v_-{}^{\gamma}} - \frac{8\pi D\beta\gamma v_2 v_-}{(v_2 + v_-)v_1{}^{\alpha}v_2{}^{\beta}v_-{}^{\gamma}} \\
\frac{d\gamma}{d\ell} &= -\frac{8\pi D\alpha\gamma v_1 v_-}{(v_1 + v_-)v_1{}^{\alpha}v_2{}^{\beta}v_-{}^{\gamma}} - \frac{8\pi D\beta\gamma v_2 v_-}{(v_2 + v_-)v_1{}^{\alpha}v_2{}^{\beta}v_-{}^{\gamma}}.
\end{aligned} \tag{B.15}$$

Chapter 6 shows how the V matrix flow in the χLL action determined by the correlation function flows found in this appendix has a natural interpretation in terms of the boost and rotation parts of the V matrix.

Bibliography

[1] K. von Klitzing, G. Dorda, and M. Pepper, Phys. Rev. Lett. **45**, 494 (1980).

[2] R. B. Laughlin, Phys. Rev. B **23**, 5632 (1981).

[3] B. I. Halperin, Phys. Rev. B **25**, 2185 (1982).

[4] R. B. Laughlin, Phys. Rev. Lett. **50**, 1395 (1983).

[5] F. D. M. Haldane, Phys. Rev. Lett. **51**, 605 (1983).

[6] X.-G. Wen, Adv. in Phys. **44**, 405 (1995).

[7] P. K. Lam and S. M. Girvin, Phys. Rev. B **30**, 473 (1984).

[8] B. I. Halperin, Phys. Rev. Lett. **52**, 1583 (1984).

[9] L. N. Pfeiffer *et al.*, Appl. Phys. Lett. **56**, 1697 (1990).

[10] A. M. Chang, L. N. Pfeiffer, and K. W. West, Phys. Rev. Lett. **77**, 2538 (1996).

[11] X.-G. Wen, Phys. Rev. B **43**, 11025 (1991); Phys. Rev. Lett. **64**, 2206 (1990).

[12] F. Milliken, C. Umbach and R. Webb, Solid State Comm., **97**, 309 (1995).

[13] A.M. Chang, L.N. Pfeiffer and K.W. West, Phys. Rev. Lett, **77**, 2538 (1996).

[14] X.-G. Wen, Int. J. Mod. Phys. B **6**, 1711 (1992).

[15] S. Tomonaga, Prog. Theor. Phys. **5**, 544 (1950).

[16] J. M. Luttinger, J. Math. Phys. **4**, 1154 (1963).

[17] F. D. M. Haldane, Phys. Rev. Lett. **47**, 1840 (1981).

[18] C. L. Kane, M. P. A. Fisher, and J. Polchinski, Phys. Rev. Lett. **72**, 4129 (1994).

[19] C. L. Kane and M. P. A. Fisher, Phys. Rev. B **51**, 13449 (1994).

[20] A. V. Shytov, L. S. Levitov, and B. I. Halperin, Phys. Rev. Lett. **80**, 141 (1998).

[21] N. Read, Phys. Rev. Lett. **62**, 86 (1989).

[22] S. C. Zhang, T. H. Hansson and S. Kivelson, Phys. Rev. Lett. **62**, 82 (1989).

[23] J. K. Jain, Phys. Rev. Lett. **63**, 199 (1989).

[24] M. D. Johnson and A. H. MacDonald, Phys. Rev. Lett. **67**, 2060 (1991).

[25] J. E. Moore and F. D. M. Haldane, Phys. Rev. B **55**, 7818 (1997).

[26] T. Giamarchi and H. J. Schultz, Phys. Rev. B **37**, 325 (1988).

[27] C. L. Kane and M. P. A. Fisher, Phys. Rev. B **52**, 17393 (1995).

[28] C. W. Misner, K. S. Thorne and J. A. Wheeler, *Gravitation* (W. H. Freeman and Co., New York, 1973), p. 69.

[29] G. L. Watson, *Integral Quadratic Forms* (Cambridge University Press, Cambridge, 1960), chaps. 1-3.

[30] F. D. M. Haldane, Phys. Rev. Lett. **74**, 2090 (1995).

[31] J. P. Eisenstein, H. L. Stormer, L. N. Pfeiffer, and K. W. West, Phys. Rev. Lett. **62**, 1540 (1989); Phys. Rev. B **41**, 7910 (1990).

[32] B. I. Halperin, Helv. Phys. Acta. **56**, 75 (1983).

[33] I. A. McDonald and F. D. M. Haldane, Phys. Rev. B **53**, 15845 (1996).

[34] K. Moon *et al.*, Phys. Rev. Lett. **71**, 4381 (1993).

[35] C. L. Kane and M. P. A. Fisher, Phys. Rev. B **46**, 15233 (1992).

[36] R. C. Ashoori, H. Stormer, L. Pfeiffer, K. Baldwin and K. West, Phys. Rev. B **45**, 3894 (1992).

[37] J. E. Moore and X.-G. Wen, Phys. Rev. B **57**, 10138 (1998).

[38] P. Fendley, A. W. W. Ludwig, and H. Saleur, Phys. Rev. B **12**, 8934 (1995).

[39] S. Ghoshal and A. B. Zamolodchikov, Int. J. Mod. Phys. A **9**, 3841 (1994).

[40] C. Chamon and E. Fradkin, Phys. Rev. B **56**, 2012 (1997).

[41] J. E. Moore and X.-G. Wen, unpublished.

[42] D. B. Chklovskii and B. I. Halperin, Physica E **1**, 75 (1997).

[43] N. P. Sandler, C. Chamon, and E. Fradkin, Phys. Rev. B **59**, 12521 (1999).

[44] J. L. Cardy, Nucl. Phys. B **270**, 186 (1986).

[45] P. Di Francesco, P. Mathieu, and D. Senechal, *Conformal Field Theory*, Springer-Verlag (1998).

[46] A. Schmid, Phys. Rev. Lett. **51**, 1506 (1983).

[47] J. E. Moore, P. Sharma, and C. Chamon, `cond-mat/9912443`, to appear in Phys. Rev. B.

[48] L. P. Pryadko, E. Shimshoni, A. Auerbach, Phys. Rev. B **61**, 10929 (2000).

[49] J. M. Kosterlitz and D. J. Thouless, J. Phys. C **6**, 1181 (1973).

[50] J. V. José, L. P. Kadanoff, S. Kirkpatrick, and D. R. Nelson, Phys. Rev. B **16**, 1217 (1977).

[51] D. R. Nelson, Phys. Rev. B **18**, 2318 (1978); D. R. Nelson and B. I. Halperin, Phys. Rev. B **19**, 2457 (1979).